LRFD PULLOUT RESISTANCE FACTOR CALIBRATION FOR SOIL NAILS INCORPORATING SURVIVAL ANALYSIS AND PLAXIS 2D

by

BRETT DEVRIES

Presented to the Faculty of the Graduate School of

The University of Texas at Arlington in Partial Fulfillment

of the Requirements

for the Degree of

MASTER OF CIVIL ENGINEERING

THE UNIVERSITY OF TEXAS AT ARLINGTON

August 2013

Acknowledgements

I would like to express my appreciation to Dr. Xinbao Yu for his constant support and guidance throughout this research. My appreciation extends to Dr. Sahadat Hossain, Dr. Laureano R. Hoyos, Dr. Anand J. Puppala, and Dr. Bhaskar Chittoori for their instruction, wisdom and guidance throughout my time at the University of Texas at Arlington. I greatly appreciate the time and effort to help me with the statistical analysis that Dr. D. L. Hawkins Jr. has extended to me.

A special thanks needs to be extended to Carmen Díaz-Caneja and Family for their constant encouragement, support and love. I am truly blessed to them in my life.

Additionally, I would like to thank Trinity Infrastructure LLC and Craig Olden, Inc. for allowing me to conduct this research. All of their employees have been helpful and friendly, but a special thanks needs to be extended to Carlos Fernández Lillo and Cynthia Zuñiga. Their insight and help has been crucial for me to conduct this research.

I appreciate all the help and support from my fellow classmates and friends, namely Asheesh Pradhan, Charles Leung and Justin Thomey. Without the help, instruction and support from all of these people I could not have completed my Masters.

July 18, 2013

Abstract

LRFD PULLOUT RESISTANCE FACTOR

CALIBRATION FOR SOIL NAILS

INCORPORATING SURVIVAL

ANALYSIS AND PLAXIS 2D

Brett DeVries

The University of Texas at Arlington, 2013

Supervising Professor: Xinbao Yu

The use of soil nail walls (SNWs) in the United States has increased since their introduction in the mid-1970's, to where currently the analysis, design and construction are commonly performed (Lazarte, 2011). These SNW designs were mostly based on ASD methods and LRFD-based methodologies were lacking until the 1998 FHWA manual on SNW design (Byrne, Cotton, Porterfield, Wolschlag and Ueblacker, 1998), which provided uncalibrated resistance factors developed from ASD safety factors. As a result, little improvement was made toward a more efficient design, until fully calibrated LRFD pullout resistance factors were provided in the NCHRP Report 701 (Lazarte, 2011). These pullout resistance factors were calibrated with a variety of load factors commonly used for retaining structures as part of a bridge substructure. Although fully calibrated resistance factors were calculated, the predicted pullout resistance was not based a specific design procedure, but rather on multiple design procedures (Lazarte, 2011).

The main objective of this study was to achieve a greater understanding of the bond strength of soil nails in North Dallas Texas. In an effort to accomplish this

objective, pullout resistance factors were calibrated for cohesive soils within the project location. Pullout resistances were determined using creep test data, field observations, and methods commonly used in tension piles. This resulted in 25 cases that met failure criteria out of the 47 verification tests conduction in cohesive soil for the LBJ Express construction project. Statistical analysis was conducted to evaluate the predicted to measured pullout resistance for the failed tests, and Survival Analysis was utilized to incorporate the non-failed tests. In addition, PLAXIS 2D was used to fit a finite element model to testing results and used to predict failure in three cases. Results from analysis test results, Survival Analysis and PLAXIS 2D were combined with the 25 failed cases along with soil nail testing results found in the NCHRP Report 701. Five soil nail databases were established from these results and utilized in the remainder of the study. Then, LRFD reliability analysis using Monte Carlo simulations were performed to calibrate pullout resistance factors at a target reliability index of 2.33 and load factors of 1, 1.35, 1.5, 1.6 and 1.75. The final step involved incorporating SNAILZ to compare the required soil nail length between the existing design method and the calibrated resistance factors for a typical SNW.

Table of Contents

List of Illustrations

List of Tables

Chapter 1

Introduction

1.1 Introduction

1.1.1 *Soil Nails*

Soil nailing is the technique of installing closely spaced steel bars encased in grout (typically six inches in diameter) within soil. When this technique is utilized to construct a wall, it is referred to as a soil nail wall (SNW) as shown in Figure 5.10. SNWs are typically constructed from the top down and as excavation proceeds, concrete or shotcrete is applied to the excavation facing. The soil nails are subjected primarily to tensile stresses and are constructed in a near horizontal orientation (Lazarte, Elias, Espinoza and Sabatini, 2003).

The use of SNWs in the United States has increased since their introduction in the mid-1970's, to where currently the analysis, design, and construction are commonly performed (Lazarte, 2011).

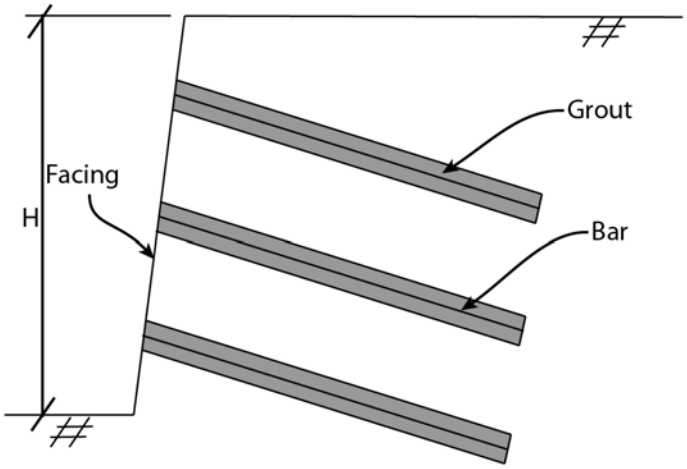

Figure 1.1: Typical soil nail wall layout.

1.1.2 *Survival Analysis*

Due to the limitations of the ultimate tensile strength of the bar or other reasons, many soil nails are not conducted to failure during the verification tests. As a result, an absolute value for the ultimate bond strength between the soil and nail is not known. It is known however, that

failure criteria will be met at a load higher than what was applied during the test (Figure 1.2). Thus, it is important to incorporate these non-failed tests when analyzing the ultimate strength between soil and nail. These non-failed tests can be effectively incorporated into the analysis process by utilizing Survival Analysis.

Survival Analysis has typically been used in the biomedical sciences, where it is applied to predicting the probability of survival, response or mean lifetime of experiments on animals or humans (Lee and Wang, 2003). Although these principles can be a benefit to civil engineering applications where tests may or may not be conducted to failure, this type of analysis has not been incorporated previously in Geotechnical Engineering applications.

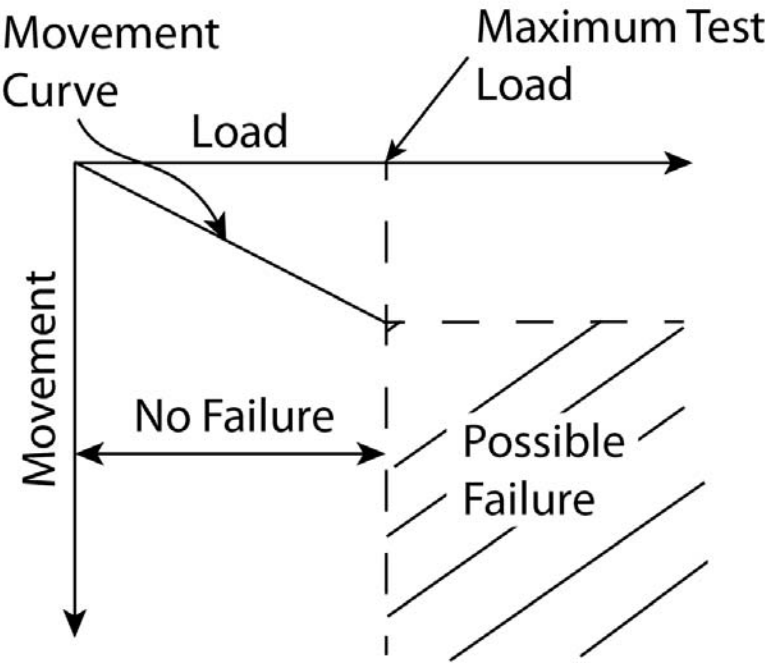

Figure 1.2: Example of a verification test not conducted to failure.

1.1.1 *PLAXIS 2D*

PLAXIS 2D was developed to analyze deformation, groundwater flow and stability in geotechnical engineering, and is intended for use by Geotechnical Engineers who may not be numerical analysis specialist (PLAXIS, 2011). It is a two-dimensional finite element program that allows the soil to be modeled by a variety of methods and has successfully been implemented

to model both SNWs and soil nail tests (Ann et al., 2004a; Ann et al., 2004b; Lengkeek and Peters; Singh and Sivakumar Babu, 2010; Sivakumar Babu and Singh, 2009; Zhang et al., 1999).

1.1.2 *Load and Resistance Factor Design*

The use of load and resistance factor design (LRFD) based methodologies for SNWs was lacking until the 1998 FHWA manual on SNW design (Byne et al., 1998), which provided uncalibrated resistance factors developed by allowable-stress design (ASD) safety factors. As a result, little improvement was made toward a more efficient design, until fully calibrated LRFD pullout resistance factors were provided in the NCHRP Report 701 (Lazarte, 2011). These pullout resistance factors were calibrated with a variety of load factors commonly used for retaining structures as part of a bridge substructure. Although fully calibrated resistance factors were calculated, the predicted pullout resistance was not based on a specific design procedure but rather on multiple design procedures (Lazarte, 2011).

The main advantage of LRFD when compared to ASD, is that LRFD addresses uncertainties in a systematic manner rather than based on experience. The LRFD method was developed to accomplish the following:

- separately account for uncertainties in loads and resistances by the use of load and resistance factors,
- offer load and resistance factors based on reliability and acceptable levels of structural reliability, and
- provide consistent levels of safety for several components which are incorporated within a structure (Lazarte, 2011).

To accomplish these tasks, a tolerable probability of failure is selected and resistance and load factors are calibrated using actual load and resistance data with probability-based techniques (Lazarte, 2011).

1.1.3 *SNAILZ*

California Department of Transportation (Caltrans) developed the program SNAILZ and according to Lazarte (2011) is the most widely used SNW design software in the United States. This program has the advantage of being free to download from the Caltrans website and easily allows for minimum factors of safety for soil nail walls along with slope stability with and without reinforcement, and tie back walls to be calculated (Caltrans, 2007).

1.2 Project Background

LBJ Express is a 2.7 billion dollar project that will improve the capacity of I-35E and I-635 located in North Dallas, Texas (Figure 1.3). When completed, this project will consist of eight lanes for general purpose traffic, two to four managed lanes, and two to three frontage road lanes. Project construction began early in 2011 and completion will occur in early 2016, resulting in dramatically expanded capacity. To complete this project, numerous temporary and permanent SNWs will and have been constructed.

Figure 1.3: Project location (Google, Inc.).

The LBJ Express construction project is underlain by flood plain and alluvial deposits associated with the Trinity River and overlays the Eagle Ford Shale Formation. The Alluvial and Flood Plain deposits consist of small gravel, sand, sandy clays, and clays which have been

deposited in the last 40,000 years, while the Eagle Ford Formation consists of highly plastic clay, weathered and unweathered shale. Temporary SNWs are constructed mainly in cohesive soil, while permanent walls are built in rock formations such as tan and gray limestone. All of the soil/rock strength parameters are conservatively estimated and remained relatively constant throughout the project.

1.3 Research Objectives

The main objective of this research is to achieve a greater understanding of the bond strength between the soil (cohesive) and grout for soil nails in North Dallas Texas. This would allow engineers to have greater confidence in the design of SNWs for both this project and SNWs in the Dallas Texas area. For the objective to be accomplished, the steps listed subsequently were conducted.

1. Collection of soil nail testing results in the North Dallas Texas area on which failure analysis of verification tests was conducted. Soil nail testing results were presented in the NCHRP Report 701 and incorporated in this study.
2. Survival Analysis was conducted to incorporate both failed and non-failed testing results. This type of statistical analysis allowed fitting normal and lognormal distributions to the testing data.
3. PLAXIS 2D was used to model verification testing results and in several cases predict the failure load.
4. Load and resistance factor design was incorporated and calibration of many resistance factors was completed for various load factors and soil nail databases.
5. The computer software SNAILZ was incorporated to compare required soil nail lengths of the existing design method to incorporating the LRFD design methods for a typical SNW.

1.4 Organization and Summary

The organization of this thesis progresses in such a manner that it will allow the reader to understand basic concepts before results and conclusions are provided. In generally the layout follows the previously listed steps 1 through 5 and the following provides a brief summary of each chapter within this thesis.

Chapter 2 provides information found in literature on the bond resistance, testing procedures, and failure classification. Also included is a summary of testing databases incorporated in this study and measured to predicted testing results and conclusions.

Chapter 3 describes the basic background information about Survival Analysis and also provides a simple example to allow for easier understanding. Results and conclusions of the Survival Analysis on the various databases are also provided.

Chapter 4 presents information about PLAXIS 2D and the steps involved to model soil nail verification tests. The various trial methods for modeling testing results are provided along with a comparison between modeling and Triaxial Test results.

Chapter 5 offers background information about the load and resistance factor design and the steps followed in this study to incorporate LRFD into the established databases. Summary and conclusions on the calibrated resistance factors are also provided.

Chapter 6 provides the reader a basic understanding of the SNAILZ programs and presents results on the required soil nail length for the established design and incorporation of the calibrated resistance factors.

Chapter 7 is the chapter where general conclusions about the methods and results from this study are provided.

Appendix A presents testing results found in this study and from the NCHRP Report 701, which are separated by chosen databases.

Appendix B offers the verification testing results from North Dallas Texas and the corresponding PLAXIS 2D fittings are shown. The fitted model parameters and predicted test results are also provided in this section.

Appendix C shows the calculations necessary for the PLAXIS and SNAILZ software to be used.

Appendix D provides the Consolidated Undrained Triaxial Testing results conducted by Terracon and included for comparison to PLAXIS results.

Chapter 2

Soil Nails

2.1 Literature Review and Background

2.1.1 *Soil Nail Bond Resistance*

Pullout failure of the soil nail is the primary internal failure that occurs within a SNW and as a result it is critical to possess a good understanding of this mechanism. To prevent pullout failure, bond resistance between the soil and grout interface is mobilized within a SNW as seen in Figure 5.10.

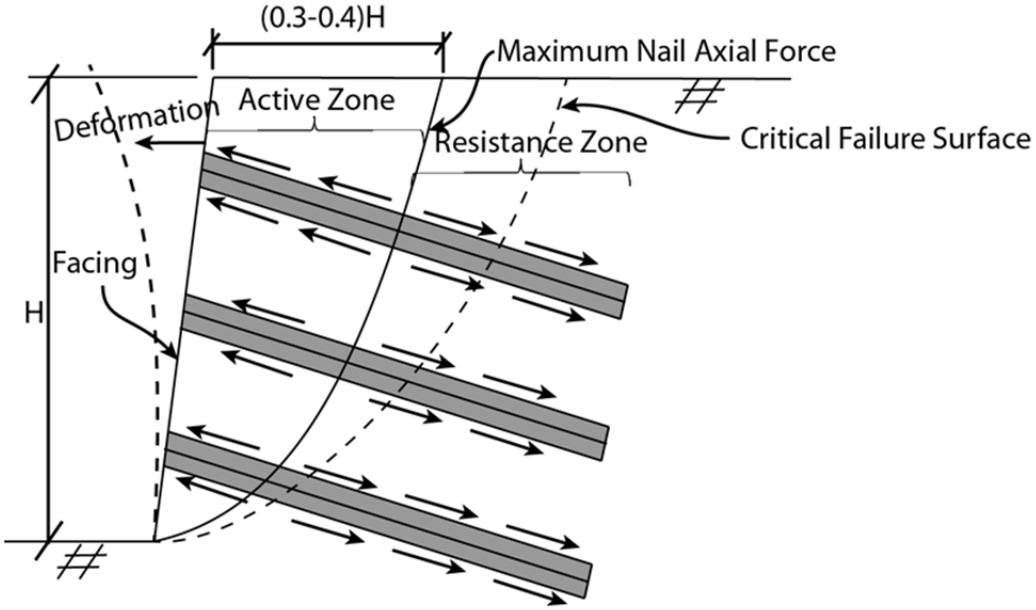

Figure 2.1: Soil nail wall behavior (modified from Byne et al., 1998; Lazarte et al., 2003[1]).

The bond resistance is activated when the wall facing deforms as a result of the soil pressure, causing the attached soil nail to experience tensile forces. A number of factors can affect the bond resistance pertaining to soil nails that are drilled and gravity grouted as:

- from the ground above:
    - soil characteristics,

[1]Lazarte et al. (2003) will be referenced to as “GEC 7 (2003)."

    - soil type, and
    - overburden pressure;
- soil nail installation methods:
    - drill-hole cleaning procedure,
    - drilling method,
    - grouting procedure,
    - grout injection method, and
    - grout characteristics (Lazarte, 2011).

The magnitude of overburden tends to have a larger effect on the bond resistance for granular soil when compared to fine-grained soils, and granular soils have a tendency to be most affected by the soil friction of the surrounding soil and the overburden pressure. For fine-grained soils, the bond strength is generally a fraction of the undrained shear strength of the surrounding soil. The ratio between the bond resistance and the undrained shear strength tends to be higher in relatively soft fine-grained soils when compared to relatively stiff (Lazarte, 2011).

Possessing techniques to estimate the bond strength of the soil nail is essential to both the preliminary and final design of SNWs and the accuracy of these correlations can decide how the SNW will perform in the field. Currently, the bond resistance of the soil nail can be estimated by the following techniques:

- from common field test,
- typical values found in literature, and
- soil nail tests (Lazarte, 2011).

These types of techniques typically apply for a wide range of soil types and conditions. Correlations between the bond strength of soil nails and standard field test such as the Standard Penetration Test (SPT) and the Pressuremeter Test (PMT) can be found in GEC 7 (2003), Lazarte (2011) and Clouterre (1993). While, typical values for a wide range of soil types

and construction methods can be found in Elias and Juran (1991) and the Post-Tensioning Institute (PTI, 2005). These values encompass a range of values and allow engineers to select typical values for a variety of conditions. The typical values from Elias and Juran (1991) are shown in Table 2.1 and include a certain degree of conservatives, and are the most widely used reference according to Lazarte (2011). The upper and lower bounds in Table 2.1 represent approximately the most and least favorable conditions for each construction method and soil type (GEC 7, 2003; Lazarte, 2011).

Table 2.1: Estimated bond strength of soil and rock (from Elias and Juran, 1991; obtained from GEC 7, 2003).

Material	Construction Method	Soil/Rock Type	Ultimate Bond Strength, q_u (kPa)
Rock	Rotary Drilled	Marl/limestone	300 - 400
		Phyllite	100 - 300
		Chalk	500 - 600
		Soft dolomite	400 - 600
		Fissured dolomite	600 - 1000
		Weathered sandstone	200 - 300
		Weathered shale	100 - 150
		Weathered schist	100 - 175
		Basalt	500 - 600
		Slate/Hard shale	300 - 400
Cohesionless Soils	Rotary Drilled	Sand/gravel	100 - 180
		Silty sand	100 - 150
		Silt	60 - 75
		Piedmont residual	40 - 120
		Fine colluvium	75 - 150
	Driven Casing	Sand/gravel	
		low overburden	190 - 240
		high overburden	280 - 430
		Dense Moraine	380 - 480
		Colluvium	100 - 180
	Augered	Silty sand fill	20 - 40
		Silty fine sand	55 - 90
		Silty clayey sand	60 - 140
	Jet Grouted	Sand	380
		Sand/gravel	700
Fine-Grained Soils	Rotary Drilled	Silty clay	35 - 50
	Driven Casing	Clayey silt	90 - 140
	Augered	Loess	25 - 75
		Soft clay	20 - 30
		Stiff clay	40 - 60
		Stiff clayey silt	40 - 100
		Calcareous sandy clay	90 - 140

Notes: Convert values in kPa to psf by multiplying by 20.9
Convert values in kPa to psi by multiplying by 0.145

Although typical values and correlations between field tests and the bond strength of the soil nail are good for preliminary design, it is necessary to conduct soil nail load tests to verify estimated values. These tests are conducted on partially grouted nails and tensile forces are applied along the axis of the bar while the movement is recorded (Figure 2.2). This procedure can allow the estimated pullout resistance between the grout/soil interface to be determined (GEC 7, 2003; Lazarte, 2011). The objectives of testing soil nails can include:

- confirming design load (DL) can be achieved for the purposed installation method and materials,
- that if a different soil type is encountered or construction methods changed, that the DL can be achieved,
- investigate if the soil nail will experience excessive time-related deformation, and
- define the ultimate load that the soil nail can resist without failing (Lazarte, 2011).

To accomplish these objectives, the following tests can be conducted on both sacrificial and non-sacrificial nails within a SNW:

- proof load test,
- verification load test, and
- creep tests (Lazarte, 2011).

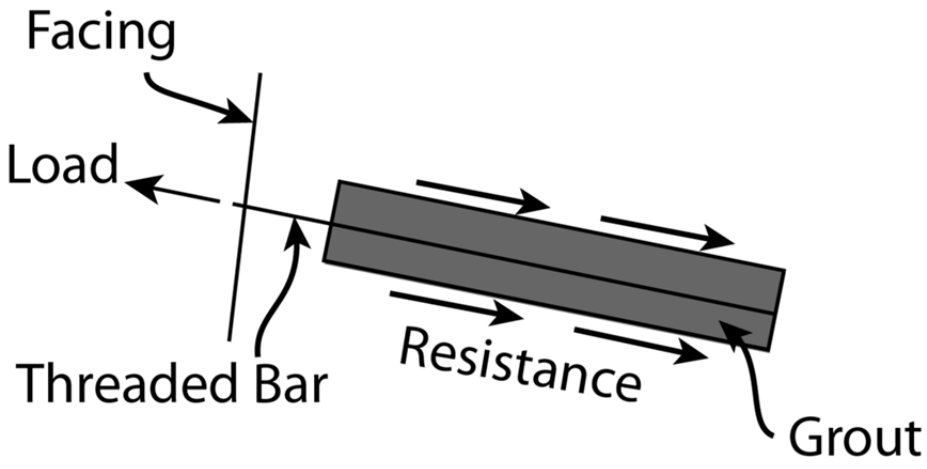

Figure 2.2: Applied load and induced resistances from the soil nail during the verification test.

Proof tests are conducted on production nails (assuming small amounts of deformation) and intended to ensure that the construction procedure used remained constant and that the nails have not been constructed in a soil layer that has yet been tested (GEC 7, 2003). The typical proof test is conducted to a maximum load of 150 percent of the DL and as a result, small amounts of deformation are usually obtained. Consequently, failure during the proof tests rarely occurs (GEC 7, 2003; Lazarte, 2011).

Verification or ultimate load tests are conducted on sacrificial nails and can be used to verify the ultimate bond strength of the soil nail. At minimum, the test should be conducted to an equivalent factor of safety of the DL, but it is recommended to test to failure (GEC 7, 2003; Lazarte, 2011).

Creep tests are conducted to ensure that the soil nail can sustain the design load throughout the life of the structure and are performed as part of the verification or proof tests. These tests are performed by measuring the movement of the soil nail over a certain period of time and failure criteria is based on experience (GEC 7, 2003; Lazarte, 2011).

2.1.1.1 Soil Nail Load Mechanics

[2]An illustration of a soil nail test and the resulting forces, stresses and elongations are shown in Figure 2.3. For all soil nail tests, the load (P) and total soil nail elongation (Δ_{tot}) is applied or measured at the SNW facing. The resisting force by the soil nail is assumed to be uniform along the grouted (bonded) length (L_B); although this relationship can be complex and depend on nail length, grout characteristics, magnitude of applied tensile force and soil conditions (Figure 2.3 (b)). Incorporating this assumption, the load transfer rate (Q) can be defined as:

$$Q = (\pi D_{DH}) q(x) \qquad 1$$

[2]For simplicity, ideas and equations shown in this section are courtesy of GEC 7 (2003) and Lazarte (2011).

where the term (πD_{DH}) is the outside perimeter of the grout and $q(x)$ is the uniform stress along the L_B. When considering a single nail segment of a soil nail and applying a tensile force (T) as shown in Figure 2.3 (a), the incremental tensile force (dT) is:

$$dT = (\pi D_{DH})qdx = Qdx \quad (2)$$

The tensile force along the unbounded length (L_U) is simplified to be constant, which is shown in Figure 2.3 (c). Where, T at distance x from the end of the bar (opposite of the facing) can be defined as:

$$T(x) = \int_0^x (\pi D_{DH})qdx = \int_0^x Qdx \quad (3)$$

When the ultimate bond strength (maximum value of $T(x)$) is achieved, the pullout capacity (R_{PO}) can be expressed as:

$$R_{PO} = T_{max} = (\pi D_{DH})q_u L_B \quad (4)$$

where q_u is the ultimate bond strength between the soil and grout. The test load (P) at failure can be equal to T_{max} and results in the following equation:

$$q = \frac{P}{(\pi D_{DH})L_B} \quad (5)$$

where the term, $(\pi D_{DH})L_B$ is the outside surface area of the grouted section over the entire bonded length of soil nail.

As shown in Figure 2.3 (c), Δ_{tot} is comprised of the deformation of the bonded length (Δ_B) and unbounded length (Δ_U). This elongation of the bar (Δ_U) as a result of the applied load can be described as:

$$\Delta_U = \frac{PL_{UB}}{EA_t} \quad (6)$$

where A_t is the cross-sectional area of the bar, and E is the elastic modulus of the bar.

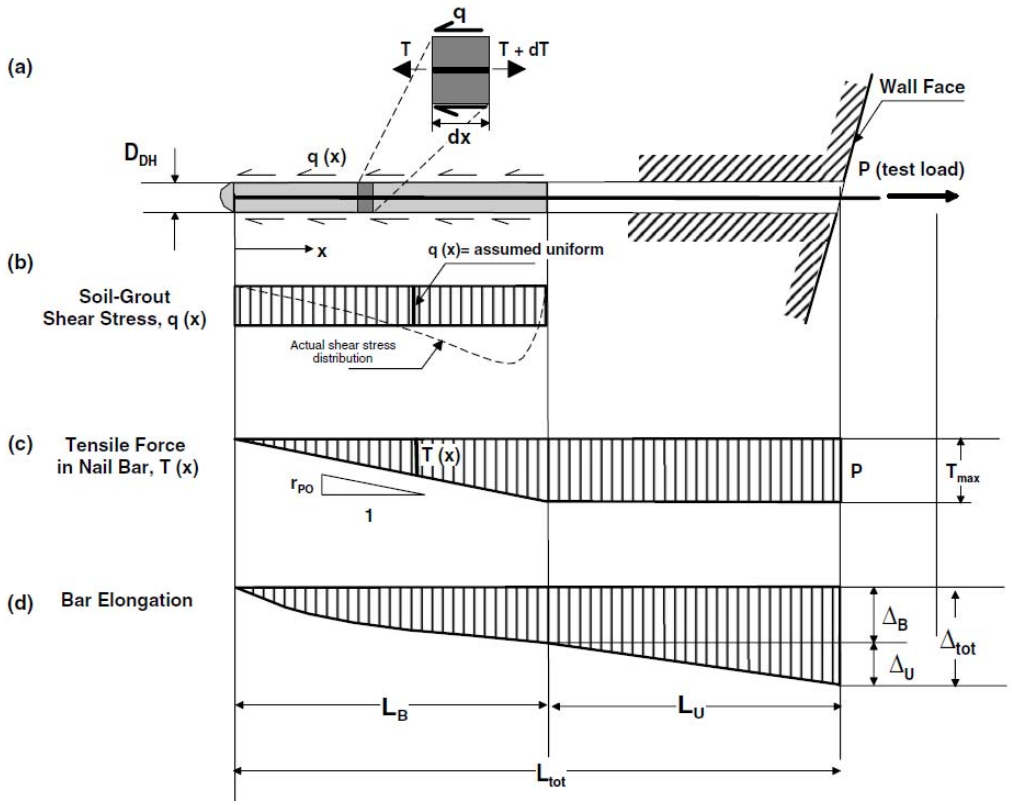

Figure 2.3: Loads and elongation in a soil nail load test (Lazarte, 2011).

It is assumed that because of the high resistance between the threaded bars and grout, bar deformation within the grout is negligible. This implies that Δ_B is only a result of the grout and soil interaction and can be expressed as:

$$\Delta_B = \Delta_{tot} - \Delta_U \qquad 7$$

These elongation concepts may be best illustrated and understood by Figure 2.4.

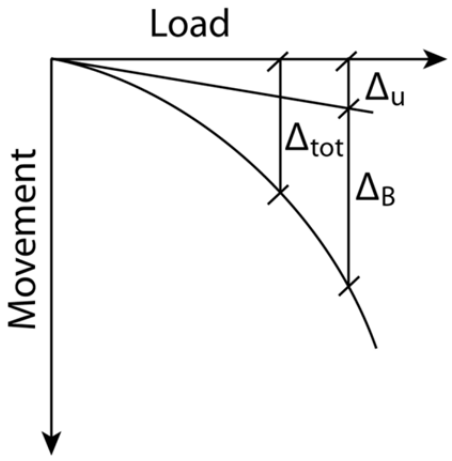

Figure 2.4: Elongation concepts from a soil nail load test (modified from Lazarte, 2011).

2.1.2 *Verification Test*

It is critical in any soil nail wall to test the strength between the soil nail grout and the surrounding soil. To accomplish this task, verification tests are conducted and also verify capacities for different conditions during construction and/or installation methods (GEC 7, 2003). In addition, verification testing can provide the following information:

- determine the ultimate bond strength if conducted to failure,
- verify of the factor of safety, and
- establish the load at which excessive creep occurs (GEC 7, 2003).

For meaningful results, verification tests should be conducted with the same construction and design methods as used for the production nails (GEC 7, 2003; Lazarte, 2011). Potentially a more economical design can be achieved if the test is conducted to failure, because the ultimate bond strength between soil and nail is determined and consequently a lower factor of safety is required. At minimum, a verification test should be conducted to twice the DL to verify the factor of safety (recommended factor of safety of 2.0) and the test load must not exceed 80 percent of the ultimate tensile strength of the soil nail bar (GEC 7, 2003; Lazarte, 2011).

A typical verification test setup is shown in Figure 2.5, and consists of at least a hydraulic ram, a reaction frame and dial gauge(s). The hydraulic ram applies the load to the soil nail and the reaction frame transfers the applied load to the SNW facing. The dial gauge(s) allow the movements of the soil nail to be measured throughout the test (GEC 7, 2003).

A typical within soil layout of a verification test is shown in Figure 2.6. This material used should be identical to the production nails; but unlike production nails, includes an unbounded length (L_{UB}) and a shorter grouted length (L_B). The unbounded length allows for the movement of the soil nail without interfering with the SNW, while exceptionally large loads are avoided by conduction the test with a shorter grouted length than the production nails. As shown in Figure 2.2, the load is applied axially and the resulting resistance by the soil/nail interface is along the entire grouted length (GEC 7, 2003; Lazarte, 2011).

Figure 2.5: Verification testing equipment and setup (Trinity Infrastructure, Inc.).

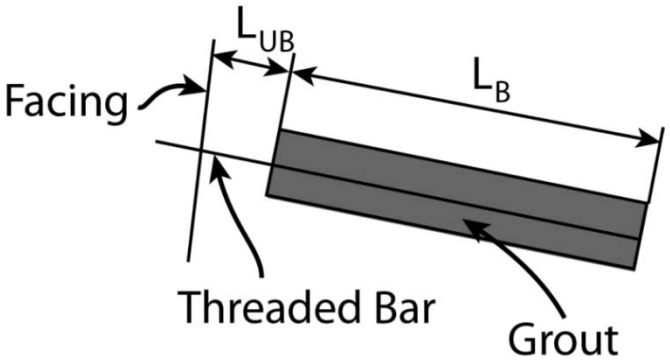

Figure 2.6: Layout of within soil structures of a soil nail during a verification test.

The standard testing schedule for the verification test is shown in Table 2.2 with design test loads (DTL) of upwards of 300 percent. A creep test is conducted at 150 percent of the design load and used to verify that the load can be carried throughout the service life (GEC 7, 2003). Confirming that the SNW will not fail throughout the service life can also be completed by measuring the difference in movement of the soil nail at certain time intervals during each load increment (usually comparison between the one and ten minute readings). It is not required to test beyond a design load of 200 percent. However, as stated before more information and possibly a more efficient design is gained if the test is conducted to failure (GEC 7, 2003; Lazarte, 2011).

Table 2.2: Typical verification test loading schedule (GEC 7, 2003).

Load	Hold Time
0.05 DTL max	1 minute
0.25 DTL	10 minutes
0.50 DTL	10 minutes
0.75 DTL	10 minutes
1.00 DTL	10 minutes
1.25 DTL	10 minutes
1.50 DTL (Creep Test)	60 minutes
1.75 DTL	10 minutes
2.00 DTL	10 minutes
2.50 DTL	10 minutes max.
3.00 DTL or Failure	10 minutes max.

2.1.3 *Interpretation of Verification Test Results*

Interpreting the verification test results is a critical aspect of defining the ultimate bond strength of the soil nail. Several procedures have been defined and used to estimate this value by GEC 7 (2003) and Lazarte (2011) and include:

- field observation,
- evaluation of test curves,
- analysis of loads using a maximum deflection criteria, and

- analysis of creep behavior.

2.1.3.1 Field Observations

This procedure can be used if in the field, observations show near or imminent failure will occur (Lazarte, 2011). It is somewhat limited in practicality because the identification of failure must be performed during the test and it may be easier to test the soil nail to a predetermined design load, independent of the deformation.

2.1.3.2 Evaluation of Test Curves

This evaluation procedure is defined when the test load curve flattens or when further attempts at increasing the load results in only deformation (Lazarte, 2011). An example of flatting of the test curve is presented in Figure 2.7 (2). Evaluating using this procedure is possibly the best at defining the ultimate bond strength, but may require relatively large loads to achieve.

It has been seen by the NCHRP Report 701 that this type of evaluation provides a better estimate when the tests are conducted in clay and clayey sand when compared to weathered rock, gravel and dense sands.

2.1.3.3 Maximum Deflection Criteria

The NCHRP Report 701 states that techniques similar to those used to estimate the ultimate compression and tension loads for deep foundation can be considered and include:

- Davission (1972) method,
- De Beer (1967 and 1968) method, and
- Brinch-Hansen (1963) method.

These techniques have the potential to work as well as they do for deep foundations because soil nails show very similar load-deformation trends to tension loads on deep foundations. However, these techniques were not very useful to identify clearly the ultimate pullout resistances for soil nails in the NCHRP Report 701.

Although may tend to be conservative, considering a maximum movement to be considered for failure has been used commonly in tension piles (Lazarte, 2011). These methods are outlined by Hirany and Kulhawy (2002) and Koutsoftas (2000), and consider the ultimate load is achieved when a movement of 0.4 to 0.5 inch is seen between the soil/nail interface. Another example of maximum movement corresponding to failure load, is in accordance to some SNW contractors, where the maximum load is established when the Δ_{tot} is equal to one inch (Lazarte, 2011). A failure criteria meeting a movement of 0.4 inch between the soil/nail interface is shown in Figure 2.7 (3).

2.1.3.4 Analysis of Creep Test

The creep test analysis can be used to ensure that the nail can adequately perform throughout the service life of the structure rather than immediate failure of the system. These types of criteria are based largely on experience as previously mentioned. Evaluated of the potential for creep is conducted during the creep test and at each ten minute load increment (Table 2.2; GEC 7, 2003). Two failure criteria listed in GEC 7 (2003) state that between the one and ten minute readings at an individual load, the movement must be greater than 1 mm (0.04 in.) or the movement between the six and sixty minute reading during the creep test must be larger than 2 mm (0.08 in.). Failure can also be concluded if the creep rate is not linear or increasing throughout the creep test load by GEC 7 (2003) or by French soil-nailing practice (Clouterre, 2002).

2.2 Analysis Procedure

The large amount of SNWs constructed to data for the LBJ Express construction project allowed for a substantial amount of testing data to be accumulated. This testing data included verification and proof testing and in various soil types. Verification tests are used to estimate the ultimate bond strength of the soil nail and thus the testing data was reduced to 91 tests, with all tests conducted with the same augured drilling and gravity grouted method. The soil conditions surrounded each soil nail were determined by engineers at Trinity Infrastructure LLC and

allowed for sorting of tests into databases for each soil type commonly found in the North Dallas area. In general, the cohesive soils in the region are associated with the Eagle Ford Formation and are classified as CH (high plasticity clay; Appendix D).

To estimate the ultimate bond strength of the soil nail, the following failure criteria were selected from those in Section 2.1.3:

1. A test load (P) having greater than 1 mm (0.04 in.) of total creep movement during a ten-minute reading.
2. Analysis of the elastic movement curve, particularly flattening of the test curve.
3. Movement of 10 mm (0.4 in.) or greater between the soil/nail interface.

A verification test that met multiple failure criteria is shown in Figure 2.7. In this figure the creep (1) and movement between soil/nail (3) failure criteria were met at a test load of 106 kN (24 kips), and the test curve exhibited flattened behavior (2) at a test load of 115 kN (26 kips). The ultimate pullout resistance was considered to be 106 kN, which is at the smallest load that met failure criteria. In many cases, the creep (1) and soil/nail movement (3) failure criteria corresponded to the same test load and defined the ultimate bond resistance.

As a result of this analysis a total of 47 verification tests were accumulated in fine-grained soil and a total of 25 met one or more of the failure criteria. In addition to the tests conducted in the North Dallas area, the tests in cohesive soil presented in NCHRP Report 701 were utilized.

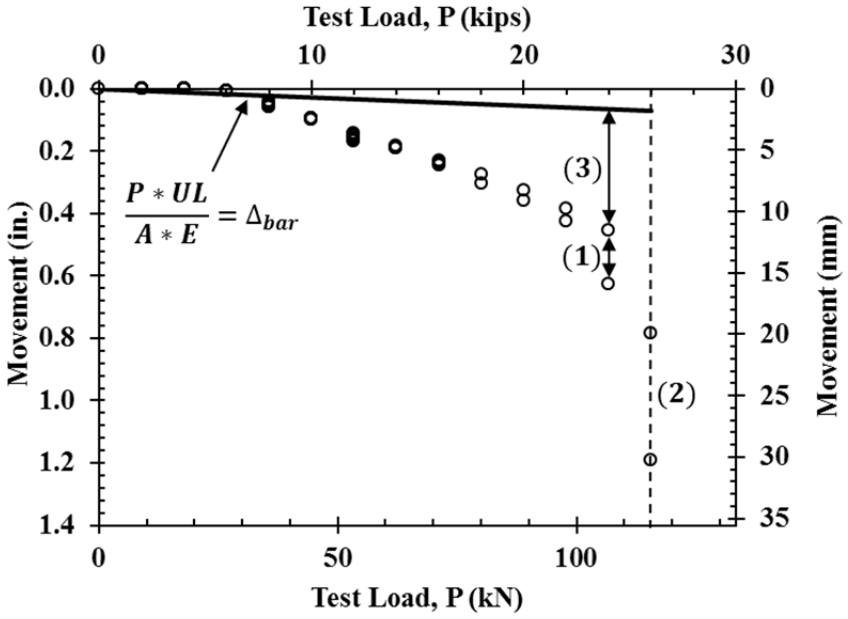

Figure 2.7: Example of elastic movement analysis of a verification test meeting multiple failure criteria.

It was necessary to divide the soil nail verification tests into databases so that various combinations of verification test results from this study and the NCRHP Report 701 can be combined. In addition, databases were combined to incorporate failed and non-failed test results and resulted in the calculation of 22 mean and standard deviations values. The databases are shown in Appendix A and described as:

- Database 1: included the 25 verification tests from North Dallas meeting failure criteria.
- Database 2: comprised of the 45 tests in cohesive soil from the NCHRP Report 701.
- Database 3: incorporated the 22 verification tests from North Dallas not meeting failure criteria.
- Database 4: contained the three verification tests that were predicted to fail by PLAXIS.
- Database 5: comprised of the 19 verification tests from North Dallas that did not meet or predicted to meet failure criteria.

For LRFD calibration to be performed, it is optimum to have all predicted values estimated by the same design method. This is the case for all verification tests from this study (Databases 1, 3, 4 and 5), where the ultimate bond strength of the soil nail is predicted by the lower end of the augured stiff clay found in Table 2.1. As a result, the predicted ultimate bond strength for all of the soil nails in North Dallas is 1,000 psf. However, predicted values found in Database 2 from the NCHRP Report 701 represent multiple prediction methods and are based on typical values found in Table 2.1 or based on engineer's local experience (Lazarte, 2011).

2.3 Results and Conclusions

To conduct LRFD calibration and Survival Analysis, the measured and predicted pullout resistance of the soil nails should be characterized. Figure 2.8 through Figure 2.15 show this comparison for databases or cumulative databases that were used throughout this study. The subsequent results and conclusions should be noted from these figures.

- The general trend in Figure 2.8 showed that the measured resistance was greater than the predicted resistance (occasionally greater than two times). There were however, two data points that disagreed with this trend and are positioned near to the 1:1 line (measured and predicted values are the same).
- The addition of the NCHRP Report 701 data to Database 1 (Figure 2.9) shifted the trend toward the 1:1 line.
- Similar trends to Database 1 are shown in Figure 2.10, when the PLAXIS predicted failures (Database 4) were incorporated.
- Almost no change in trend was shown when Database 4 was included with Databases 1 and 2, as shown in Figure 2.11.
- Figure 2.12 incorporated non-failed tests to Database 1 and resulted in a slight increase in tendency toward a higher bias[3]. It is important to note that the highest bias values

[3] Bias is defined as measured values divided by predicted and will be defined in greater detail within Section 5.1.5.

were non-failed test results, and an additional test value was incorporated near the 1:1 line (bias equal to 1.0).

- As shown in Figure 2.13, the addition of non-failed tests (Database 3) to Databases 1 and 2 resulted in insignificant change. Again, it is important to note that the highest bias values were shown to be non-failed test results.
- The addition of non-failed tests (Database 5) to Databases 1 and 4 increased the trend toward larger bias values (Figure 2.14). The highest bias values in the cumulative database were again non-failed test results.
- When all data values from literature and this study are combined, the results are shown in Figure 2.15. This resulted in a very similar trend to when Databases 1, 2 and 3 were combined and the highest bias values were non-failed tests.
- It should be noted that Craig Olden, Inc. has conducted all verification tests for the LBJ Express construction project.

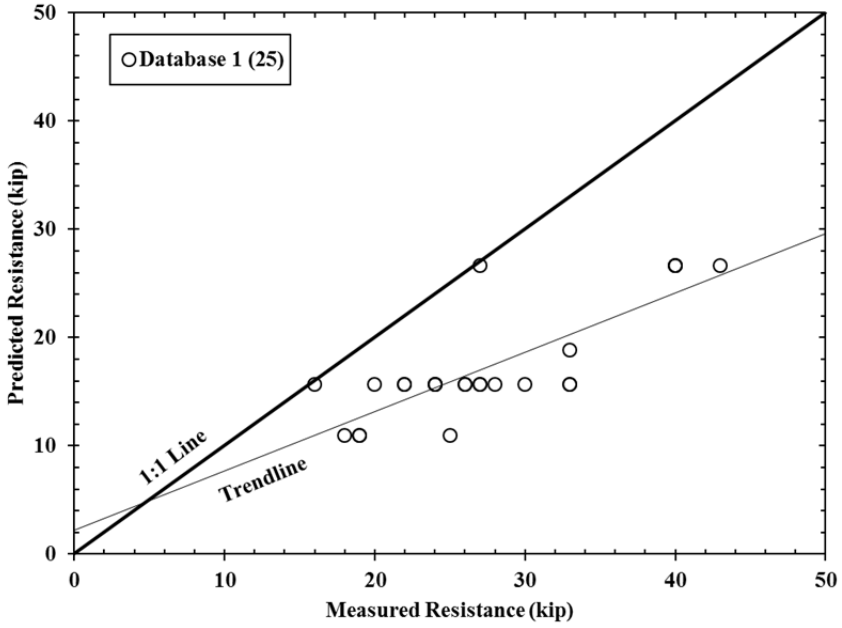

Figure 2.8: Measured and predicted pullout resistance for Database 1.

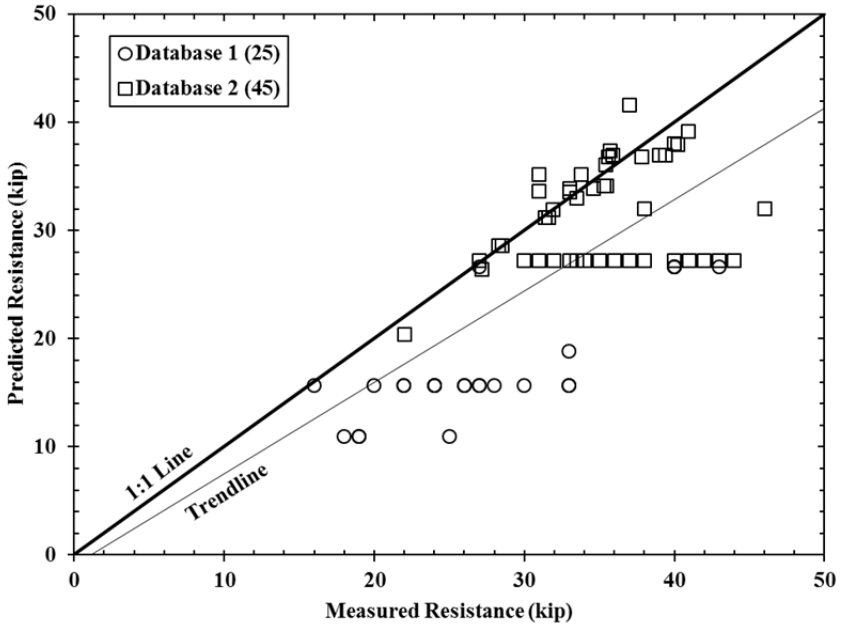

Figure 2.9: Measured and predicted pullout resistance for Databases 1 and 2.

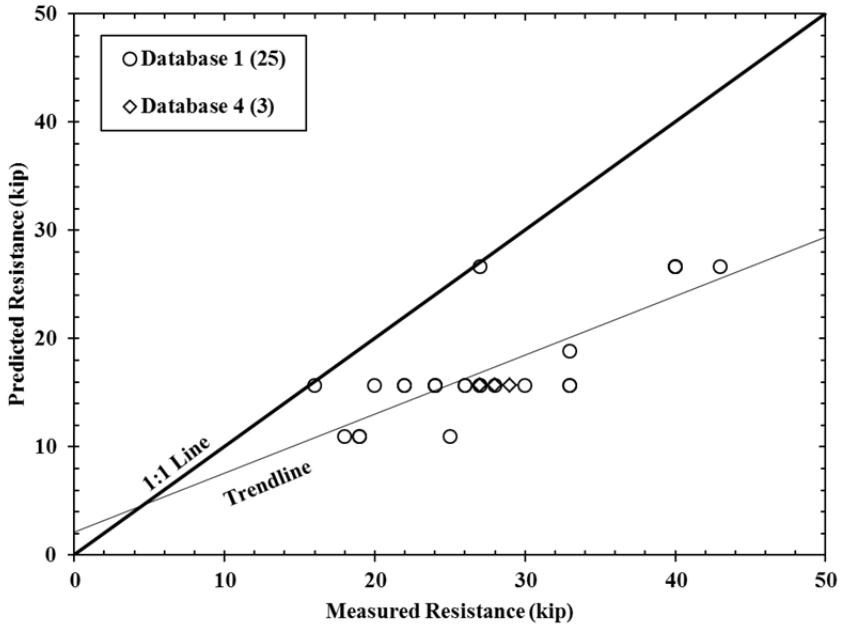

Figure 2.10: Measured and predicted pullout resistance for Databases 1 and 4.

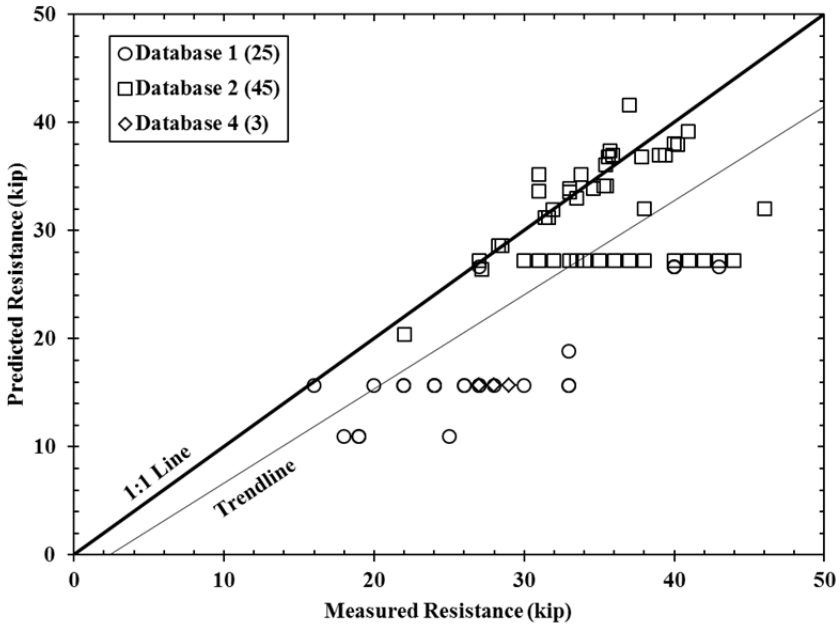

Figure 2.11: Measured and predicted pullout resistance for Databases 1, 2 and 4.

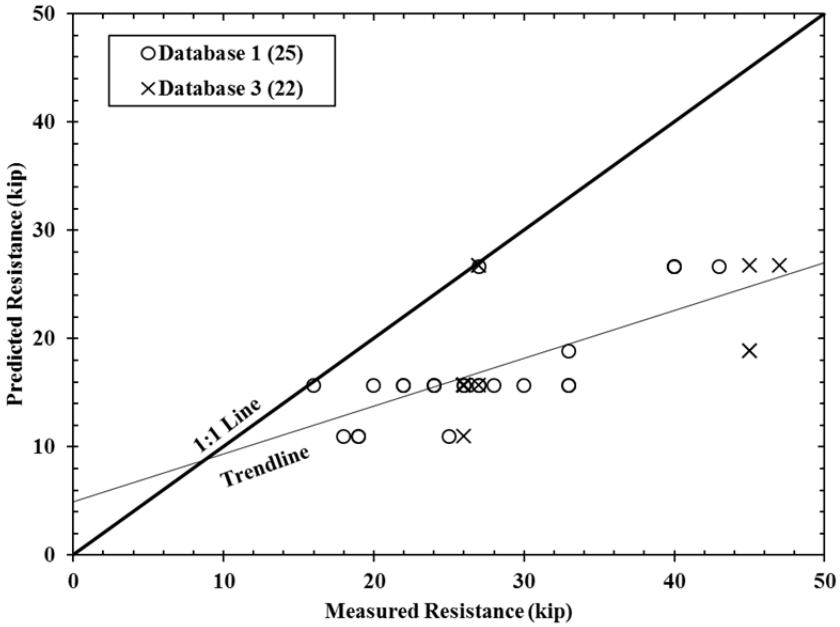

Figure 2.12: Measured and predicted pullout resistance for Databases 1 and 3.

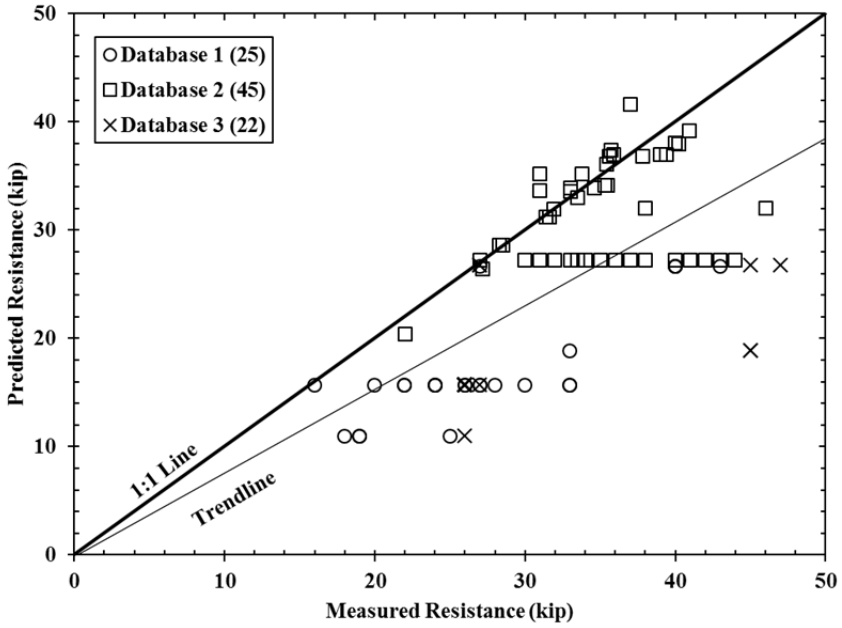

Figure 2.13: Measured and predicted pullout resistance for Databases 1, 2 and 3.

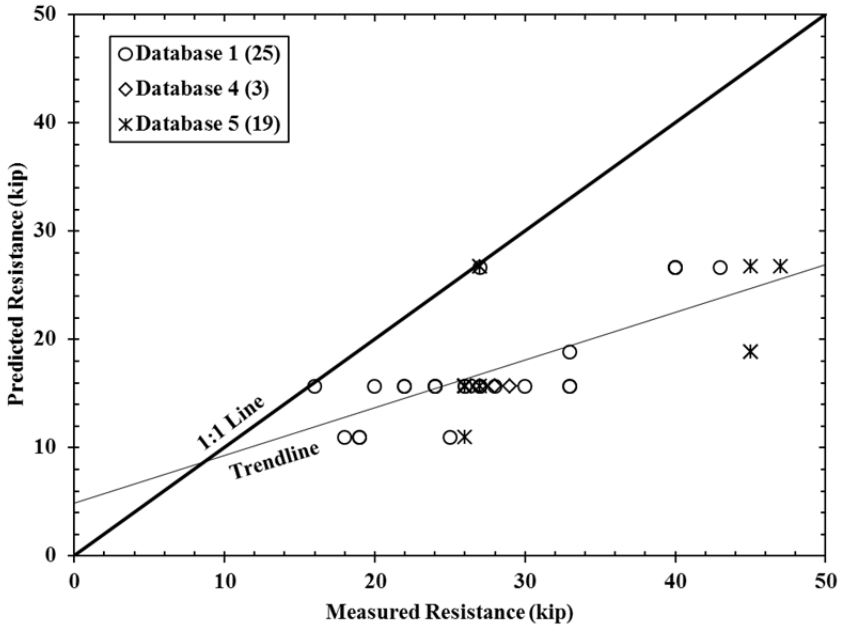

Figure 2.14: Measured and predicted pullout resistance for Databases 1, 4 and 5.

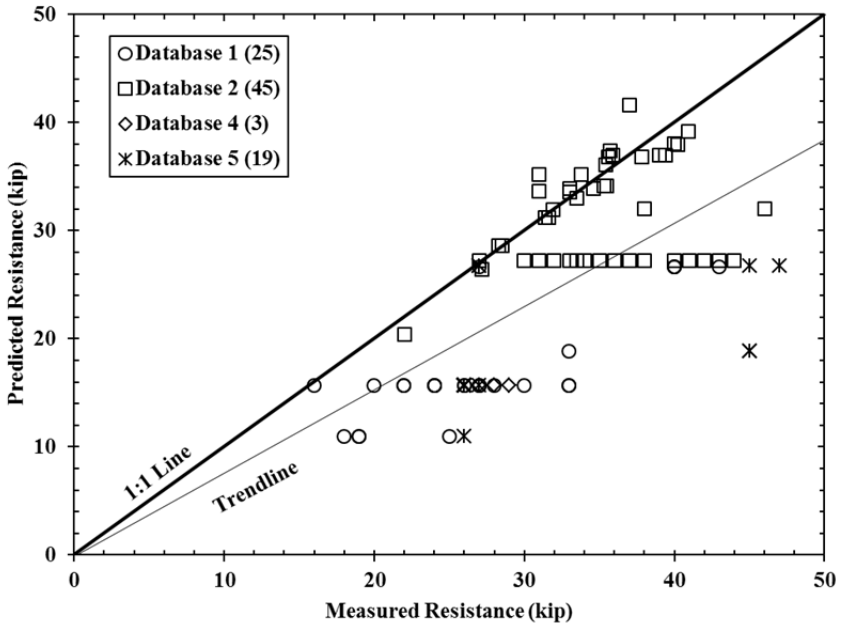

Figure 2.15: Measured and predicted pullout resistance for Databases 1, 2, 4 and 5.

Chapter 3

Survival Analysis

3.1 Literature Review and Background

3.1.1 *Background*

In Survival Analysis, the interest is in a defined time (or load[4]) required to achieve a defined failure point, known as the survival time (Cox and Hinkley, 1984; Lee and Wang, 2003). For the survival time to be precisely determined, a few requirements must be met and include:

- origin of time must be defined,
- scale for measuring the passage of time must be established, and
- failure has to be clearly defined (Cox and Hinkley, 1984).

In the case of soil nail verification tests, the survival time is the loads up to where the nail meets one or more of the failure criteria, the origin is at a load of zero and scale is the load increments.

One of the most important features of survival analysis is to incorporate tests not conducted to failure. When the verification test is not conducted to failure, the exact survival load is unknown and referred to as a censored observation. When the verification test is conducted to a load where a failure criterion is met, it is referred to as an uncensored observation. There are three types of censoring:

- Type I: observe for a fixed period of time,
- Type II: to wait until a fixed portion of the subjects have died, and
- Type III: when the time is random (Cox and Hinkley, 1984; Lee and Wang, 2003).

Type I and type II are called singly censored data, while type III is called randomly censored (Lee and Wang, 2003). Verification tests are conducted to 80 percent of the ultimate tensile strength of the bar or a predetermined design load, and are thus considered Type I censored data. All three of these types of censoring are considered right censoring, because

---

[4]The terms failure time and failure load will be used interchangeably and refer to the same definition.

they occur at the end (right side) of the observation (Lee and Wang, 2003) and occurs when the final load applied to the soil nail is not large enough to result in one of the failure criteria being met.

To conduct Survival Analysis, analytical methods such as parametric and nonparametric must be used. Nonparametric methods can be calculated by hand and usually completed first to allow comparison to the parametric method. Parametric approaches are used when a distribution is selected and fitted to the available data (Lee and Wang, 2003).

3.1.2 *Functions of Survival Time*

A set of survival time's distribution can be characterized by the following functions:

- survivorship function,
- probability density function, and
- hazard function (Lee and Wang, 2003).

These functions can be used interchangeably but it may be practical to use a certain function to illustrate a particular aspect of the data (Lee and Wang, 2003). As a result, only the survivorship function or survival function will be defined.

3.1.2.1 Survivorship Function (Survival Function)

When L is taken as the survival time, the distribution of L can be defined by the survivorship function. This survivorship function is denoted by $S(l)$ and is the probability that a failure criterion is not met before load (l) as:

$$S(l) = P(a\ soil\ nail\ does\ not\ fail\ before\ l) = P(L > l) \quad 8$$

This allows for the cumulative distribution function $F(l)$ of L to be defined as:

$$S(l) = 1 - P(a\ soil\ nail\ fails\ before\ l) = 1 - F(l) \quad 9$$

It stands to reason that the probability of a soil nail surviving a load of zero is 100 percent, and any soil nail surviving to an infinite load has a probability of zero as:

$$S(l) = \begin{cases} 1, & for\ l = 0 \\ 0, & for\ l = \infty \end{cases} \quad 10$$

When censored observations are not present in the data, the survivorship function is estimated as the proportion of nails failing at a load greater than l:

$$\hat{S}(l) = \frac{number\ of\ nails\ failing\ at\ a\ load\ greater\ than\ l}{total\ number\ of\ verification\ tests} \qquad 11$$

where the circumflex ($\widehat{\ }$) represents an estimate of the survivorship function. When censored observations are present, $\hat{S}(l)$ cannot always be determined and it is no longer appropriate to estimate $S(l)$ (Lee and Wang, 2003). As a result, nonparametric or parametric methods may be required to conduct Survival Analysis.

3.1.3 *Nonparametric Methods*

Nonparametric methods are useful when censored and uncensored data are present and it is suggested to use nonparametric methods to analyze survival data before fitting a distribution. The estimates obtained from the nonparametric methods and accompanying graphs can be helpful to find a distribution that fits the data (Lee and Wang, 2003). Several nonparametric methods are available to estimate the survival functions:

- Kaplan and Meier Product-Limit (PL), and
- Life-Table technique (Lee and Wang, 2003).

Kaplan and Meier PL method and the Life-Table technique are very similar and thus only the PL method will be discussed.

3.1.3.1 Product-Limit (PL) Estimates of Survivorship Function

The PL method of estimating the survivorship function was developed by Kaplan and Meier (1958), and is useful when the estimate is based on individual survival times (Lee and Wang, 2003).

A simple case where all of the soil nails are observed to failure and thus the survival loads are exact and known can be considered first. Let $l_{(1)}$,$l_{(2)}$,….,$l_{(n)}$ be the exact survival loads of the n verification tests conducted. This group of nails can be assumed as a random sample from a much larger population of nails with similar properties. Relabeling the n survival

loads ($l_{(1)}$,$l_{(2)}$,….,$l_{(n)}$) in ascending order such that $l_{(1)} \leq l_{(2)} \leq \cdots \leq l_{(n)}$ allows the survivorship function at any particular load ($l_{(i)}$) to be estimated as (Lee and Wang, 2003):

$$\hat{S}\left(l_{(i)}\right) = \frac{n-i}{n} = 1 - \frac{i}{n} \quad 12$$

where $n-i$ is the number of verification tests surviving longer than $l_{(i)}$. If two or more $l_{(i)}$ are equal (tied observations), the largest i value is used. As an example, if $l_{(2)} = l_{(3)}$, then (Lee and Wang, 2003):

$$\hat{S}\left(l_{(2)}\right) = \hat{S}\left(l_{(3)}\right) = \frac{n-3}{n} \quad 13$$

this will result in a conservative estimate for the tied observations. Similar to Equation 10, every nail has not failed at a load of zero, and no test survives longer than $l_{(n)}$. This allows the following to be defined (Lee and Wang, 2003):

$$\hat{S}\left(l_{(0)}\right) = 1 \quad 14$$

$$\hat{S}\left(l_{(n)}\right) = 0 \quad 15$$

In practice, $\hat{S}(l)$ is computed at every distinct survival load, since the $\hat{S}(l)$ remains constant between load intervals where no soil nails are seen to fail. It is recommended by Lee and Wang (2003) that the PL survivorship function should be plotted as a step function. However, when the survival curve must be used to estimate the median survival load, a smooth curve may provide a better estimate (Lee and Wang, 2003). This method only works if all of the verification tests are conducted to failure, if this is not the case the PL estimate given by Kaplan and Meier (1958) must be used to estimate $\hat{S}(l)$.

The PL estimate of the probability of surviving any particular load is the product of the same estimate up to the preceding load ($\hat{S}(l-1)$), and the observed survival rate at that particular load (p_l), such that (Lee and Wang, 2003):

$$\hat{S}(l) = \hat{S}(l-1)p_l \quad 16$$

The PL estimates can be calculated by the use of a table and incorporate the following equation:

$$\hat{S}(l) = \prod_{l_{(r)} \leq l} \frac{n-r}{n-r+1} \qquad 17$$

where the n survival loads are relabeled in increasing magnitude such that $l_{(1)} \leq l_{(2)} \leq \cdots \leq l_{(n)}$, $l_{(r)}$ is an uncensored load and l goes through the positive integers in which $l_{(r)} \leq l$ (Lee and Wang, 2003).

A few critical features of the PL estimates of the survivorship function are provided subsequently.

- The Kaplan-Meier estimates are limited to the load interval in which all observations are seen. The PL estimate is zero when the largest observation is uncensored, but if the largest observation is censored, then the PL estimate can never be equal to zero and is undefined beyond the largest observation (censored).
- An estimate of the median can be made by taking the L at which $\hat{S}(t) = 0.5$ on the survival curves estimated by the PL method; however, the solution may not be unique.
- If the largest observation is censored and greater than 50 percent of the observations are censored, then the median survival time cannot be estimated.
- The reason an observation is censored must be unrelated to the cause of failure, and the PL method is not appropriate to use when inappropriate censoring is incorporated.
- The confidence interval may deserve more attention than just the point estimate $\hat{S}(l)$ and a 95 percent confidence interval for $S(l)$ is (Lee and Wang, 2003):

  $$S(l) = \hat{S}(l) * 1.96 * S.E.[\hat{S}(l)] \qquad 18$$

  where $S.E.$ is the standard error of $S(l)$.

3.1.4 *Parametric Methods*

Parametric methods allow selection of a distribution such as the commonly used normal or lognormal distributions to be incorporated into Survival Analysis (Cox and Hinkley, 1984; Lee and Wang, 2003). These models are often complex and may require the use of statistical programs such as SAS® to compute the mean and standard deviations for the normal and lognormal distributions.

3.1.4.1 Estimation of μ and σ^2 for Data with Censored Observations

For samples comprised of singly censored observations, the data consists of n total observations with r exact survival loads (uncensored) and are $l_1, l_2, \ldots l_r$. When the data is considered lognormally distributed, $Y = \log L$ which has normal distribution with mean μ and variance σ^2. With censored observation within the data are $l_{r+1}^+, l_{r+2}^+, \ldots l_n^+$, and the likelihood function is defined as (Lee and Wang, 2003):

$$l(\mu, \sigma^2) = -\frac{r \log(2\pi\sigma^2)}{2} - \sum_{i=1}^{r}\left(\log l_i + \frac{(\log l_i - \mu)^2}{2\sigma^2}\right) + \sum_{i=r+1}^{r}\left\{\int_{l_i^+}^{\infty} \frac{1}{x\sqrt{2\pi\sigma^2}} \exp\left[-\frac{1}{2\sigma^2}(log\, x - \mu)^2\right] dx\right\} \quad 19$$

The maximum likelihood estimate (MLE) of μ and σ^2 can be obtained by solving the following two equations (Lee and Wang, 2003):

$$\sum_{i=1}^{r}\frac{\log l_i - \mu}{\sigma^2} + \sum_{i=r+1}^{r}\frac{\int_{l_i^+}^{\infty}\frac{\log x - \mu}{x\sigma^2\sqrt{2\pi\sigma^2}}\exp\left[-\frac{1}{2\sigma^2}(log\, x - \mu)^2\right]dx}{\int_{l_i^+}^{\infty}\frac{1}{x\sqrt{2\pi\sigma^2}}\exp\left[-\frac{1}{2\sigma^2}(log\, x - \mu)^2\right]dx} = 0 \quad 20$$

$$-\frac{n}{2\sigma^2} + \sum_{i=1}^{r}\frac{(\log l_i - \mu)^2}{2\sigma^4} + \sum_{i=r+1}^{r}\frac{\int_{l_i^+}^{\infty}\frac{(\log x - \mu)^2}{x2\sigma^4\sqrt{2\pi\sigma^2}}\exp\left[-\frac{1}{2\sigma^2}(log\, x - \mu)^2\right]dx}{\int_{l_i^+}^{\infty}\frac{1}{x\sqrt{2\pi\sigma^2}}\exp\left[-\frac{1}{2\sigma^2}(log\, x - \mu)^2\right]dx} = 0 \quad 21$$

When SAS® is used, the estimated parameters of the lognormal and normal distribution mean ($\hat{\mu}$) and standard deviation ($\hat{\sigma}$) are (Lee and Wang, 2003):

$$\hat{\mu} = INTERCEPT \quad 22$$

$$\hat{\sigma}^2 = SCALE^2 \quad (23)$$

The complexity of these equations demonstrates the importance of using statistical software such as SAS®.

3.2 Analysis Procedure

In an effort to calculate the statistical parameters (μ and σ) to be incorporated into the LRFD resistance factors, nonparametric and parametric Survival Analysis was conducted. These analyses were conducted on Databases (Appendix A) and Cumulative Databases results shown in Section 2.3, and allowed non-failed test to be incorporated into the LRFD pullout resistance factor calibration. When only failed tests were seen such as in Database 1 and 2, Survival Analysis provided a best fit distribution to the data. As recommended previously (Section 3.1.1), a nonparametric method (Kaplan and Meier PL method) was used for comparison of the distributions (normal and lognormal) assumed in the parametric analysis. The procedure for conducting nonparametric and parametric methods are as follows (Lee and Wang, 2003):

- nonparametric:
    1. let n be the total number of soil nails whose survival load are censored or uncensored,
    2. relable the n survival loads in order of increasing magnitude such that $l_{(1)} \leq l_{(2)} \leq \cdots \leq l_{(n)}$,
    3. rank the n survival loads such that they are consecutive integers 1, 2,…,n,
    4. establish values for r, which are equal to the rank integer if the survival load is uncensored. If the survival load is censored, then no rank is given,
    5. calculate p_l for each uncensored observation using the following equation:

$$p_l = \frac{n-r}{n-r+1} \quad (24)$$

    6. calculate $\hat{S}(l)$ using Equation 16 or 17;

- parametric:
    1. select a distribution that is predicted to fit the data,
    2. choose a statistical software such as SAS®, and
    3. write code such that the output will provide the desired statistical parameters such as shown in Figure 3.1 for an assumed lognormal distribution.

```
options ls=69 ps=50;
data one;
infile '\\tsclient\E\SAS\Example.csv'
        dlm=',' ;
input number bias failure $;
censor=(failure='yes'); *censor=1 if lifetime is observed, = 0 if observation
is censored;
proc print;
data one; set one;
 bl=bias;
proc print;
run;
proc lifereg data=one outest=parmdat covout;
 model bl*censor(0) =   /dist=lnormal;
 output out=outfile cdf=f p=quantile q=.50  std=se_quant
                    xbeta=uhat;
run;
```

Figure 3.1: Example of SAS® code for parametric Survival Analysis (modified from code provided by Dr. Hawkins).

3.2.1 *Example Problem*

A simple example of nonparametric and parametric method calculations can be useful for understanding. In this example, tests are seen to fail (uncensored) at loads of 2, 7, 7 and 20 kips; and tests are conducted to but not seen to fail at loads of 4 and 15 kips. The table format PL nonparametric method is shown in Table 3.1. Results of the parametric (assuming normal and lognormal distributions) and nonparametric analysis are shown in Figure 3.2 and Table 3.2.

Table 3.1: Calculation of the PL estimate survivorship functions for the example problem.

Failure Load, L (kip)	Rank (i)	r	$\frac{n-r}{n-r+1}$	$\hat{S}(l)$
2	1	1	$\frac{(6-1)}{(6-1+1)}=\frac{5}{6}$	$\frac{5}{6}$
4*	2	-	-	-
7	3	3	$\frac{(6-3)}{(6-3+1)}=\frac{3}{4}$	$\frac{5}{6}*\frac{3}{4}=0.625^{a}$
7	4	4	$\frac{(6-4)}{(6-4+1)}=\frac{2}{3}$	$\frac{5}{6}*\frac{3}{4}*\frac{2}{3}=0.4167^{a}$
15*	5	-	-	-
20	6	6	$\frac{(6-6)}{(6-6+1)}=0$	0

[a]0.4167 is used as $\hat{S}(7)$, for a conservative estimate.
*indicates a censored test.

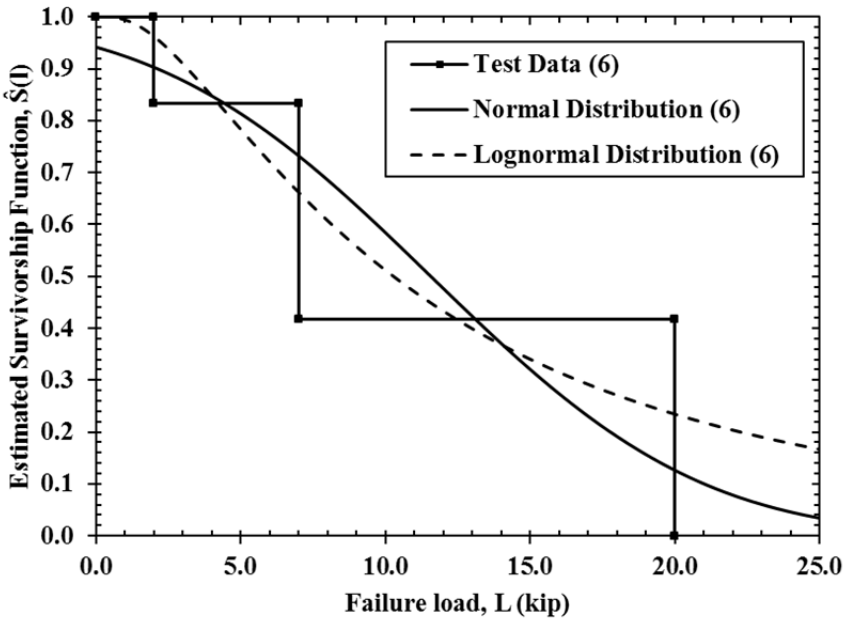

Figure 3.2: Parametric and nonparametric estimated survivorship functions of the example problem.

Table 3.2: Results of parametric analysis using SAS® for the example problem.

Distribution	Mean (μ)	Standard Deviation (σ)
Normal	11.567	7.367
Lognormal	2.333	0.919

3.3 Results and Conclusions

Parametric analysis results from SAS® are shown in Table 3.3 and for easy comparison the normally distribution μ_{PO} and σ_{PO} values are provided in Figure 3.3 and Figure 3.4 (similar trends are shown for the lognormal distribution). Noted results and explanations from these tables and figures are listed following.

- Databases or cumulative databases with tends closer to the 1:1 line (as shown in Section 2.3) showed lower mean values than those cumulative databases with tendencies toward higher bias values.
    - Results from this study tend to have high bias values (farther away from the 1:1 line) and thus when the bias values that are closer to the 1:1 line are incorporated in the data, it resulted in a decrease in the mean.
- Incorporating Database 2 with any distribution, lowered the mean and increased the standard deviation.
    - This is a result of the bias values having a tendency toward a bias value of 1.0 for Database 2. This trend was not shared by data from this study and resulted in higher uncertainty (higher standard deviation).
- Incorporating non-failed test databases (3 and 5) resulted in higher mean and standard deviation values.
    - The exact failure load is not known for non-failed testing results, and thus added uncertainty was associated with non-failed test and resulted in higher standard deviations.
- Incorporating PLAXIS prediction results (Database 4) with Database 1 showed slightly greater mean and slightly reduced standard deviation values.
    - Database 4 had slightly higher mean of the bias values when compared to Database 1, and thus will result in a slightly higher mean value.

- When more values showing similar trends were added to a database, the standard deviation tended to decrease.

In addition, it is important to compare the testing results incorporating nonparametric methods to the normal and lognormal distribution computed by the SAS® program using parametric methods. The comparisons are shown in Figure 3.5 through Figure 3.12 and discussed subsequently.

- When the estimated distribution values are to the left (lower bias values) of the test data, then the distribution was underestimating the test results and a conservative estimate was established.
- It is important to note that these figures show a trend to overestimate the tail (values close to $\hat{S}(bias)$ equal to 1.0) with the exception of when Database 2 was incorporated with another database(s) (Figure 3.6, Figure 3.8 and Figure 3.10).
- Note that as stated in Section 3.1.3.1, the PL estimate of the estimated survivorship function (nonparametric method) will not reach a value of zero when the highest bias values within a database are censored. The occurrence of this circumstance was noted in Section 2.3 and is presented in Figure 3.9, Figure 3.10 and Figure 3.11.
- For all cases, the parametric distribution showed a good correlation with the nonparametric method, but parametric distributions overestimated or underestimated nonparametric results at certain bias values.

Finally, comparison between the parametric and nonparametric methods using bias, measured resistance (kip) and measured resistance (psf) was conducted. This type of comparison was conducted on Databases 1 and Combined Databases 1 and 2 to illustrate the important conclusions. Figure 3.5, Figure 3.13 and Figure 3.15 show the comparison for Database 1, while Databases 1 and 2 are presented in Figure 3.6, Figure 3.14 and Figure 3.16.

- The nonparametric and parametric methods showed the same trend in Figure 3.5 (bias) and Figure 3.15 (measured resistance in psf), while Figure 3.13 showed different results.
    - This is the result of the normalization of the measured resistance in psf and bias values and the fact that all of the predicted values incorporated into the bias were the same value in psf. The measured resistance in kip is not normalized and thus results in a different trend for the Survival Analysis.
- All three of the results for the nonparametric and parametric analysis methods shown in Figure 3.6, Figure 3.14 and Figure 3.16 show different trends.
    - Although the measured resistance in psf and bias values are normalized, the predicted values for Database 2 are not the same value in psf and thus the results of the Survival Analysis will be different.

Table 3.3: Results of parametric analysis using SAS® for selected databases.

Database(s)	Distribution	Number of Tests Included		Mean (μ_{PO})	Standard Deviation (σ_{PO})
		Failed	Non-Failed		
1	Normal	25	0	1.622	0.289
	Lognormal	25	0	0.467	0.187
1 and 2	Normal	70	0	1.305	0.332
	Lognormal	70	0	0.236	0.243
1 and 4	Normal	28	0	1.639	0.278
	Lognormal	28	0	0.479	0.180
1, 2 and 4	Normal	73	0	1.325	0.339
	Lognormal	73	0	0.250	0.247
1 and 3	Normal	25	22	1.849	0.392
	Lognormal	25	22	0.605	0.239
1, 2 and 3	Normal	45	22	1.474	0.449
	Lognormal	45	22	0.354	0.316
1, 4 and 5	Normal	28	19	1.821	0.370
	Lognormal	28	19	0.588	0.225

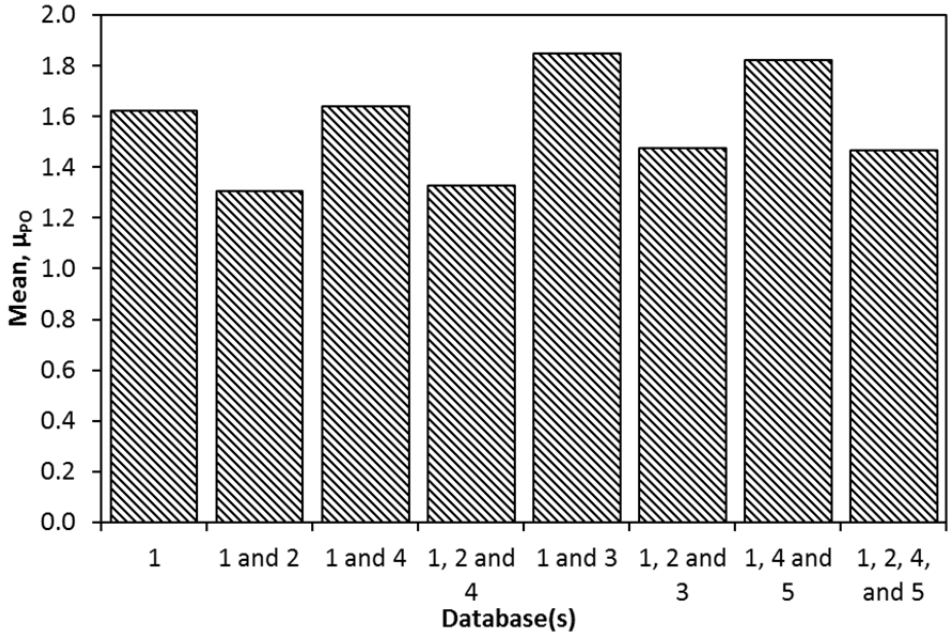

Figure 3.3: Summary of mean (normally distributed) values calculated by Survival Analysis for the Databases.

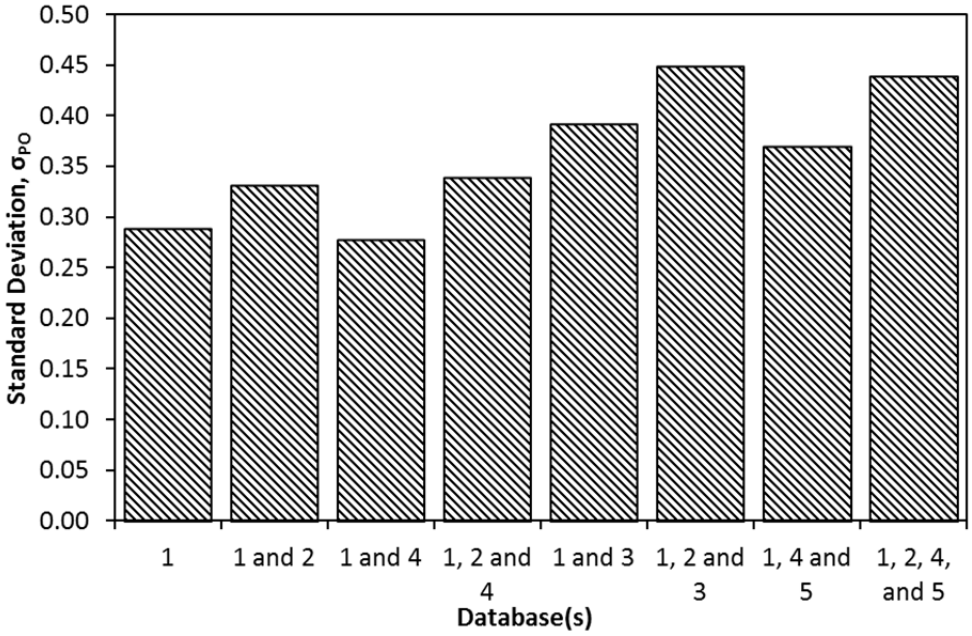

Figure 3.4: Summary of standard deviation (normally distributed) values calculated by Survival Analysis for the Databases.

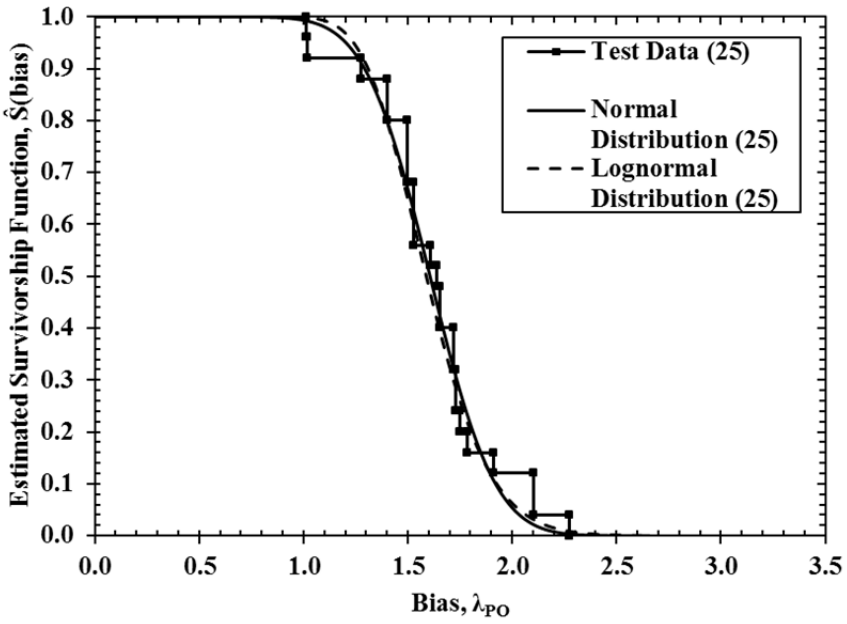

Figure 3.5: Parametric and nonparametric estimated bias survivorship functions of Database 1.

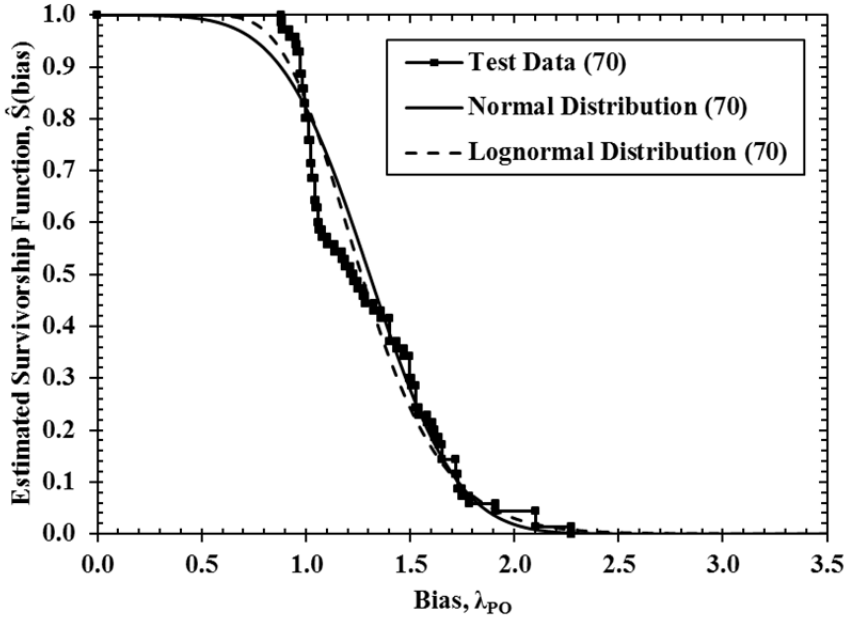

Figure 3.6: Parametric and nonparametric estimated bias survivorship functions of Databases 1 and 2.

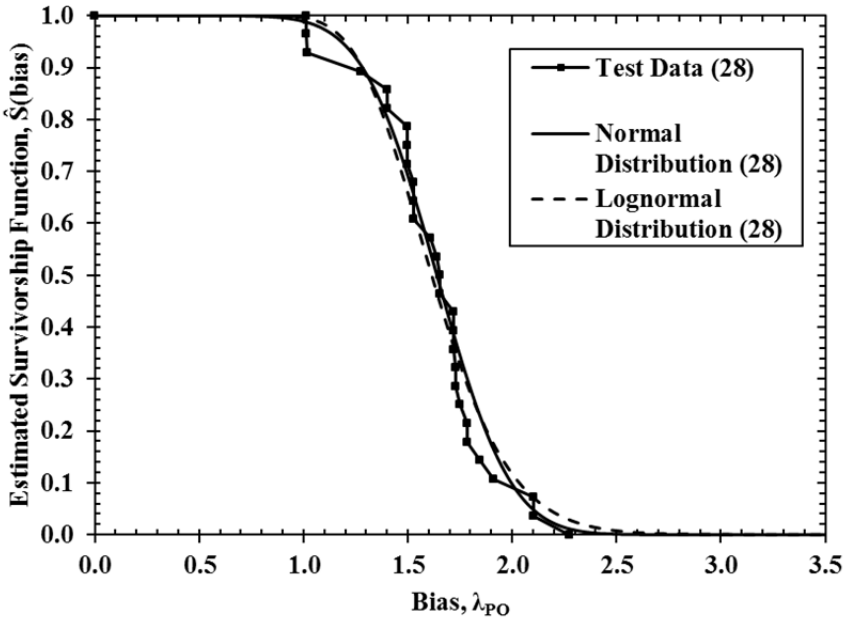

Figure 3.7: Parametric and nonparametric estimated bias survivorship functions of Databases 1 and 4.

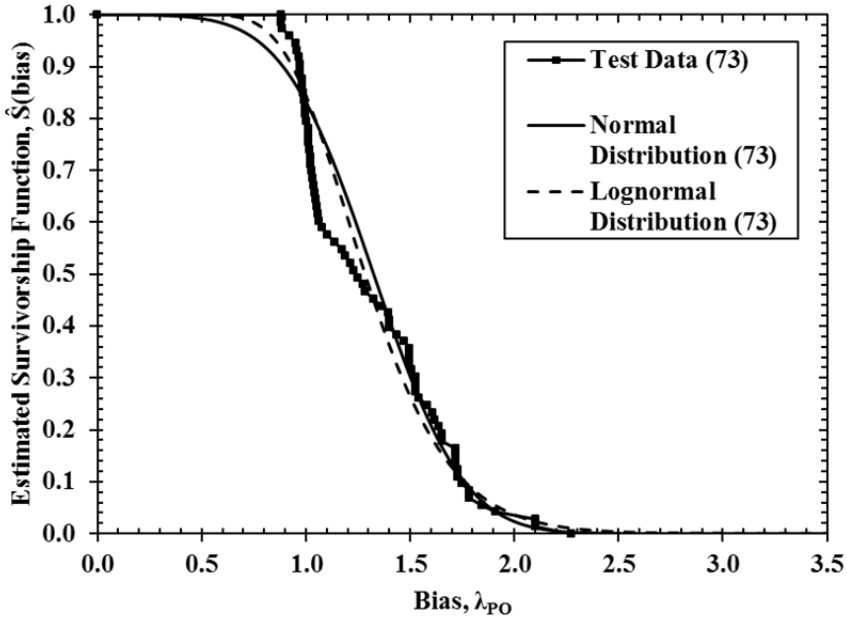

Figure 3.8: Parametric and nonparametric estimated bias survivorship functions of Databases 1, 2 and 4.

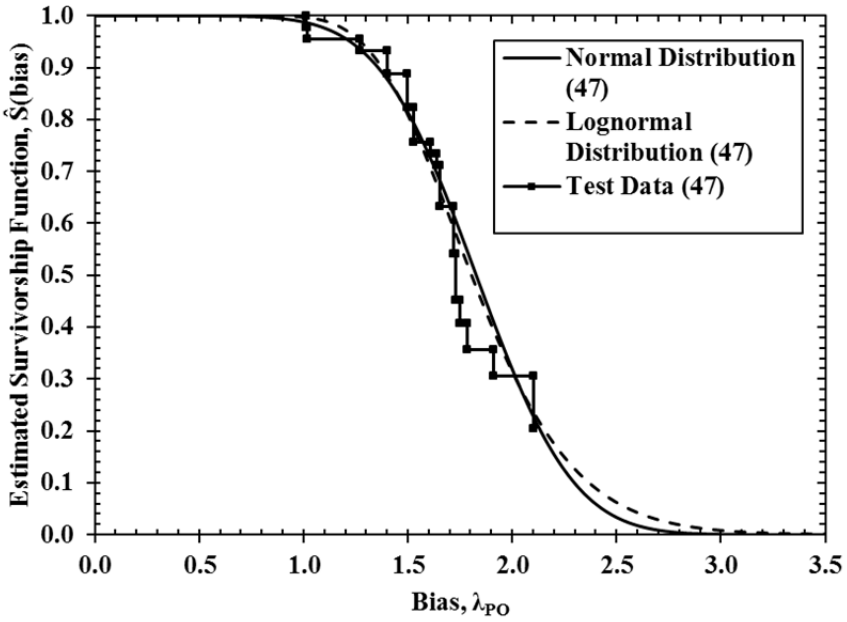

Figure 3.9: Parametric and nonparametric estimated bias survivorship functions of Databases 1 and 3.

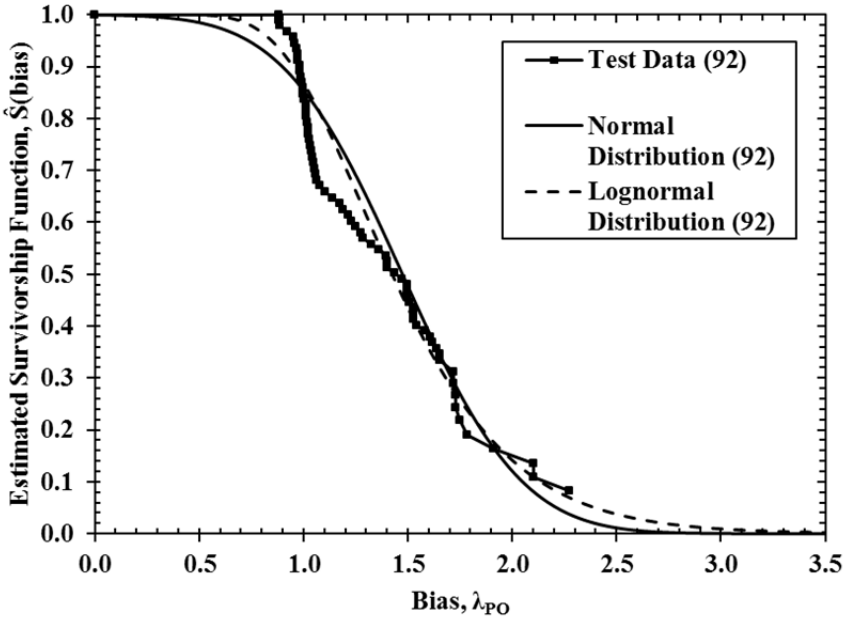

Figure 3.10: Parametric and nonparametric estimated bias survivorship functions of Databases 1, 2 and 3.

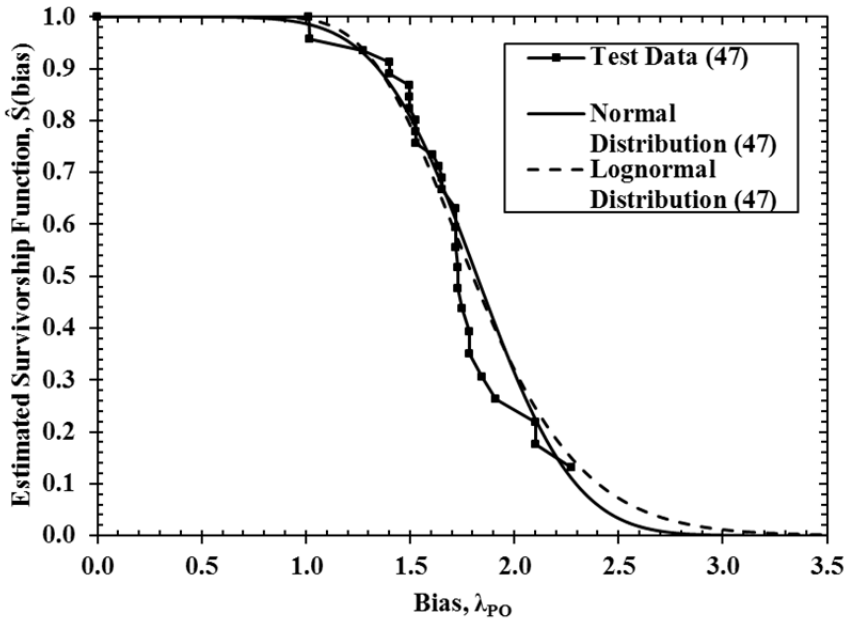

Figure 3.11: Parametric and nonparametric estimated bias survivorship functions of Databases 1, 4 and 5.

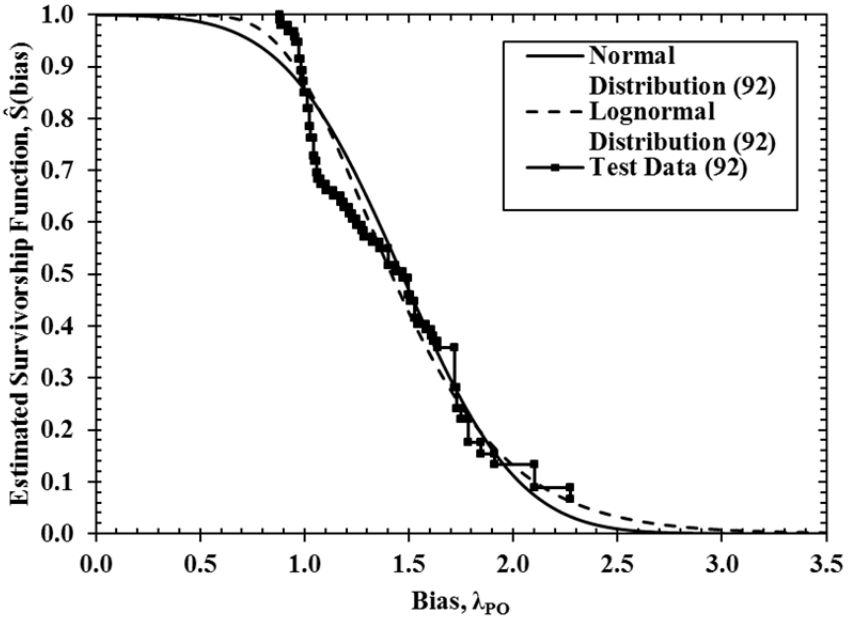

Figure 3.12: Parametric and nonparametric estimated bias survivorship functions of Databases 1, 2, 4 and 5.

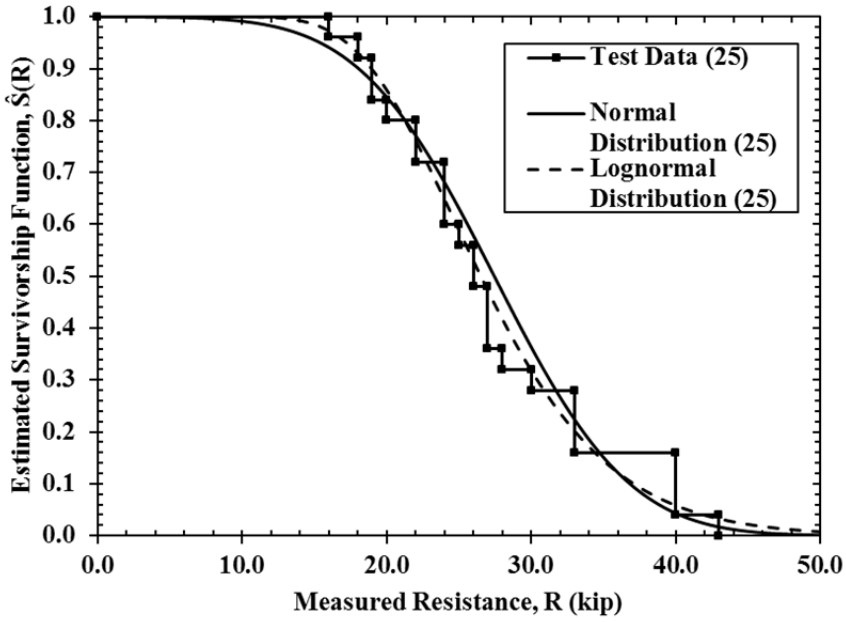

Figure 3.13: Parametric and nonparametric estimated measured resistance (kip) survivorship functions of Database 1.

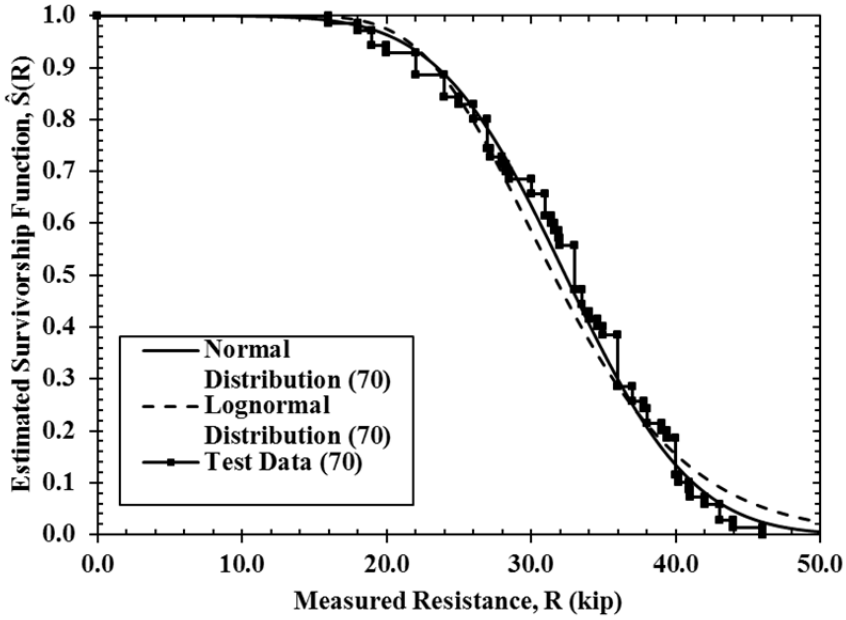

Figure 3.14: Parametric and nonparametric estimated measured resistance (kip) survivorship functions of Databases 1 and 2.

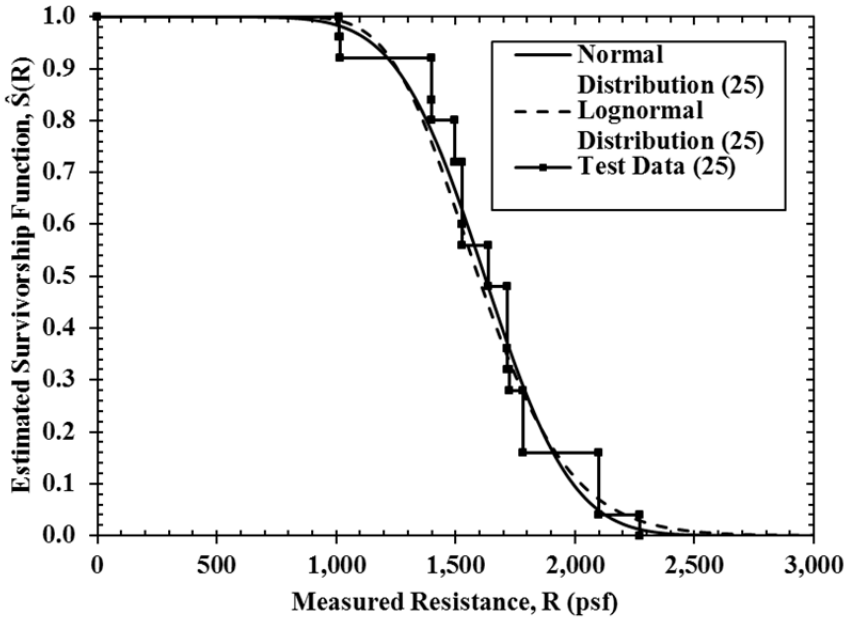

Figure 3.15: Parametric and nonparametric estimated measured resistance (psf) survivorship functions of Database 1.

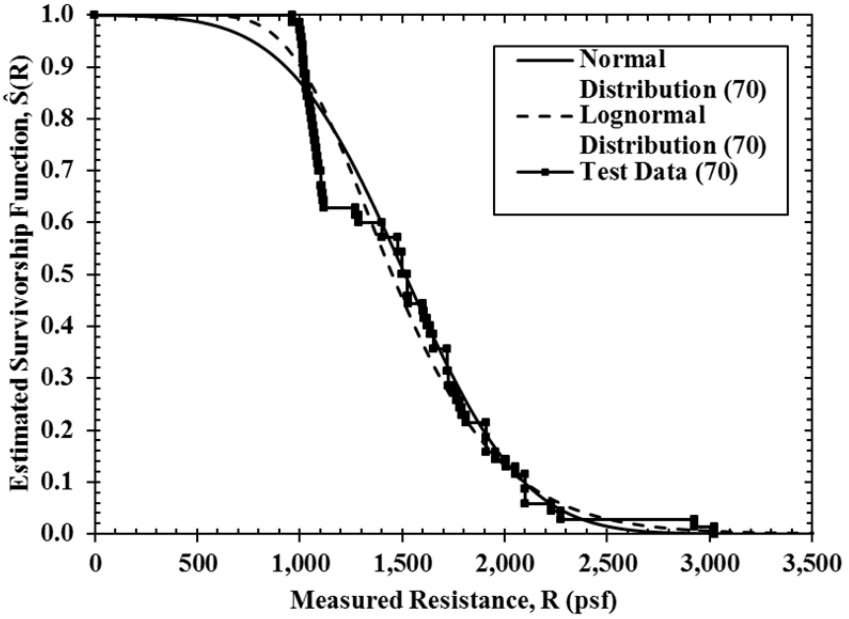

Figure 3.16: Parametric and nonparametric estimated measured resistance (psf) survivorship functions of Databases 1 and 2.

Chapter 4

PLAXIS 2D

4.1 Literature Review and Background

4.1.1 *Model*

Geometries in PLAXIS can be represented as either Plane strain or Axisymmetric as shown in Figure 4.1. Each of these geometries has their own benefits and cases where a particular model will be beneficial over the other.

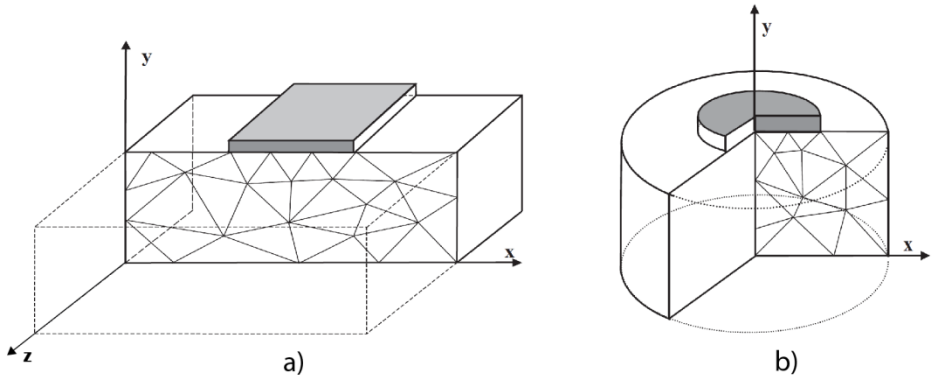

Figure 4.1: Example of layout of Plane Strain (a) and Axisymmetric (b) in PLAXIS (modified from PLAXIS, 2011).

4.1.1.1 Plane Strain Model

The Plane Strain model is shown in Figure 4.1 (a) and is useful when the loading is over a particular length in the z-direction. It is assumed that the displacements and strains in the z-direction are zero, but the normal stresses are fully accounted for (PLAXIS, 2011).

This type of model is especially useful when analyzing a specific section of a SNW and analyzing the most critical section of the SNW in PLAXIS 2D allows the entire SNW to be analyzed with the just one column of soil nails. Researchers such as Singh and Sivakumar Babu (2010) have used PLAXIS 2D with the Plane Strain model to successfully simulate SNWs, such as the section of a SNW shown in Figure 4.2.

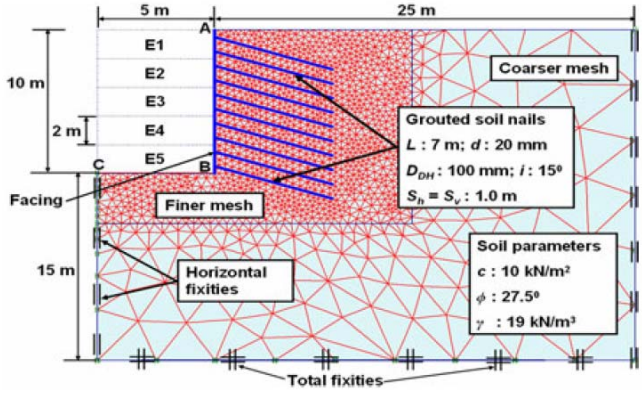

Figure 4.2: Example of the Plane Strain model in PLAXIS (Singh and Sivakumar Babu, 2010).

4.1.1.2 Axisymmetric Model

The Axisymmetric model allows for circular structures with reasonably identical radial direction deformation and stress states to be simulated. This type of model is shown in Figure 4.1 (b) and is used for circular structures with uniform cross sections and loads about the axis.

It is presented in the PLAXIS (2011) Tutorial Manual that the Axisymmetric model has been used to simulate driving a pile, and this simulation shares many of the same characteristics as the verification test of soil nails (Figure 4.3). In addition, dynamic and static soil nail pullout test simulations using the Axisymmetric model have been studied by Ann et al. (2004b). Only comparison between the simulated dynamic and static tests were conducted in the article; however, similar trends from the simulation and in-situ tests of the load and displacement curves were presented (Ann et al., 2004b).

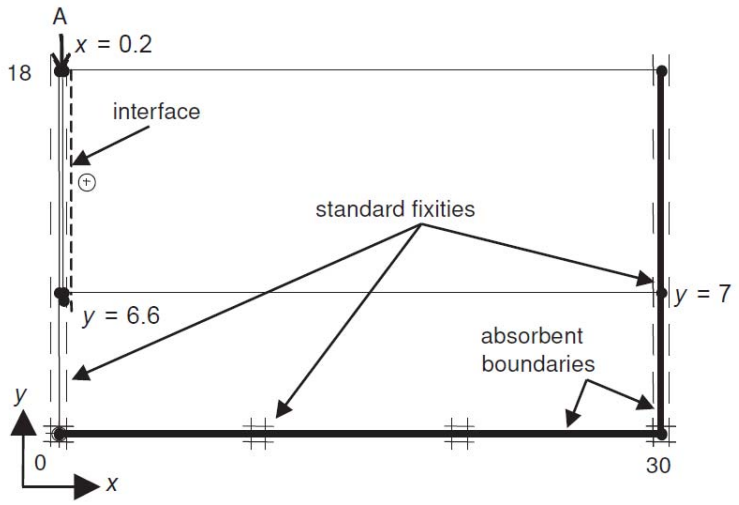

Figure 4.3: Example of the Axisymmetric model in PLAXIS (PLAXIS, 2011).

4.1.1 *Elements*

Both 6- or 15-node triangular elements can be selected to model soil or other materials; and by using these elements, displacements and stresses can be simulated. Figure 4.4 shows the 15-node triangle (a) and 6-node triangle (b), which are the only types of elements available in PLAXIS 2D (PLAXIS, 2011).

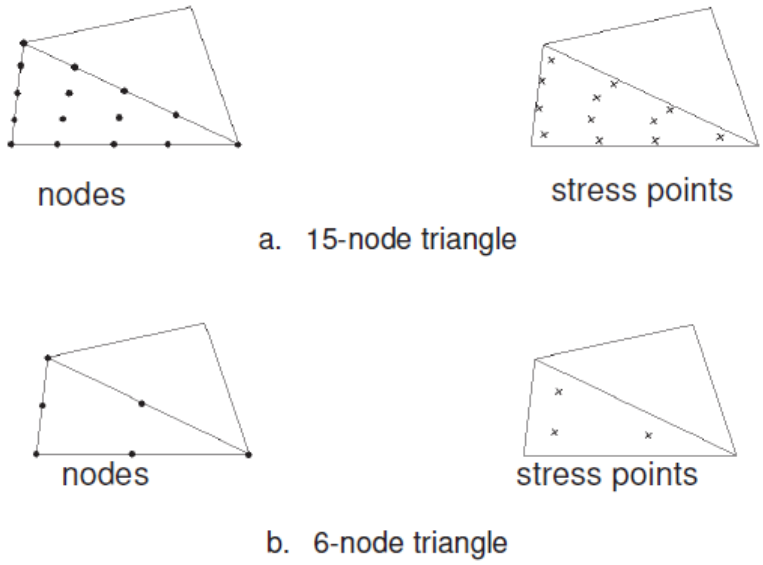

Figure 4.4: Position of nodes and stress point in elements (PLAXIS, 2011).

4.1.1.1 15-Node Element

The15-node triangular element provides a forth order interpolation for displacement and numerical integration involving twelve stress points (gauss points). It results in a high quality stress results for difficult problems, but leads to longer calculation times (PLAXIS, 2011).

4.1.1.2 6-Node Element

Numerical integrations involving three stress points and second order interpolation for displacement are provided by the 6-node triangular element. Compared to the 15-node element, the 6-node produces less precise estimates of deformation but can provide acceptable results for standard deformation analysis (PLAXIS, 2011).

4.1.2 *Gravity and Acceleration*

The Earth's normal gravity is set at 9.8 m/s^2 by default in PLAXIS, but it is possible to change this value to accommodate certain engineering applications (PLAXIS, 2011). This type of adjustment was proposed by Ann et al. (2004b), where the gravity was taken as zero to simulate soil nail tests.

4.1.3 *Geometry*

The geometry of the structure and soil must be defined at the beginning of the finite element modeling and consists of:

- points,
- clusters,
- lines,
- walls,
- plates,
- tunnel linings,
- loadings, and
- soil-structure interactions (PLAXIS, 2011).

The clusters are generated by PLAXIS, but the other geometry and structural objects must be generated by the user. Additionally, the user should define not only the initial conditions, but also the conditions present throughout various calculation phases (PLAXIS, 2011).

4.1.3.1 Geometry Line

The geometry line consists of points and lines, and allows the user to define structures and soil clusters. The geometry line is typically the first geometry parameter defined in the finite element analysis (PLAXIS, 2011).

Geometry lines can be used to define structures such as piles (PLAXIS, 2011) and soil nails (Ann et al., 2004b). If conducted correctly, defining geometry lines as structures can allow accurate estimations of deformation for the structure.

4.1.3.2 Plates and Geogrids

Plates are used to model slender structural objects within the soil. These structures typically have significant bending and normal stiffness and can simulate structures that extend into the z-direction (Plane Strain model) such as the following:

- walls,
- plates,
- soil nails,
- shells, and
- linings (PLAXIS, 2011).

Plate's behavior in PLAXIS 2D is defined by an elasto-plastic material behavior, where the elastic behavior is defined by:

- bending stiffness (EI),
- normal stiffness (EA), and
- Poisson's ratio (ν; PLAXIS, 2011).

The material behavior of plates is governed by the following three equations relating the forces and strains on the structure (PLAXIS, 2011):

$$N = EA\varepsilon \quad (25)$$

$$Q = \frac{kEA}{2(1+\nu)}\gamma^* \quad (26)$$

$$M = EI\kappa \quad (27)$$

where γ^* is the modified shear strain, k is the shear correction factor ($^5/_6$), Q is the shear force, and I is the moment of inertia. The maximum bending moment (M_P) and maximum axial force (N_P) can be defined when plasticity or elasticity are considered and shown in Figure 4.5. When Equations 25 and 26 are calculated and results are within the diamond (Figure 4.5), then elastic deformation occurs; and the boundaries of the diamond shape are where the ultimate combination of forces resulting in plastic behavior occur (PLAXIS, 2011).

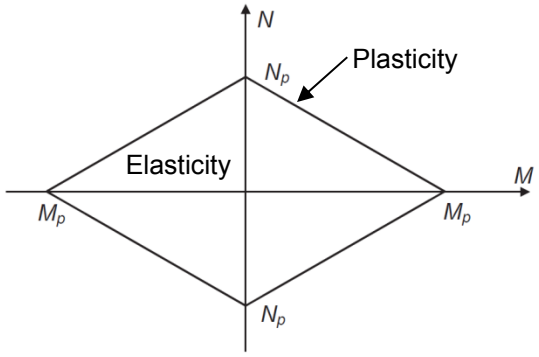

Figure 4.5: Combinations of maximum bending moment and axial force for plates (modified from PLAXIS, 2011).

The use of plates to simulate soil nails was completed by Sivakumar Babu and Singh (2009) and can account for the bending stiffness that could occur during the construction period of a SNW.

Behavior of geogrids in PLAXIS 2D are dependent on the tension stiffness (E) and the cross sectional area (A). It is important to note that geogrids can only withstand tension forces

and when elastoplastic behavior is selected, the relationship between tensile force (N) and strain can be defined as Equation 25 (PLAXIS, 2011).

A geogrid in PLAXIS can be used to simulate such structures as:

- soil nails,
- geogrids, and
- geotextiles (PLAXIS, 2011).

Sivakumar Babu and Singh (2009) showed that geogrids can be used to simulate soil nails, but this type of structures does not account for the bending stiffness to be simulated. Ignoring the bending stiffness when simulating a SNW result in substantial changes in the calculated factor of safety; however, it is common to ignore this during traditional SNW design (FHWA, 2007; Sivakumar Babu and Singh, 2009).

A small section of a row within a SNW can be seen in Figure 4.6 with the horizontal spacing between nails is S_H, but when using the Plane Strain model special considerations must be addressed. The PLAXIS 2D Plane Strain model extends into the z-direction one unit but assumes that plates and geogrids extend to infinity as shown in Figure 4.7. As a result of the differences between the field and PLAXIS model, an equivalent elastic modulus (E_{eq}) must be incorporated. This procedure also allows the E_{eq} to account for the separate elastic modulus of the bar and the grout within the soil nail.

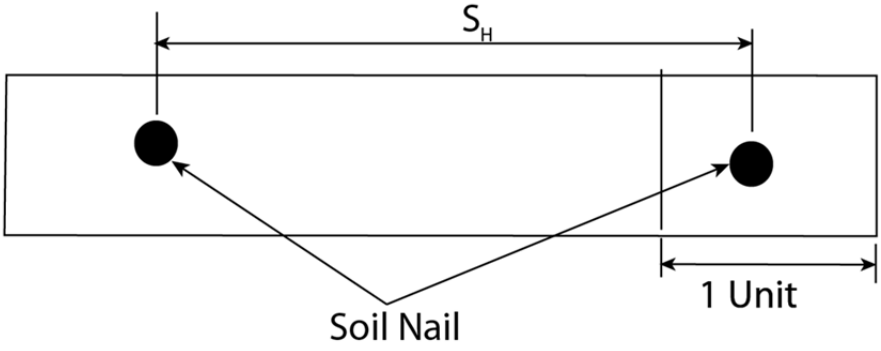

Figure 4.6: Layout of a row of soil nails within a SNW.

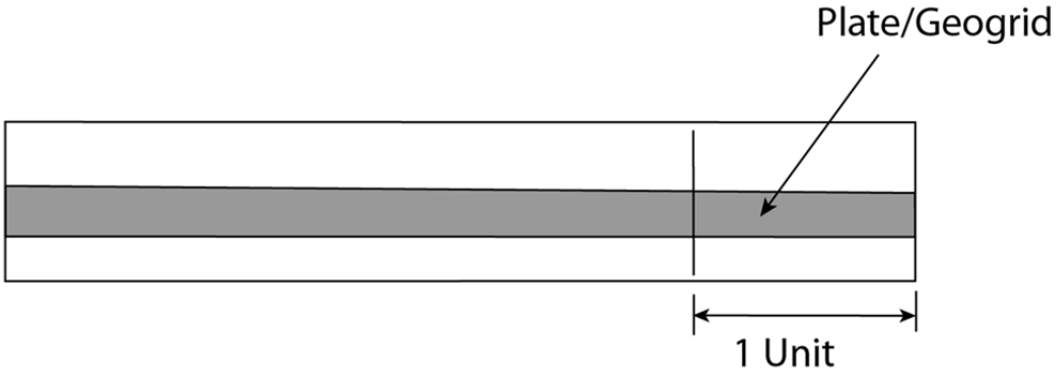

Figure 4.7: Layout of plates and geogrids in PLAXIS.

An equation defining the equivalent modulus of elasticity is (Singh and Sivakumar Babu, 2010; Sivakumar Babu and Singh, 2009):

$$E_{eq} = E_n\left(\frac{A_n}{A}\right) + E_g\left(\frac{A_g}{A}\right) \quad 28$$

where E_n is the modulus of elasticity of the bar, A_n is the cross-sectional area of the bar, A is the total area of the soil nail, E_g is the modulus of elasticity of the grout and A_g is the grouted area $(A - A_n)$. Using E_{eq} from Equation 28, the axial stiffness for plates and geogrid, and bending stiffness for plates can be calculated as:

$$EA = \frac{E_{eq}}{S_H}\left(\frac{\pi D_{DH}^2}{4}\right) \quad 29$$

$$EI = \frac{E_{eq}}{S_H}\left(\frac{\pi D_{DH}^4}{64}\right) \quad 30$$

where D_{DH} is the drill hole diameter (Singh and Sivakumar Babu, 2010; Sivakumar Babu and Singh, 2009).

4.1.4 *Interfaces*

Interfaces are usually placed at the union between the soil and structure in PLAXIS 2D and incorporate a virtual thickness used to define material properties within the region. This

virtual thickness allows for elastic deformation to be generated, and more elastic deformation can occur when the virtual thickness is larger (PLAXIS, 2011).

The roughness of the interaction between the structure and nail can be simulated by the use of a strength reduction factor (R_{inter}). This factor allows modeling of the soil strength parameters (cohesion, friction angle and dilantancy angle) to be related to the interface strength such as the wall friction and adhesion (PLAXIS, 2011).

It can be seen by Wang and Richwien (2002) that soil nails tested by pullout tests have a R_{inter} value greater than 1.0. However, PLAXIS allows a R_{inter} value of 1.0 or less and thus a value of 1.0 has been implemented by Sivakumar Babu and Singh (2009).

A rigid interface between the soil and structure is integrated when a value of 1.0 for R_{inter} is chosen; and as a result, PLAXIS does not reduce the strength of the surrounding soil. Consequently, the cohesion, friction angle and dilantancy angle for the material interacting within the interface is not changed; however, ν is altered to a value of 0.45 (PLAXIS, 2011).

4.1.4.1 Interface Elements

The interface elements and how they are connected to the soil elements are shown in Figure 4.8 and although a gap is shown for the interface elements, the formulation of the finite element considers the node pairs at identical coordinates. The node pairs can move independently and allow for deferential settlements such as slipping and gapping (PLAXIS, 2011).

When local slip is induced at the interface, the local disturbance remains local with accordance to the Newton-Cotes integration (PLAXIS, 2011; Van Langen, 1991). The rate of deformation and maximum deformation at the interface caused by the local desturbance depends on the interface properties such as the interface friction angle and cohesion (Van Langen, 1991).

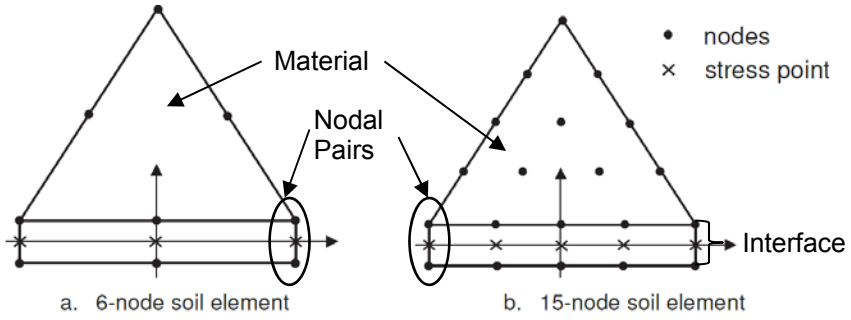

Figure 4.8: Distribution of nodes and stress points in interface elements and their connection to soil elements (modified from PLAXIS, 2011).

4.1.4.2 Interfaces Around Corner Points

When corners in stiff structures are present, ending the interface at the tips of the structure (Figure 4.9) may result in erroneously high peaks in the strains and stresses. This problem can be resolved by extending the interfaces beyond that of the corners, as shown in Figure 4.10 (PLAXIS, 2011). The concept of placing interfaces beyond the corners or ends of a structure can be extended to plates and geogrids.

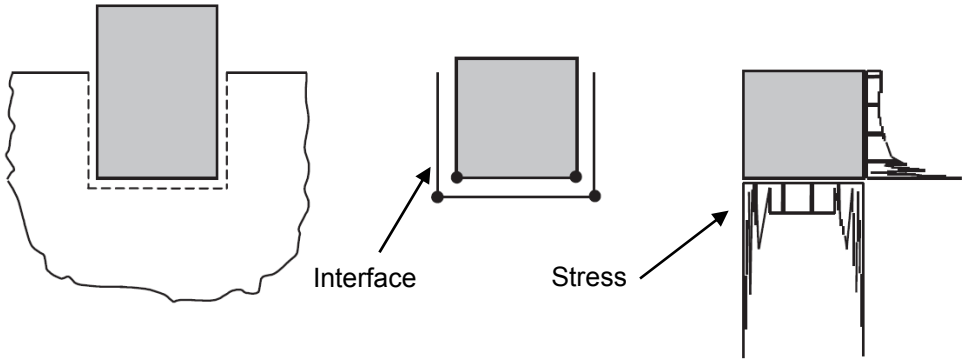

Figure 4.9: Corner points causing poor quality stress results (modified from PLAXIS, 2011).

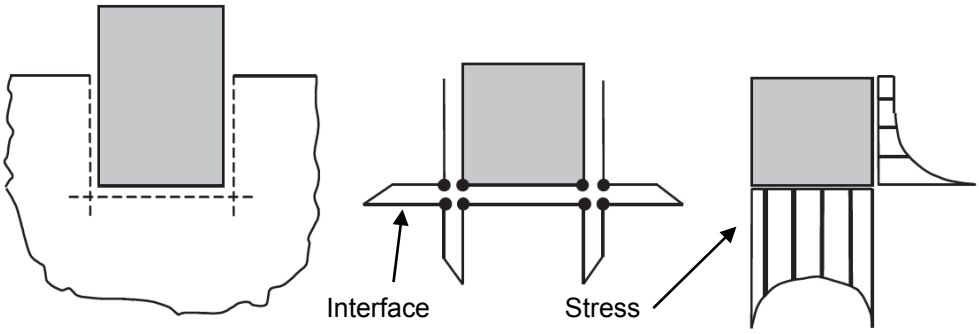

Figure 4.10: Corner points with improved stress results (modified from PLAXIS, 2011).

4.1.5 *Boundary Conditions*

The position of the boundary of the model in relation to the structure may affect the results of the finite element calculation. Thus, it is important to place the boundaries of the model at a sufficient distance from the boundary conditions as to not affect the results (Ann et al., 2004b; PLAXIS, 2011; Sivakumar Babu and Singh, 2010; and Singh and Sivakumar Babu, 2009).

4.1.6 *Fixities*

Fixities are locations in which displacement is equal to zero and in PLAXIS 2D include the following options:

- total fixities as shown in Figure 4.11 (a),
- vertical fixities as seen in Figure 4.11 (b), and
- horizontal fixity, as presented in Figure 4.11 (c; PLAXIS, 2011).

Total fixities are locations where displacements are equal to zero in both the x- and y-directions; where vertical and horizontal fixities have displacements equal to zero in the y- and x-direction, respectively.

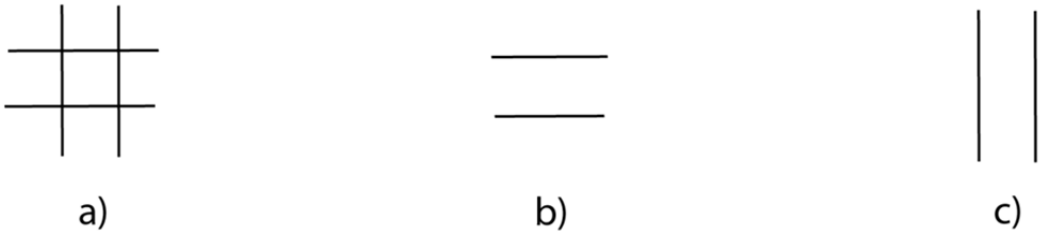

Figure 4.11: Icons in PLAXIS 2D indicating total (a), vertical (b) and horizontal fixities (c).

4.1.7 *Loads*

A load(s) can be applied to the system by either the addition of distributed or point load(s). Each of these types of loads can be in the x- and/or y-direction with a maximum of two load systems for each type of load in the simulation (PLAXIS, 2011).

4.1.7.1 Distributed Loads

In PLAXIS 2D, applied distributed loads resemble line loads; however, their units are force per area. As indicated in Figure 4.12, distributed loads are shown in only the x- and y-directions but extend one unit into the z-direction (PLAXIS, 2011). Not only can distributed loads apply a load on a structure, but can be used to incorporate a soil overburden pressure onto a structure when the acceleration of gravity is set to zero (Ann et al., 2004b).

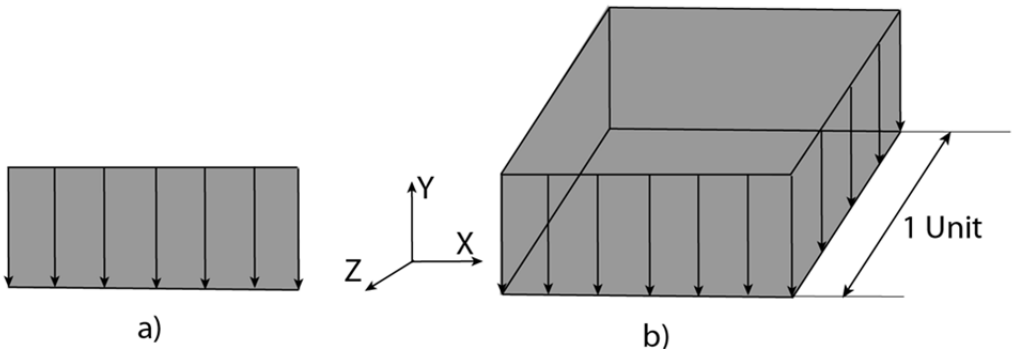

Figure 4.12: Distributed load in shown (a) and modeled (b) in PLAXIS 2D.

4.1.7.2 Point Loads

Applying a point load may change depending on which model (Plane Strain or Axisymmetric) or location is chosen. A point load applied at the axis ($x = 0$) in the Axisymmetric model must be calculated as follows:

$$Input\ Load = \frac{Actual\ Load}{2\pi} \quad (31)$$

Although a point load is shown in PLAXIS, it is applied to a circle section of one radian (Figure 4.13). If however, a point load is applied to any other location in the Axisymmetric model or to any point in the Plane Strain model, the point load is actually a line load for one unit in the z-direction (Figure 4.14; PLAXIS, 2011).

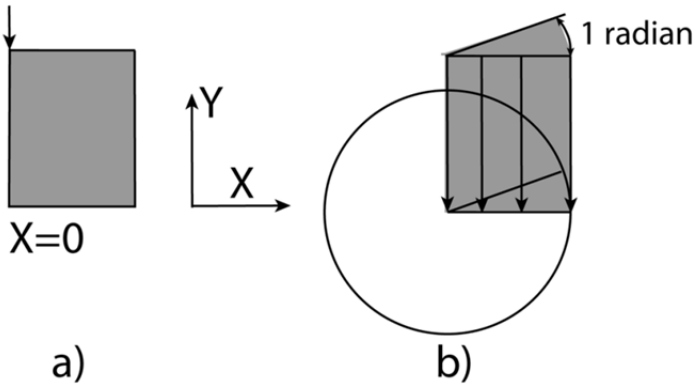

Figure 4.13: Axisymmetric point load at ($x = 0$) shown (a) and modeled (b) in PLAXIS 2D.

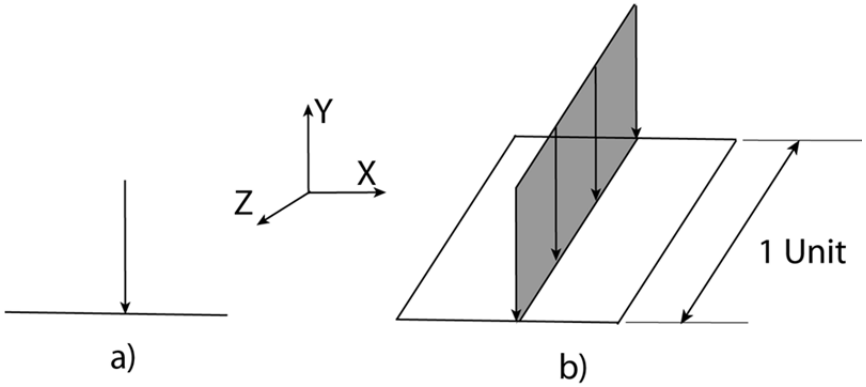

Figure 4.14: Point load shown (a) and modeled (b) in PLAXIS 2D.

4.1.8 *Mesh Generation*

To perform finite element calculations, the input geometry is divided into finite elements and the composition of these elements is referred to as a mesh. The finite element mesh can be generated automatically by PLAXIS 2D; however, these generated meshes may not provide sufficient accuracy to produce acceptable results. Consequently, it is recommended by Ann et al. (2004b); PLAXIS (2011); Sivakumar Babu and Singh (2010); and Singh and Sivakumar Babu (2009) that the mesh should be refined surrounding critical structures such as soil nails. A refined mesh may cause computational times to increase but the accuracy of results is improved (Sivakumar Babu and Singh, 2009). PLAXIS (2011) recommends that the preliminary analysis is conducted with a relatively coarse mesh and then refinement is completed once an acceptable model is established.

4.1.9 *Material Models*

PLAXIS incorporates many models and levels of sophistication that can be used to represent soil, rock and structures. The four models found in literature to simulate soil nails and the surrounding soils are as follows:

- Linear Elastic (LE) model,
- Mohr-Coulomb (MC) model,
- Hardening Soil (HS) model, and
- Hardening Soil with small-strain stiffness (HSsmall) model (Ann et al., 2004a; Ann et al., 2004b; Lengkeek and Peters; Singh and Sivakumar Babu, 2010; Sivakumar Babu and Singh, 2009; Zhang et al., 1999).

4.1.9.1 Linear Elastic (LE) Model

The Linear Elastic model is represented by Hooke's law of isotropic linear elasticity and is primarily used for stiff structures such as concrete in soils, because it is too limited to simulate soil behavior. This type of model allows for the material stiffness to be defined in terms of the Young's modulus (E) and ν (PLAXIS, 2011).

4.1.9.2 Mohr-Coulomb (MC) model

The Mohr-Coulomb model follows the linear elastic perfectly plastic model that is shown in Figure 4.15. This principle follows that the material will behave elastically (no permanent strain (ε)) until the applied stress (σ) is large enough to cause the material to behave plastically (permanent strains). Although concepts of the linear elastic perfectly plastic model with Mohr-Coulomb failure criterion can be discussed in depth, it is enough to understand that the elastic and plastic behavior is based upon a few critical input parameters. The elastic behavior of the material obeys Hooke's law for isotropic linear elasticity based on input parameters, E and ν, while the plastic behavior depends on the cohesion (c), internal friction angle (φ) and dilantancy angle (Ψ; PLAXIS, 2011).

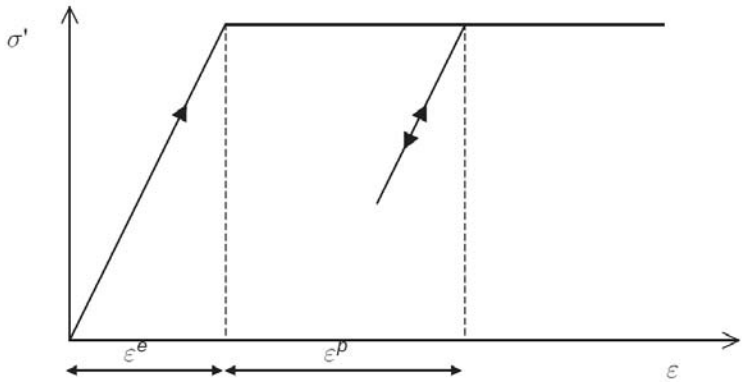

Figure 4.15: Idea of the linear elastic perfectly plastic model (PLAXIS, 2011).

4.1.9.2.1 Young's Modulus

The Young's modulus is used as a stiffness modulus in the Mohr-Coulomb model and is usually defined as either the initial slope of the stress-strain curve (E_0) or the secant modulus at 50 percent strength (E_{50}) as shown in Figure 4.16. It is recommended by PLAXIS (2011) that E_0 can be used for materials with a large linear elastic range and E_{50} used for loading situations. When unloading is involved, it would be more appropriate to use the unload-reload modulus (E_{ur}) and is typically taken as three times E_{50} (PLAXIS, 2011).

The values for E_{50} and E_{ur} have a tendency to increase as the confining pressure increases, and thus it is important to incorporate Triaxial Test results with similar confining pressures as the model.

Typical values for E_0 and E_{50} can be found in literature for various soils and range from 700 to 30,000 kPa (14,700 to 630,000 psf; Ann et al., 2004a; Lengkeek and Peters; Singh and Sivakumar Babu, 2010; Sivakumar Babu and Singh, 2009; Zhang et al., 1999).

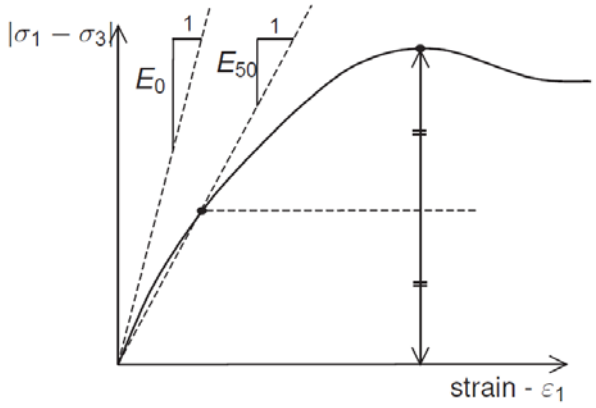

Figure 4.16: Definition of E_0 and E_{50} for standard Drained Triaxial Test results (PLAXIS, 2011).

4.1.9.2.2 Poisson's Ratio, Cohesion, Friction Angle and Dilantancy Angle

Poisson's ratios can be defined as the ratio of change of length to the initial length when a load is applied. For clay soils, typical values are taken as approximately 0.3 (Ann et al., 2004a; PLAXIS, 2011; Singh and Sivakumar Babu, 2010; Sivakumar Babu and Singh, 2009; Zhang et al., 1999).

The cohesion and friction angle of the soil can be taken from Direct Shear or Triaxial Tests. These two parameters should be well known to anyone with a Geotechnical engineering background and will not be discussed further.

The dilantancy angle is the contact angle of the soil particles from horizontal (Figure 4.17) and tend to be equal to zero for most clays (Bolten, 1986; PLAXIS, 2011).

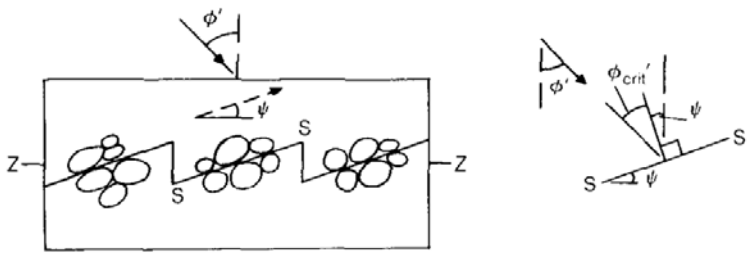

Figure 4.17: The saw blades model of dilantancy (Bolten, 1986).

4.1.9.3 Hardening Soil (HS) Model

The Hardening Soil model incorporates decreasing stiffness and the development of irreversible plastic strains as the material is loaded. The underlining concept in the HS model is that the relationship between the axial strain and deviator stress follows the hyperbolic model purposed by Duncan and Chang (1970). The basic concept behind the HS model can be seen in Figure 4.18 and differs from the hyperbolic model by incorporating the following:

- theory of plasticity rather than elasticity,
- includes soil dilantancy, and
- introduces a yield cap (PLAXIS, 2011).

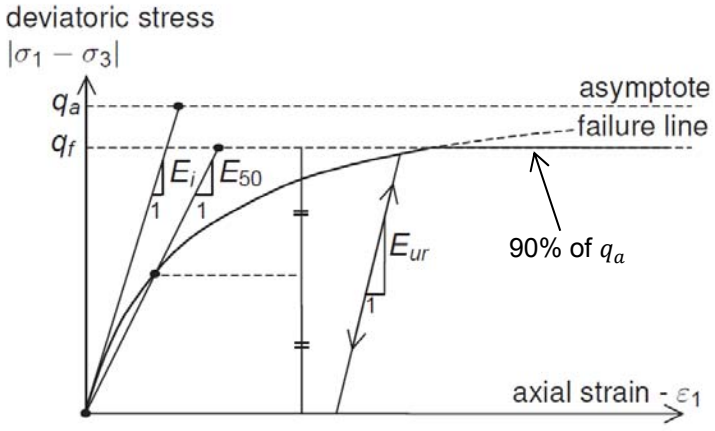

Figure 4.18: Hyperbolic stress-strain relation in primary loading for a standard Drained Triaxial Test (modified from PLAXIS, 2011).

In addition to the cohesion, friction angle and dilantancy angle parameters defined in the Mohr-Coulomb model, the Hardening Soil model requires the following:

- stress dependent stiffness according to the power law (m),
- plastic straining due to primary deviatoric loading (E_{50}^{ref}),
- plastic straining due to primary compression (E_{oed}^{ref}), and
- elastic unloading and reloading (E_{ur}^{ref}; PLAXIS, 2011).

Many of these parameters are presented in Figure 4.18 and can be estimated from Triaxial Tests.

4.1.9.3.1 Stiffness Moduli E_{50}^{ref}, E_{oef}^{ref} and E_{ur}^{ref} and power m

The value for E_{50}^{ref} can be approximated by taking the tangent of the stress-strain curve at a halfway point between the x-axis and 90 percent of the maximum deviator stress (q_a; Figure 4.18). E_{oed}^{ref} can usually be taken as the same value as E_{50}^{ref}, and E_{ur}^{ref} is typically considered as three times E_{50}^{ref}. The m value denotes the amount of stress dependency that the material possesses and can be taken as 1.0 for soft clays but has been seen to vary between 0.5 and 1.0. As a result of the modulus of elasticity from the Mohr-Coulomb model taken as E_{50}, E_{oed}^{ref} can be seen to be very similar to those stated in Section 4.1.9.2.2 (Ann et al., 2004a; PLAXIS, 2011; Singh and Sivakumar Babu, 2010; Sivakumar Babu and Singh, 2009; Zhang et al., 1999).

4.1.9.4 Hardening Soil with Small-Strain Stiffness (HSsmall) Model

The Hardening Soil with small-strain stiffness model is very similar to the HS model but incorporates truly elastic behavior for the material for small strains (PLAXIS, 2011). This type of model was not incorporated in this study and thus will not be explained further.

4.1.10 *Drainage Type*

PLAXIS offers a choice of different drainage model such as drained and various types of undrained behavior. It has been seen in a similar study conducted by Ann et al. (2004a), that the soil is taken as drained and allows the model to exclude the calculation of excess pore pressures while providing reasonable estimates (PLAXIS, 2011).

4.1.11 *Types of Analysis*

PLAXIS provides a variety of types of analysis including:

- plastic,
- plastic drained,
- consolidation (EPP and TPP),
- factor of safety, and
- updated mesh (PLAXIS, 2011).

Although a variety of analysis types are available, plastic analysis with updated mesh was selected for this study and will be discussed further. Plastic analysis with or without updated mesh have provided accurate results for simulation of soil nails (Ann et al., 2004a; Singh and Sivakumar Babu, 2010; Sivakumar Babu and Singh, 2009; Zhang et al., 1999).

4.1.11.1 Plastic Analysis

Plastic analysis is conducted for analysis of elastic-plastic deformation with undrained behavior. The deformation is in accordance to the small deformation theory and for the material models used in this study, does not allow the accommodation of time effects (PLAXIS, 2011).

4.1.11.2 Updated Mesh Analysis

This updated mesh analysis can be incorporated into the plastic, plastic drained, consolidated and factor of safety analysis and is typically utilized when large deformations are expected. As the name implies, updated mesh analysis reestablishes the mesh at the beginning of each calculation phase. According to Sivakumar Babu and Singh (2009), the updated mesh analysis results in a marginal influence on a SNW analysis, but results in greater computation time.

4.2 Analysis Procedure

The procedure to model verification tests in PLAXIS 2D involved a five step process that varied depending on if the Plane Strain or Axisymmetric models were utilized. The

subsequent procedure successfully allowed PLAXIS 2D to model failed and non-failed test results.

4.2.1 *Step 1*

This step involved defining the project properties and model that will be used; and the selected properties and model are as follows:

- Plane Strain or Axisymmetric model,
- the 15-node element was used, as it provided the most accurate results for deformation analysis, and
- geometry dimensions of the simulation were selected such that there was enough space for the boundaries of the model to be within the defined geometry.

4.2.2 *Step 2*

The second step involved defining the geometry and boundary conditions (fixities). The geometry and boundary conditions varied depending on if the Plane Strain or Axisymmetric model were chosen for the analysis and discussed subsequently.

4.2.2.1 Plane Strain Analysis Method

The Plane Strain model allowed for many options to model the soil nail (LE, geogrid and plate) and allowed for the inclination angle of the soil nail from horizontal to be modeled. Noted qualities that were incorporated in the Plane Strain model geometry are defined next and shown in Figure 4.19.

- Horizontal fixities were applied to both vertical boundaries of the soil and total fixities applied to the bottom boundary. The left boundary simulated the facing of the SNW, while all boundaries prevented erroneous soil failure at those locations.
- Geogrid, plate, or LE material models (simulating the soil nail) were placed at a depth corresponding to the depth of the verification test in the field. These material models were also placed at a three foot distance from the left boundary to simulate the

unbounded length, and a sufficient distance from the right and bottom boundaries to prevent boundary interference (Sections 4.1.5 and 4.1.6).

- Interface was extended beyond the edges of the material to prevent stress calculation problems as stated in Section 4.1.4.2 and 1.0 was selected for R_{inter} as recommended by researchers (Section 4.1.4).
- A point load was applied to the axis of the simulated soil nail (Section 4.1.7.2).

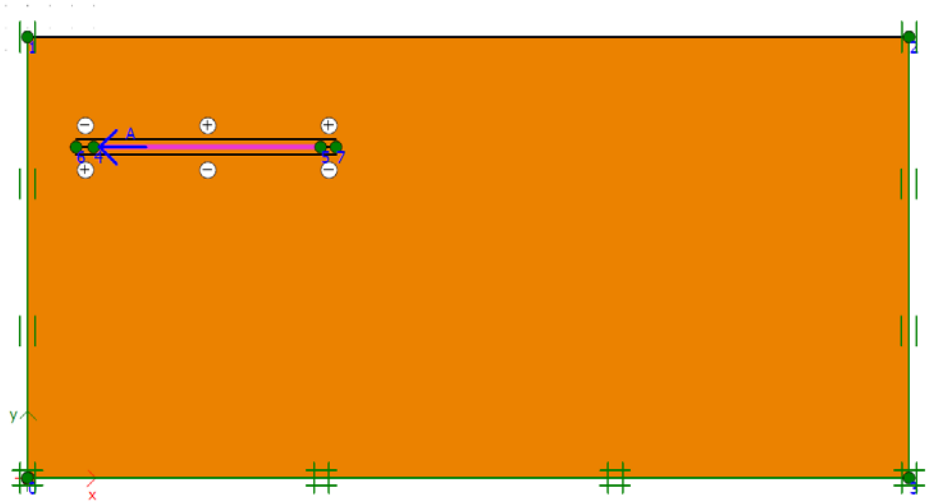

Figure 4.19: Example of Plane Strain model to simulate a soil nail verification test (geogrid).

4.2.2.2 Axisymmetric Analysis Method

This model only allowed the soil nail to be analyzed using the LE model and did not allow the inclination to be incorporated. However, the Axisymmetric model lends itself well to modeling a verification tests shown in Figure 4.20. Noted qualities of simulating a verification test in PLAXIS 2D using the Axisymmetric model are stated subsequently and are very similar to the study conducted by Ann et al. (2004b).

- The soil nail was modeled as a LE material.
- The clay in-front of the soil nail was removed to simulate the unbounded length.
- The interface is extended beyond the soil nail to avoid stress calculation complications.
- The R_{inter} values was taken as 1.0 as recommended in Section 4.1.4.

- Vertical fixities were applied to the top and bottom boundaries of the model while horizontal boundaries were applied to left boundary and to where the soil was removed.
    - These fixities were placed to prevent erroneous failures of the modeled soil.
- A horizontal distributed load is applied to the right side of the model and allows simulation of the soil overburden pressure (Section 4.1.7.1). No fixities were applied to this side so the distributed load could be applied to the soil nail.
- A point load is applied along the axis of the simulated soil nail (at $x = 0$) and the actual load was adjusted with Equation 31 (Section 4.1.7.2).

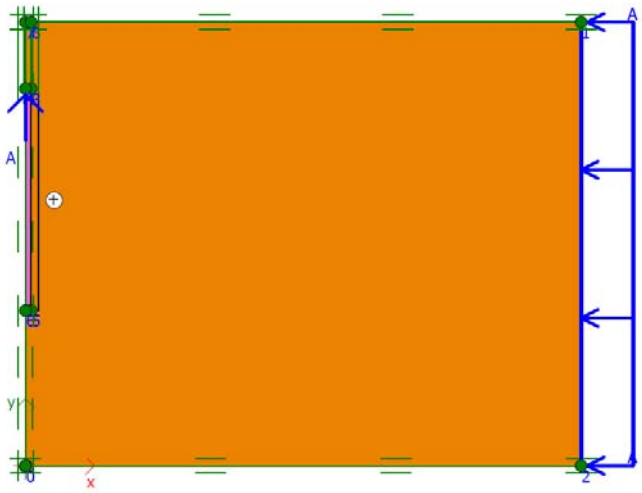

Figure 4.20: Example of Axisymmetric model to simulate a soil nail verification test.

4.2.3 *Step 3*

This step involved defining the material models that will simulate the in-situ soil nail and surrounding soil. As stated earlier, the LE model was used to approximate the soil nail in both the Axisymmetric and Plane Strain models; and geogrid and plate allowed simulation of the soil nail for only the Plane Strain model. These input parameters for the soil nail models were in accordance with Sections 4.1.3.2 (geogrids and plates) and 4.1.9.1 (LE model). The surrounding soil was either simulated as a MC or HS model, and allowed for different types of

verification testing results to be approximated. The LE, MC and HS material models were reviewed in Section 4.1.9.

4.2.4 *Step 4*

The mesh was generated in this step. Although it is known that finer meshes result in longer computation time (Section 4.1.8), the global coarseness was set at “very fine” and refinement was conducted about the soil nail (Figure 4.21, PLAXIS, 2011).

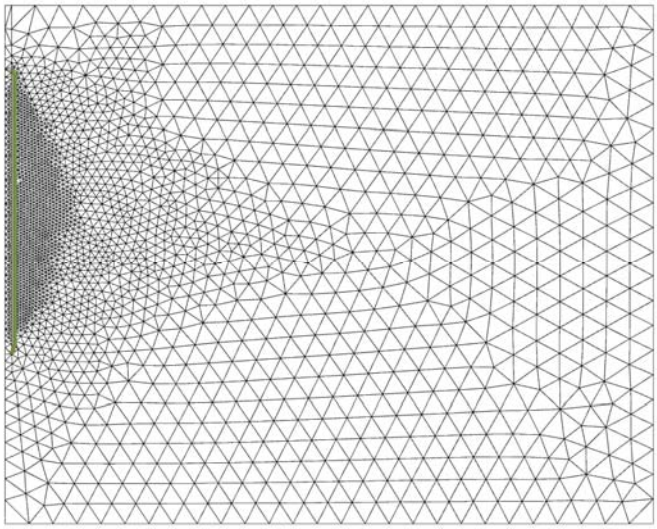

Figure 4.21: Example of the generated mesh for the Axisymmetric model.

4.2.5 *Step 5*

The final step in each model for the PLAXIS analysis involved the calculation phase. Plastic calculation with updated mesh was selected as it allowed for large deformations to be analyzed (Sections 4.1.11.1 and 4.1.11.2). It should also be noted that to allow the distributed load in the Axisymmetric method to simulate the overburden soil pressure, the gravity was set as zero and that time was not a factor in the calculation phase (Sections 4.1.2 and 4.1.11.1). Each applied load during the verification tests were considered as one calculation phase and allowed the deformation as a result of that load to be estimated.

4.2.6 *Models Tested to Simulate a Verification Test*

Various models were tested to establish which model would provide quality results for all of the PLAXIS 2D fittings to verification test data. Each of these models were conducted with the MC and HS material models. As the Axisymmetric model lend itself to modeling a verification tests, soil properties were established with the Axisymmetric model to fit the test results for each soil model (MC or HS) and then comparison between models was simulated. The models attempted include the following:

- [1]: Axisymmetric model,
- [2]: Plane Strain with the soil nail modeled by geogrid (horizontal orientation),
- [3]: Model [2] but with geogrid at an orientation of 15 degrees below horizontal,
- [4]: Model [2] but with half of the verification test load applied to the PLAXIS 2D model,
- [5]: Plane Strain model with a plate (horizontal orientation) representing the soil nail,
- [6]: Model [5] with the plate at an orientation of 15 degrees below horizontal,
- [7]: Model [5] but with half of the verification test load applied to the PLAXIS 2D model,
- [8]: Plane Strain with LE model representing the soil nail (horizontal orientation), and
- [9]: Model [8] but with half of the verification test load applied to the PLAXIS 2D model.

4.2.6.1 Results of Tested Models

General results and conclusions of testing various models for comparison to the testing curve are stated subsequently.

- The Axisymmetric model [1] showed the greatest correlation with the test curve because the material properties were adjusted to fit the test curve. As a result, this model was used to conduct the PLAXIS fitting to field test curves.
- Models with geogrid acting as the soil nail ([2] and [3]) resulted in much larger deformations than field testing results (Figure 4.22 and Figure 4.23). For these models to resemble the test curve, unrealistically high soil parameters were required in PLAXIS 2D. To achieve results close to what was shown in the verification tests (with

reasonable soil parameters), the applied load at each load increment was reduced by half (model [4]).

    - Differences in results between field tests and PLAXIS 2D were likely a result of inconsistencies between the field tests and the Plane Strain model such as how the Plane Strain modeled the load and soil nail in the z-direction.

- A plate acting as a soil nail in PLAXIS 2D ([5], [6] and [7]) resulted in very similar trends as models [2], [3] and [4] (Figure 4.24 and Figure 4.25). It is important to note that inclining the plate or geogrid resulted in greater calculated deformations and the discrepancy increased with the increase in load.
- Similar trends were found to the plate and geogrid model when the soil nail was modeled as a LE material ([8] and [9]). When the soil nail is modeled by LE material and the soil is modeled by MC, the results showed very similar trends to the previous models. However, very similar trends to the Axisymmetric model were found when the soil was modeled by the HS model and the load was equal to half of the applied load.

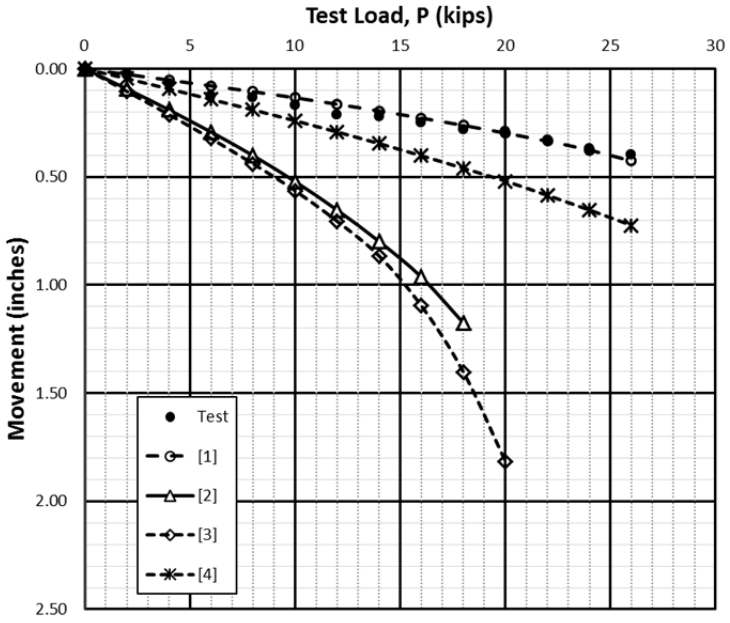

Figure 4.22: Comparison of PLAXIS 2D (MC) verification test models [1], [2], [3] and [4] (geogrid).

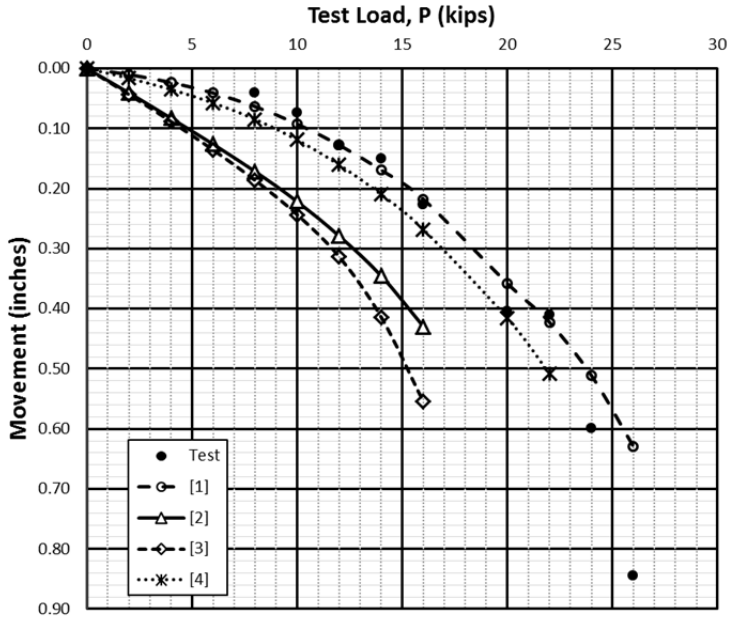

Figure 4.23: Comparison of PLAXIS 2D (HS) verification test models [1], [2], [3] and [4] (Geogrid).

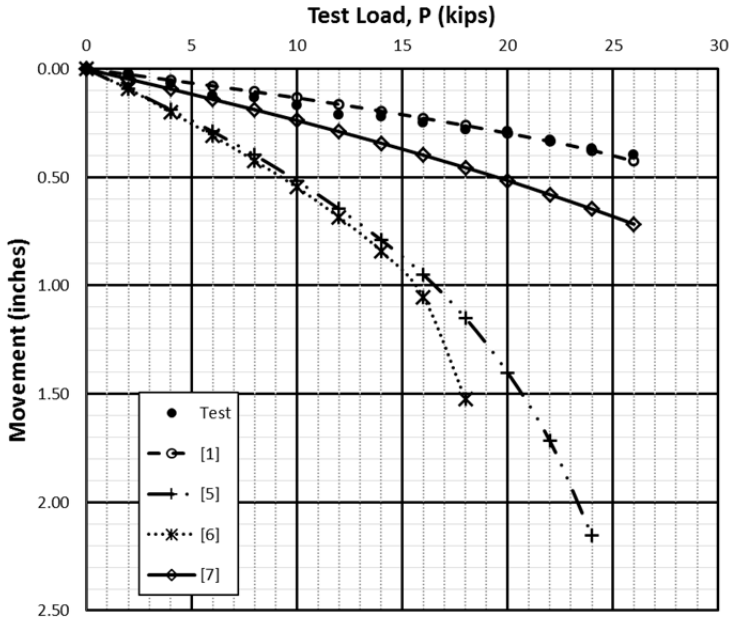

Figure 4.24: Comparison of PLAXIS 2D (MC) verification test models [1], [5], [6] and [7] (plate).

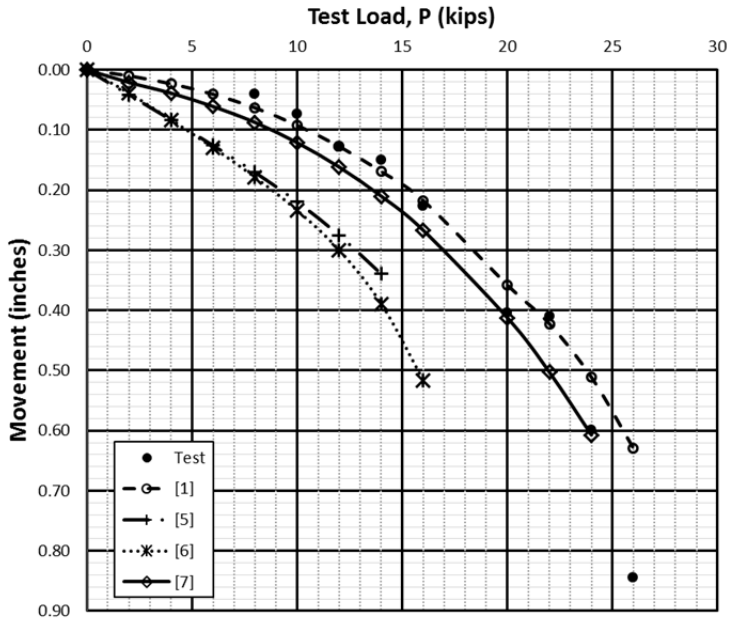

Figure 4.25: Comparison of PLAXIS 2D (HS) verification test models [1], [5], [6] and [7] (Plate).

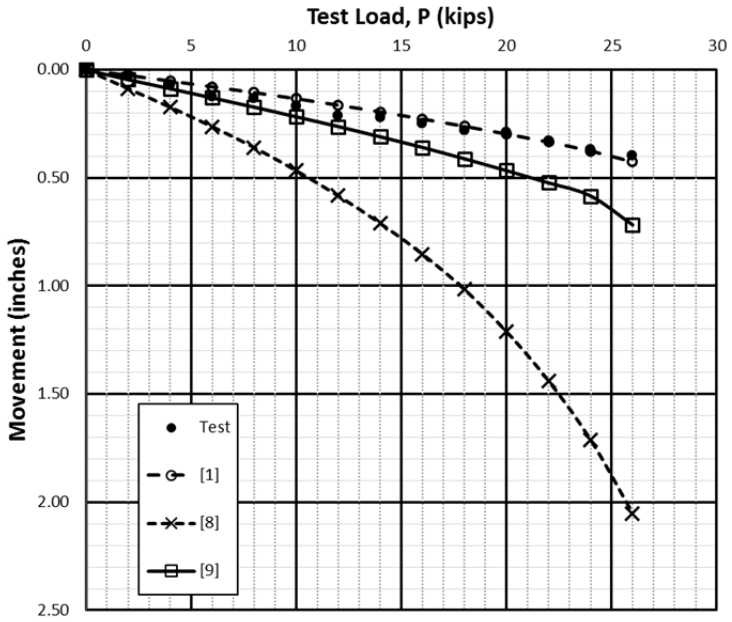

Figure 4.26: Comparison of PLAXIS 2D (MC) verification test models [1], [8] and [9] (LE model).

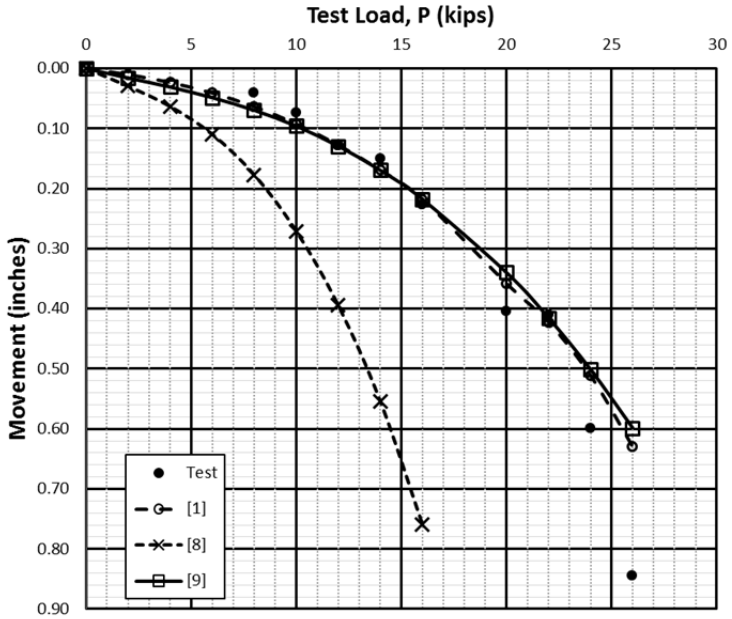

Figure 4.27: Comparison of PLAXIS 2D (HS) verification test models [1], [8] and [9] (LE model).

4.2.7 *Comparison of Changes in Model Parameters*

After the Axisymmetric method was select to model the verification test, it was vital for efficient calibration between PLAXIS and testing results to test which parameters changed the load-movement curve. Many parameters remained constant or shown to not substantially affect the modeled test curve; however, parameters that resulted in substantial changes in the test curves are shown in Figure 4.28 through Figure 4.31. Only the HS model is shown in the figures because the MC model resulted in similar changes. The following conclusions are noted subsequently and affected the trial and error method of curve fitting.

- Changes in the modulus of elasticity resulted in a change in the initial slope of the test curve, but did not change the failure load (Figure 4.28).
- Figure 4.29 and Figure 4.30 show that changes in cohesion and friction angle resulted in little change in the initial slope of the curve, but resulted in substantial changes in the failure load.

- Large changes in the overburden pressure on the soil nail resulted in changes in the slope of the curve and failure load as shown in Figure 4.31.

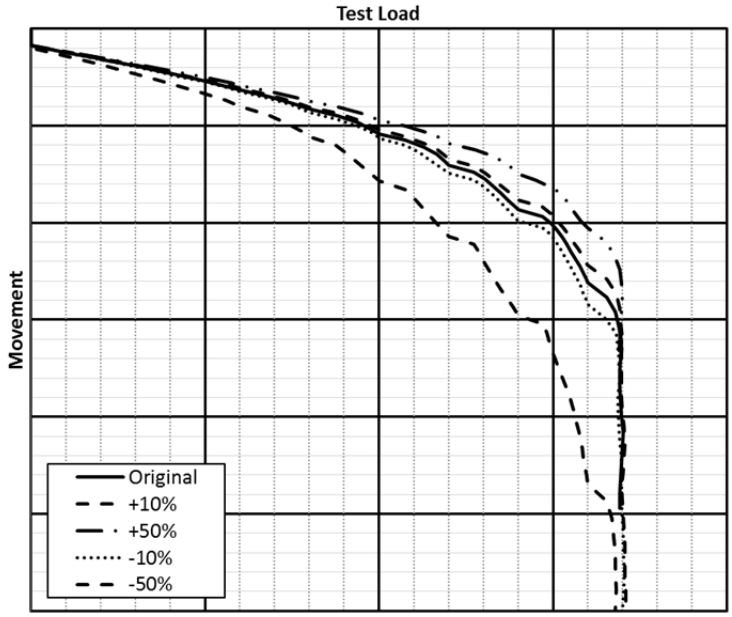

Figure 4.28: Comparison between changes in E_{50}^{ref} for the Axisymmetric and HS model.

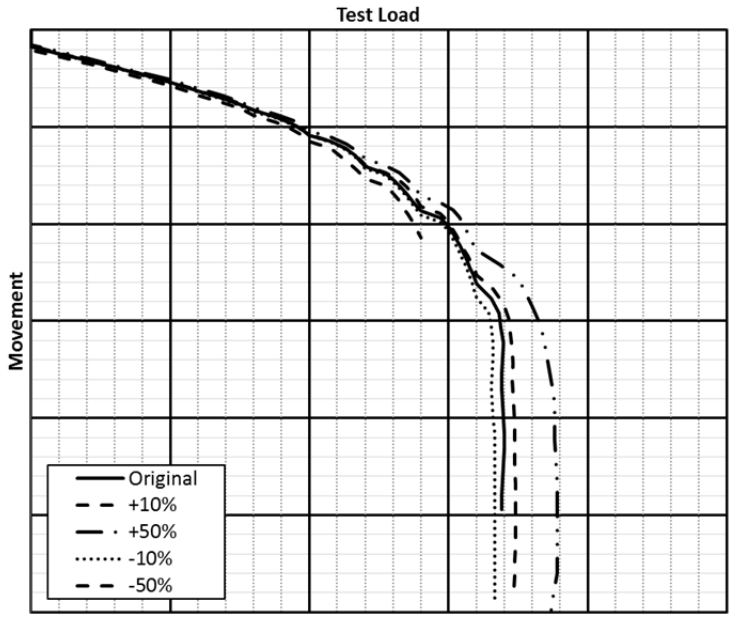

Figure 4.29: Comparison between changes in cohesion for the Axisymmetric and HS model.

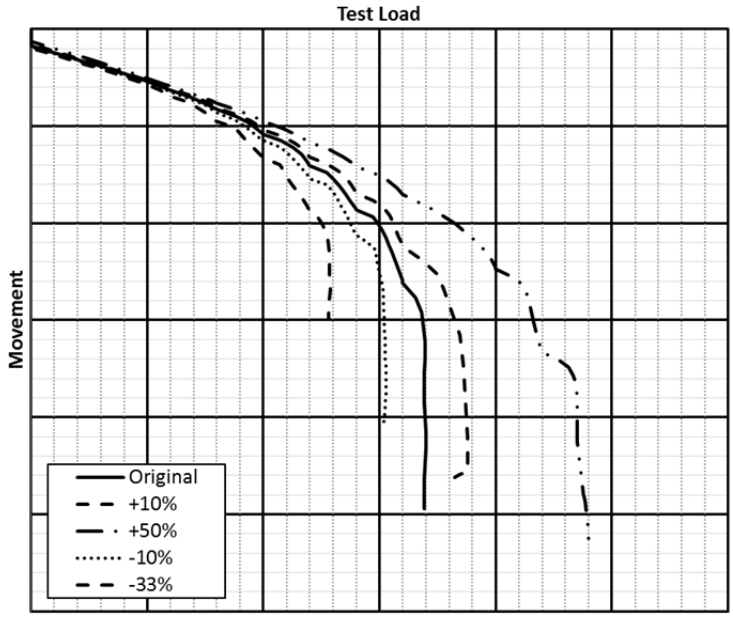

Figure 4.30: Comparison between changes in friction angle for the Axisymmetric and HS model.

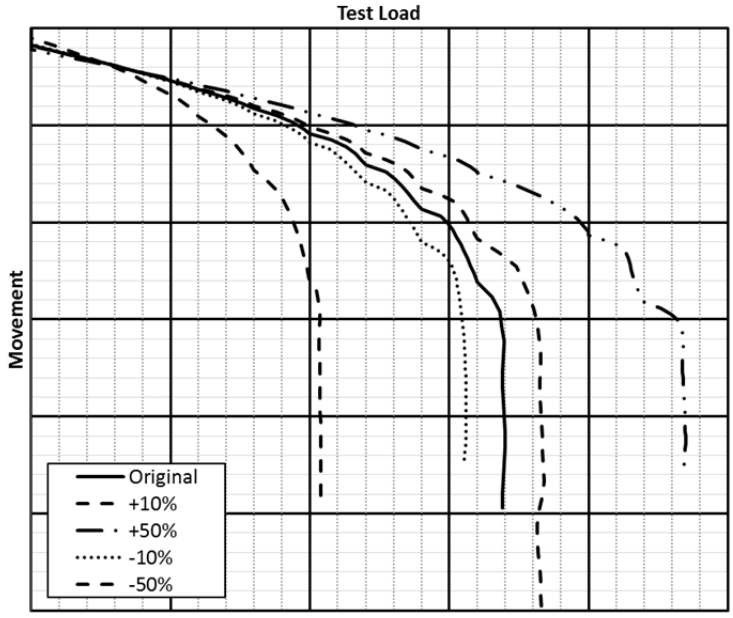

Figure 4.31: Comparison between changes in overburden pressure for the Axisymmetric and HS model.

4.3 Results and Conclusions

PLAXIS 2D fitting of the test curve was conducted on all tests meeting failure criteria and results are presented in Appendix B. The trial and error method for curve fitting was conducted to fail the PLAXIS 2D model and field verification tests at the same load. Comments and conclusions on the PLAXIS 2D Axisymmetric verification test fitting results are following.

- PLAXIS 2D allowed two of the three failure criteria used to estimate the ultimate bond strength (Section 2.2) to be utilized. The displacement in relation to a certain time increment was excluded because time was not a factor in the PLAXIS analysis model.
- The deformation of the soil nail and surrounding soil was greatest around the soil nail and decreases as the distance from the nail increased (Figure 4.32).
- Three non-failed tests were able to be predicted to failure using PLAXIS.
    - The reason for the relatively low amount of predicted failed tests was because many field tests were not conducted to a deformation that allowed prediction of failure to be conducted.
- It is shown in Appendix B that movement in the field tested soil nails does not commence when the first load is applied. This lack of movement was not able to be incorporated in the PLAXIS model, leading to an overestimate of movement at relatively low applied loads. It should be noted that the test results for figures in Appendix B, are only the maximum movement at the particular load.
- In general the PLAXIS model fit the testing results well, but not all of the movements in the testing results were accounted for.
    - This is a result of the relatively simple PLAXIS 2D model that was used, which cannot account for all variables found in the field.
- The HS model had a greater fit to the field tests results when they followed a hyperbolic path and MC fit the curves when they followed a more linear trend.
- It should be noted that the HS model was used in eight of the nine lowest bias results.

- This may be a result of the fact that when failure is imminent, the testing curve resembles a hyperbolic rather than a linear trend.

Figure 4.32: Example of the deformation of the soil nail and surrounding soil in PLAXIS 2D.

In addition, comparisons between Consolidated Undrained Triaxial Tests on cohesive soils in the project area (Appendix D) and PLAXIS parameters are shown in Figure 4.33 through Figure 4.40. As a result of the shallow depths of the verification tests (5 to 15 feet), the lowest confining pressure from each set of Triaxial Tests were used for comparison. Appendix D shows that the Triaxial Tests confining pressure tends to be higher than the confining pressure of the verification tests. Comments and conclusions of the comparison are stated following.

- Comparison between tested and PLAXIS cohesion for the MC and HS models are presented in Figure 4.33 and Figure 4.34. The MC cohesion results were higher on average (1,085 lb/ft^2) when compared to the HS (800 lb/ft^2) and testing results (439 lb/ft^2).
    - This verifies results found in literature that the R_{inter} value should be greater than 1.0, to increase the cohesion of the soil at the soil/nail interface (Section 4.1.4).

- The MC and HS model showed relatively the same trend for friction angle and most of the PLAXIS results showed a higher friction angle than the average from Triaxial testing (Figure 4.35 and Figure 4.36).
    - Similar to cohesion, this confirms a necessity to incorporate a higher than 1.0 value for R_{inter}; however, this value should only be slightly above a value of 1.0.
- The MC results showed a trend well below the minimum E_0 found in testing (Figure 4.37), but the HS model shows a trend towards the minimum E_0 values with the exception of three cases (Figure 4.38).
    - It was stated in Section 4.1.9.2.1 that E_0 should only be used for soils with large linear elastic range and should not be used for the soils in this study.
- PLAXIS MC results for E' showed a tendency to be between the minimum and average of the Triaxial Tests results, where the HS model tended to be slightly higher than the average (Figure 4.39 and Figure 4.40). This is an interesting observation because the PLAXIS results typically show higher values than Triaxial Test results, but the elastic modulus showed the opposite trend. It should be noted that testing E values from the Triaxial Tests were obtained graphically (Sections 4.1.9.2 and 4.1.9.3) and thus may slightly affect results.

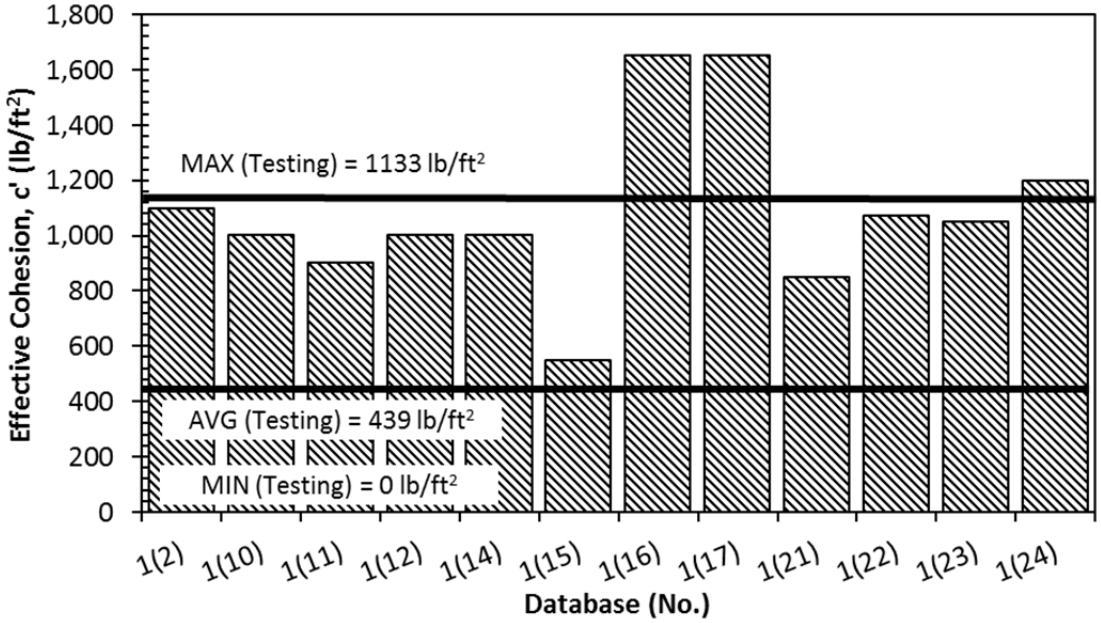

Figure 4.33: Comparison of cohesion between PLAXIS simulation (MC) and Triaxial Test results.

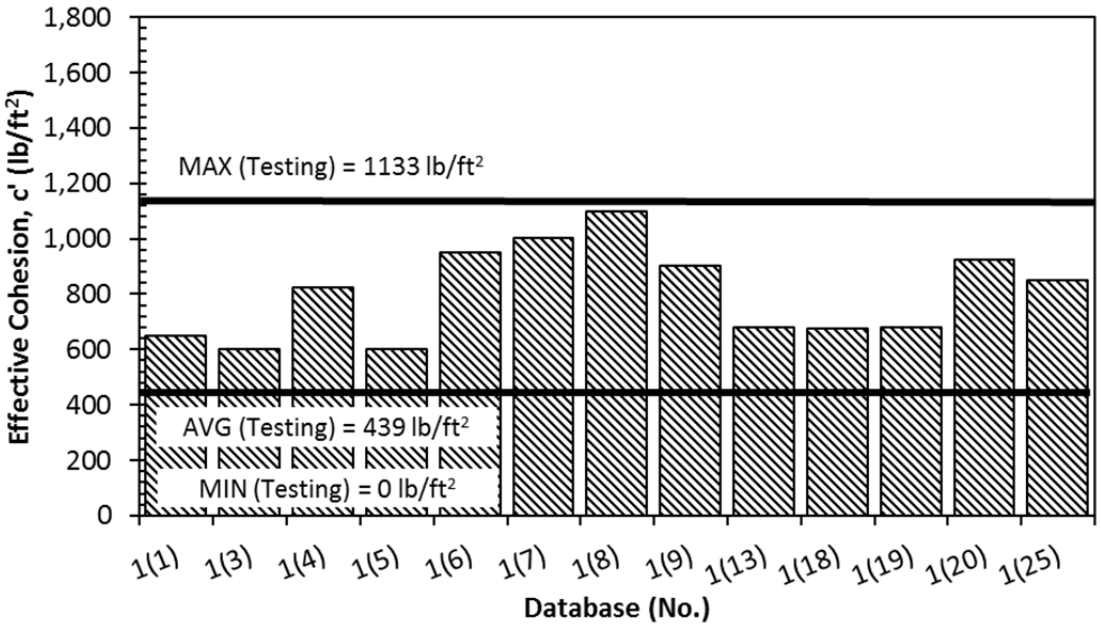

Figure 4.34: Comparison of cohesion between PLAXIS simulation (HS) and Triaxial Test results.

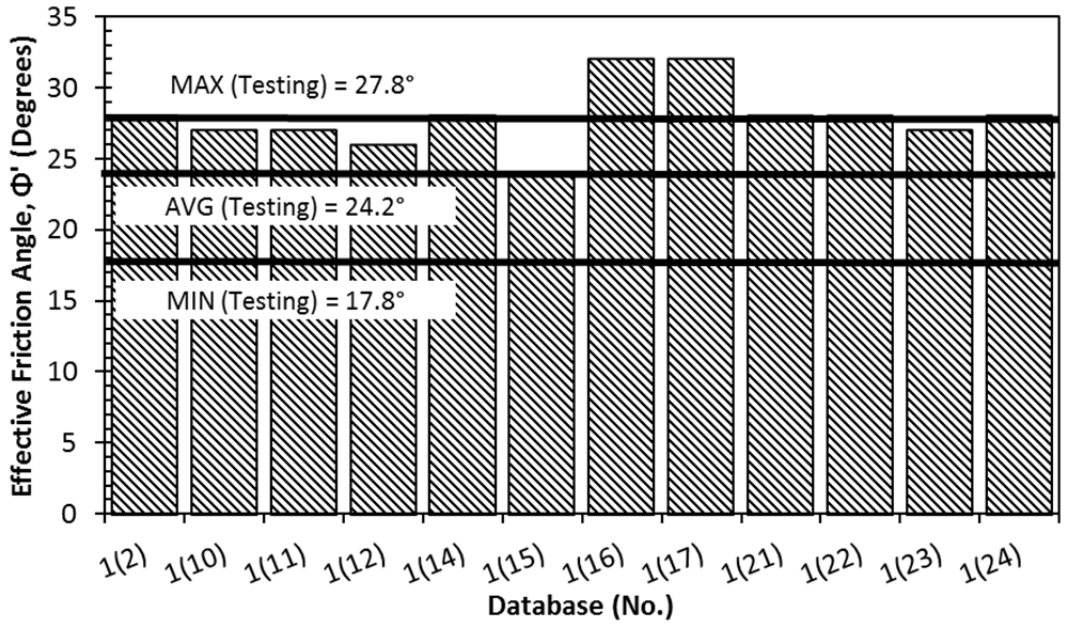

Figure 4.35: Comparison of friction angle between PLAXIS simulation (MC) and Triaxial Test results.

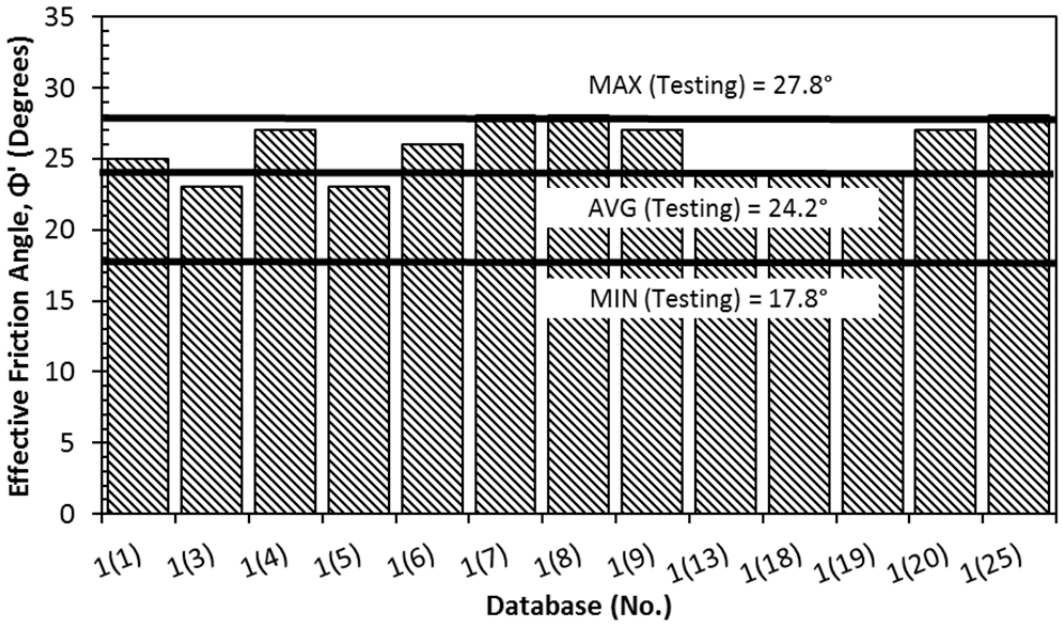

Figure 4.36: Comparison of friction angle between PLAXIS simulation (HS) and Triaxial Test results.

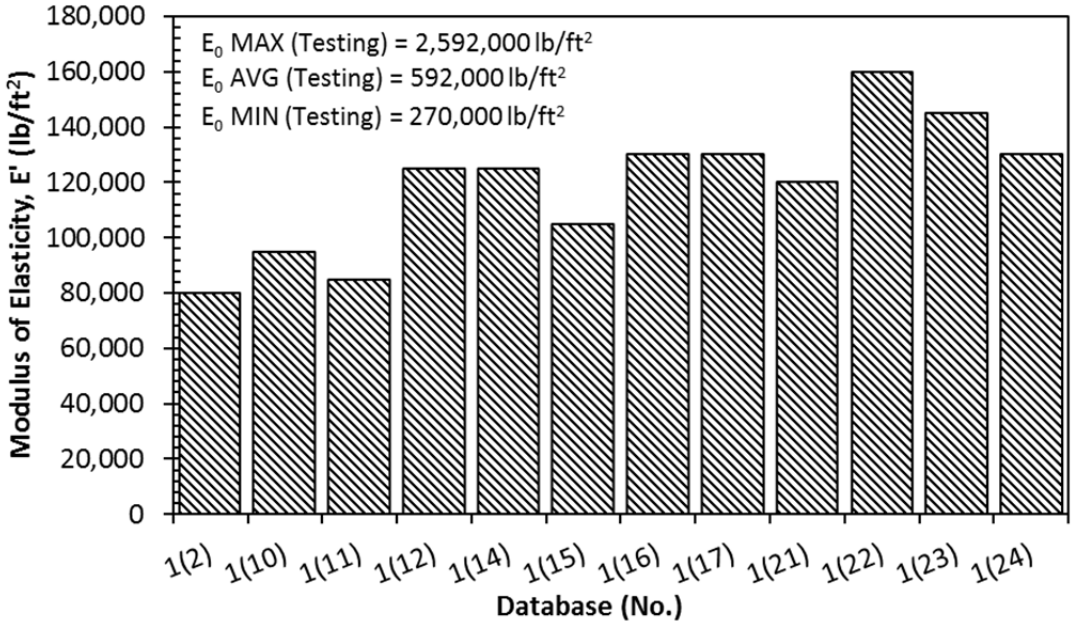

Figure 4.37: Comparison of modulus of elasticity between PLAXIS (E') simulation (MC) and Triaxial Test results (E_0).

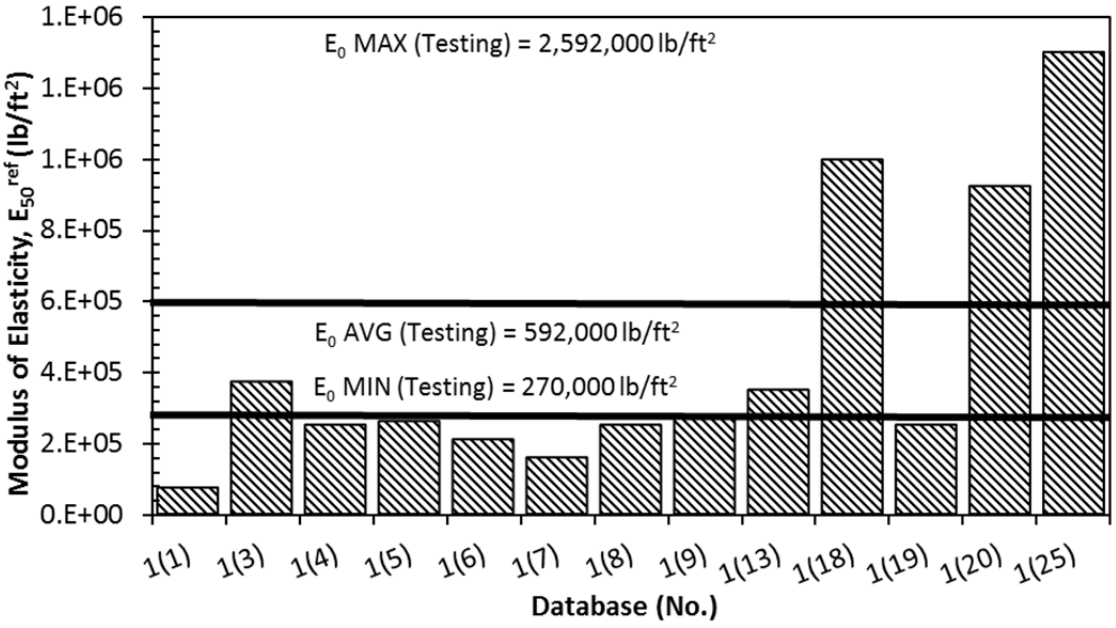

Figure 4.38: Comparison of modulus of elasticity between PLAXIS (E_{50}^{ref}) simulation (HS) and Triaxial Test results (E_0).

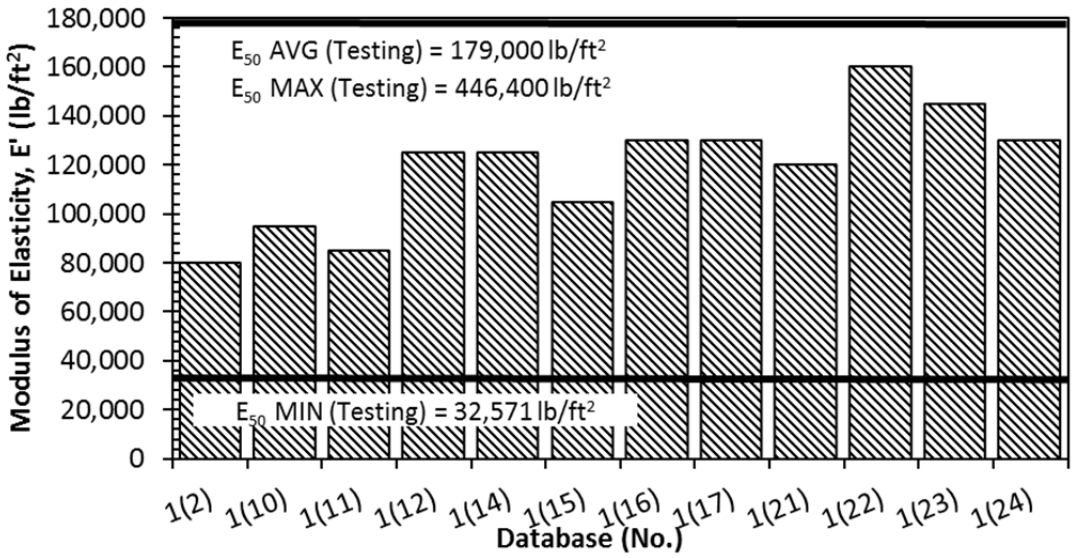

Figure 4.39: Comparison of modulus of elasticity between PLAXIS (E') simulation (MC) and Triaxial Test results (E_{50}).

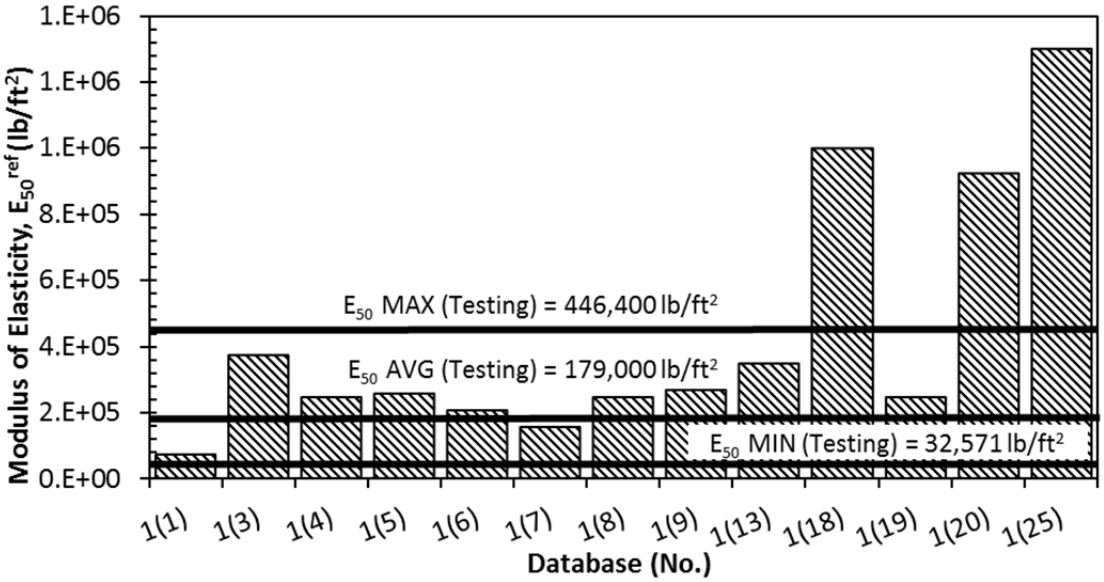

Figure 4.40: Comparison of modulus of elasticity between PLAXIS (E_{50}^{ref}) simulation (HS) and Triaxial Test results (E_{50}).

Chapter 5

Load and Resistance Factor Design

5.1 Literature Review and Background

5.1.1 Background

The traditional ASD method relies on selecting a factor of safety based on experience and in some cases can provide reasonably economic and safe designs. Rather than basing designs on experience, LRFD method addresses and quantifies uncertainties in the design in a systematic manner and incorporates load and resistance factors. The load factor normally is used to increase the predicted load applied to the structure while the resistance factor normally decreases the predicted resistance provided by the structure (AASHTO, 2007; Allen et al., 2005; Lazarte, 2011). These factors are incorporated in the design procedure and the LRFD method can provide the following:

- load and resistance factors account for separate uncertainties in the loads and resistances,
- uses acceptable levels of structural reliability to provide the reliability-based load and resistance factors, and
- provides a consistent level of safety for structures with several components (Lazarte, 2011).

Limitations of the LRFD method include:

- developing resistance factors to meet individual situations requires statistical data related to that situation,
- the resistance factor must correspond to a particular design method, and
- implementing LRFD design procedures requires a change for engineers who may be accustom to the ASD method (FHWA, 2001).

Resistance and load factors are calibrated using probability-based techniques and allow a tolerable probability of failure to be selected. These factors are calculated using actual load and resistance data, and represent a major advantage over the ASD method (Lazarte, 2011).

The limit state allows the load and resistance factors to be related and is defined when the structure (or component) has reached a level of stress, displacement, or deformation that affects its performance. There are four types of limit states commonly used in bridge design:

- Strength Limit states,
- Service Limit states,
- Extreme-Event Limit states, and
- Fatigue Limit states (AASHTO, 2007; Lazarte, 2011).

5.1.1.1 Strength Limit States

These limit strength states are those related to the stability and strength of the structure's components throughout its life. The resistance that the structure or soil provides at or near failure is incorporated into this limit state, and is commonly referred to as the ultimate strength (nominal resistance). The design equation used for the Strength Limit state is:

$$\emptyset R_n \geq \sum_{i=1}^{N} \gamma_i \eta_i Q_i \qquad 32$$

where $\emptyset$ is a non-dimensional resistance factor related to R_n, R_n is the nominal resistance of the structural component, N is the number of load types considered, γ_i is a non-dimensional load factor associated with Q_i, η_i is a load-modification factor and Q_i is the load associated with the nominal resistance (AASHTO, 2007; Lazarte, 2011).

The resistance and load factors are separate and represent statistical parameters related to each component that can be used to account for:

- magnitude of the applied loads uncertainty,
- material variability,
- uncertainty in the prediction by the design method, and

- other uncertainty sources (Nowak and Barthurst, 2005).

For geotechnical engineering, the nature and variability associated with the load is different than the resistance and thus the use of the separate parameters is justified.

It is common to reduce the nominal resistance factors and thus a ∅ value less than 1.0 is typical; on the contrary, load factors are usually increased and thus a value for γ_i greater than 1.0 is common (AASHTO, 2007; Allen et al., 2005; Lazarte, 2011). The structure's redundancy, importance and ductility is accounted for by η_i and usually lies between 0.95 and 1.05 (Lazarte, 2011).

Typically, the load applied to the structure is known and thus the resistance required to exceed this load can be calculated (Equation 32). It is important to relate the load and resistance factors through the limit state equation and rearranging Equation 32 allows such a relation to be defined as (Nowak and Barthurst, 2005; Lazarte, 2011):

$$R_n = \frac{\gamma_i}{\emptyset_R} Q_i \qquad 33$$

5.1.1.2 Service Limit State

Inadequate conditions can occur during the normal operation of the structure but may not cause failure, can be defined as the Service Limit state. The types of conditions defining the Service Limit state can include:

- excessive settlement,
- excessive deformation, and
- cracking (Lazarte, 2011).

These types of Service Limit states can notably affect the structures:

- overall stability,
- slope stability, and
- other stability states (AASHTO, 2007).

For the Service Limit state, the design equation used can be expressed as:

$$S_{TOLERABLE} \geq S_{MAX} \quad (34)$$

where $S_{TOLERABLE}$ is the maximum value of S (settlement or deformation) that the structures can tolerate before affecting functionality, and S_{MAX} is the maximum calculated value of S that is expected to occur under normal operation (Lazarte, 2011).

The Strength Limit state (Equation 32) with load factors (γ_i and η_i) equal to 1.0 can define the Service Limit state for the stability of a structure. However, this requires an assumption that the structure is under normal operating conditions (Lazarte, 2011).

5.1.1.3 Extreme-Event Limit States

The Extreme-Event Limit state has a return period that exceeds the design life of the structure but can cause large loads when they occur. These types of events can include:

- ice formation,
- seismic events,
- vehicle collisions, and
- vessel collision (Lazarte, 2011).

For Extreme-Event Limit states, the Strength Limit state (Equation 32) is commonly used, but incorporates higher load factors than those used for the Strength Limit state (AASHTO, 2007; Lazarte, 2011).

5.1.1.4 Fatigue Limit States

When repetitive loads are applied to and can affect the performance of a structure, it is categorized as a Fatigue Limit state. The stress levels of the applied load are significantly lower than the Strength Limit states and common examples include:

- dynamic loads, and
- vehicular loads (Lazarte, 2011).

5.1.2 *Calibration Concepts*

The loads and resistances are considered random independent variables and are typically either normally or lognormally distributed (Baecher and Christian, 2003; Lazarte, 2011).

Normally distributed load and resistances are shown in Figure 5.1, with the resistance values generally greater than those of the load. In addition, the resistance distribution typically has a wider distribution than the load as a result of the higher uncertainty.

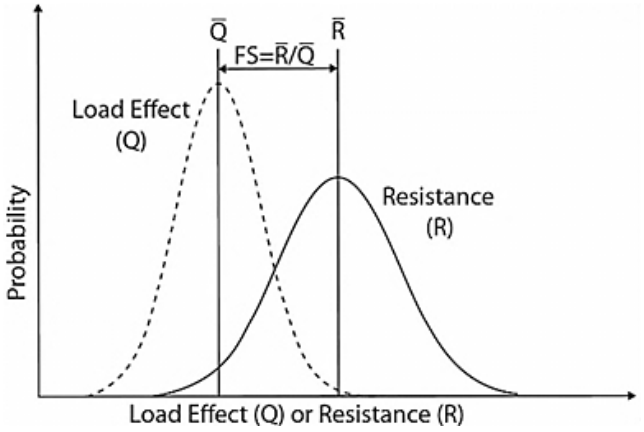

Figure 5.1: Probability density functions for load and resistance.

Although Equation 32 is beneficial for understanding of the concepts associated with the Strength Limit state, when η_i is taken as 1.0 it can be amended as:

$$\emptyset_R R_n - \gamma_i Q_i \geq 0 \qquad 35$$

The limit state equation corresponding to Equation 35 can be expressed as:

$$g = R - Q \geq 0 \qquad 36$$

where g is the safety margin, and R and Q are random variables representing the resistance and load. The safety margin acts to combine the load and resistance into one distribution and is used to define the probability of failure (P_f) as shown in Figure 5.2. The P_f is the probability that $g \leq 0$ and is typically represented by the reliability index (β), which is also shown in Figure 5.2 (Allen et al., 2005).

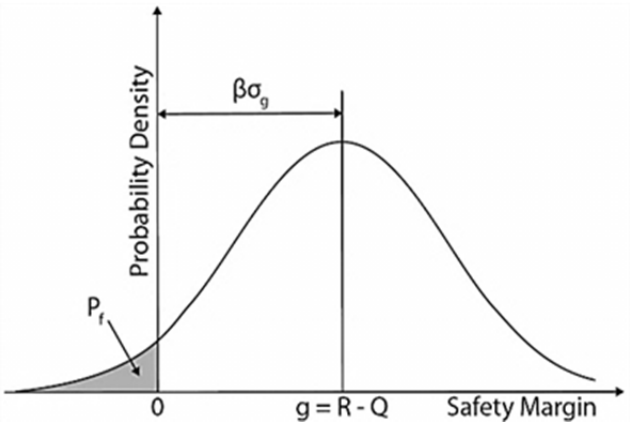

Figure 5.2: Probability density function of the safety margin.

5.1.3 *Selection of the Target Reliability Index*

In LRFD, the value of β is the implied factors of safety from the ASD method, thus the selection of the target reliability index (β_T) is crucial aspect of the calibration process that can drastically effect the calibrated resistance factor. A relationship between β and P_f is shown in Figure 5.3, and provides an indication of what β_T value should be utilized in the calibration process for a certain structure. It is also important to use available literature to decide which β_T should be used, such as the value of 2.33 used in the NCHRP Report 701 for the pullout resistance factor calibration.

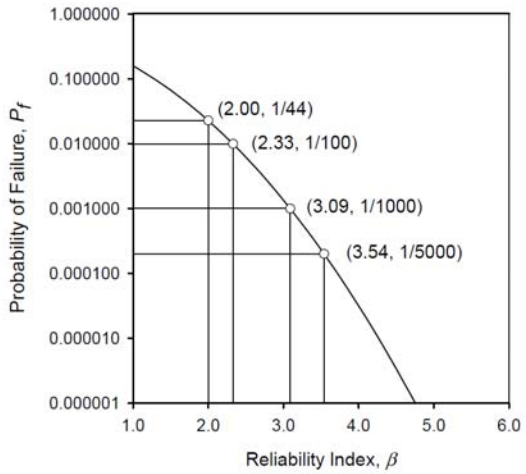

Figure 5.3: Relationship between *β* and P_f for a normally distributed function (Allen et al., 2005).

Additionally, accounting for the limit state that will be used and the consequences if the limit state is exceeded is crucial when considering what β_T value to use for calibration (Allen et al., 2005). As a result, it may be appropriate to choose a higher β_T (lower P_f) when using the Strength Limit state when compared to calibration conducted using the Service Limit state. This is because a failure by the Strength Limit state can cause failure of the system, where exceeding the Service Limit state may only cause excessive deformation or settlement. It also stands, that for higher redundant structures, a lower β_T and as a result higher P_f could be used because a failure in one part of the structure may not cause failure of the entire structure Allen et al., 2005; Lazarte, 2011).

5.1.4 *Approaches for Calibration of Load and Resistance Factors*

LRFD calibration is the process in which values are assigned to load and resistance factors. This type of calibration process can be conducted by using:

- engineering judgment,
- fitting to other codes such as the ASD method, and
- reliability based procedures (FHWA, 2001).

Each of these procedures have their advantages and disadvantages; however, using reliability based procedures for the LRFD calibration could result in the greatest benefit over the ASD method (Lazarte, 2011).

5.1.4.1 Engineering Judgment

This method requires a substantial amount of experience about the design and could be beneficial because it incorporates design practices that have been seen to be safe and cost-effective. Disadvantages of this calibration projects are that the results typically do not have a uniform level of conservatism and may be unintentionally biased (FHWA, 2001; Lazarte, 2011).

5.1.4.2 Fitting to Other Codes

The resistance factors calculated with this method are calibrated using the factor of safety values from the ASD method and generally do not achieve a more uniform margin of

safety. Although mathematically simple, this design approach may not address all sources of uncertainty. Fitting ASD methods to LRFD is commonly the first to be used to calculate load and resistance factors and ensures that the LRFD design is not radically different than the ASD design (FHWA, 2001; Lazarte, 2011). Resistance factors can be calibrated with this method by utilizing the following equation (among others):

$$\emptyset \geq \frac{\sum \gamma_i Q}{FS \sum Q_i} \qquad 37$$

where all of the variables have been defined in Section 5.1.2.

5.1.4.3 Reliability Based Procedures

An acceptable probability of failure for the structure is defined and resistance and load factors calibrated in this method are based on empirical data. Although reliability based procedures are more complex when compared to the other two methods, they may provide insight on the bias and uncertainties associated with design formulas (Lazarte, 2011).

There are several levels of probabilistic design (Level I, II and III) associated with this calibration procedure. Level III is a fully probabilistic method and requires knowledge on the probability distribution of the loads and resistances and correlations between variables. As a result, this method is the most complex and is not typically used for geotechnical applications (FHWA, 2001).

Level I probabilistic method is the first-order-second-moment (FOSM) method, and the random load and resistance variables and their mathematical derivatives used to calculate the reliability index are approximate. In this method, events related to the load are assumed to be independent of the resistance. The β value is a linear approximation of the load and resistance about their mean values and allows for closed-form approximations of resistance factors (FHWA, 2001; Lazarte, 2011).

Level II probabilistic method is known as the advanced first-order-second-moment method (AFOSM) and requires that a reliability index is assumed and then compared to the

calculated value. This process is repeated until the β_T and the calculated β values are within a small tolerance (FHWA, 2001; Lazarte, 2011).

5.1.4.4 Calibration Procedures in Literature

LRFD calibrations for soil nail pullout resistance factors are provided in AASHTO (2007) and the NCHRP Report 701. The resistance factors calculated by AASHTO (2007) are based on fitting to other codes (ASD method) and as a result did not improve upon the ASD method. The calibration procedure which improved upon the resistance factors provided by AASHTO (2007) was the NCHRP Report 701. These calibrated resistance factors follow the Strength Limit Level I and II reliability based procedures with Monte Carlo simulations.

5.1.5 *Developing Statistical Parameters and Probability Density Functions for the Resistance and Load*

Given the existing data for the resistance and load, the following statistical parameters must be established:

- bias,
- mean,
- standard deviation,
- coefficient of variation, and
- type of distribution (typically normal or lognormal; Allen et al., 2005; Lazarte, 2011).

Before the calibration process can begin, it is important to assess the quality and quantity of data. Both of these factors can have a large effect on the outcome of the calibration process and determine the accuracy of results. The questions that should be answered when assessing the quality and quantity of data are provided subsequently.

- If enough is known about the data to be confident in the results?
- Does the data adequately represent the variability in the methods used and encompass all sources of uncertainty?

- Is there enough data, that the data can be accurately characterized by the mean, standard deviation and cumulative distribution function?
- Have the outliers been identified and removed from the data (Allen et al., 2005)?

If all of these questions are answered, then the normal and lognormal distributions can be established and require the use of the following equations.

If Equations 33 and 36 are combined, the Strength Limit state function can be defined as:

$$g = \frac{\gamma_i}{\emptyset_R} Q_i - Q_i \quad (38)$$

where Q_i represents independent random variables related to either the resistance or load.

The bias of the data allows the accuracy of the design method used to be evaluated and can be defined as:

$$Bias = X_i = \frac{Measured}{Predicted} \quad (39)$$

where the measured value is from testing and a design method is used to establish the predicted value. Incorporating the fitted bias deformation into Equation 39 results in:

$$g = \frac{\gamma_i}{\emptyset_R} X - X \quad (40)$$

If the soil nail resistances or loads follow a normal distribution, the random values can be generated as:

$$X = \lambda + (\sigma z) \quad (41)$$

where λ is the normal mean of the bias from the load or resistance, σ is the standard deviation of the mean of the bias, z is the inverse normal function ($\Phi^{-1}(u_{ia})$) and u_{ia} is a random number between 0 and 1 representing a probability of occurrence (Allen et al., 2005; Lazarte, 2011).

In the event that the load or resistance of the soil nail follows a lognormal distribution, the random values can be generated as follows:

$$X = EXP\left(\mu_{ln} + (\sigma_{ln} z)\right) \quad (42)$$

where μ_{ln} is the lognormal mean of the bias, and σ_{ln} is the lognormal standard deviation of the bias from the load or resistance (Allen et al., 2005; Lazarte, 2011).

From the normal distribution parameters, the μ_{ln} and σ_{ln} parameters can be determined by the following two equations:

$$\sigma_{ln} = \sqrt{\ln\left(\frac{\sigma}{\lambda} + 1\right)} \quad 43$$

$$\mu_{ln} = \ln(\lambda) - \frac{\sigma_{ln}^2}{2} \quad 44$$

This bias value can be calculated for both the load and resistance values, and the normal or lognormal distributions can be fitted to the bias data (Figure 5.4; Allen et al., 2005). The fitted distribution is also referred to as the cumulative density function (CDF; Allen et al., 2005). It is important to note that the distributions should be fitted to the higher bias (head) values for load data and lower bias (tail) values for the resistance. These ideas can be justified because higher bias load values can normally only be greater than the lower resistance bias values are presented in Figure 5.1 (Allen et al., 2005; Lazarte, 2011).

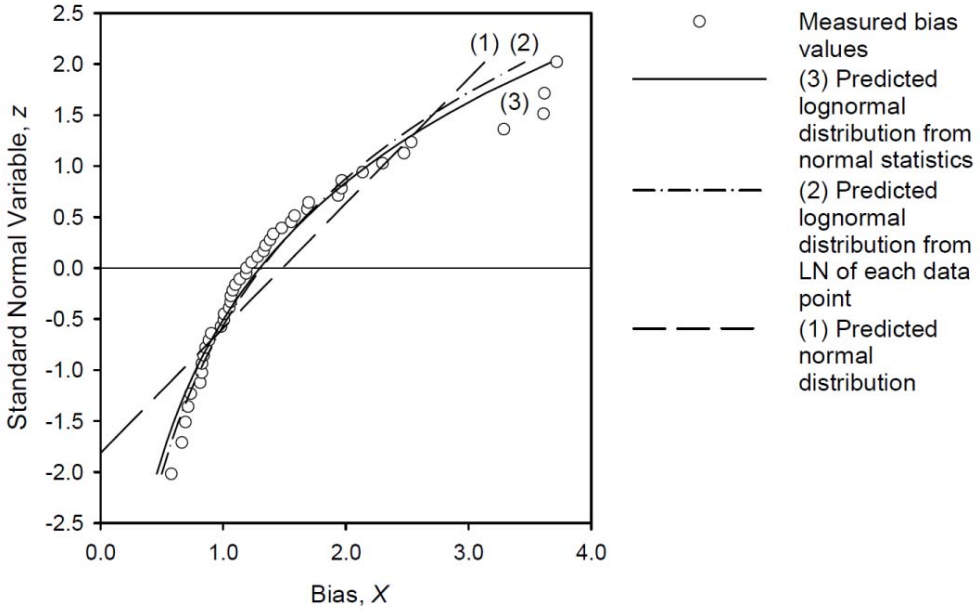

Figure 5.4: Standard normal variable as a function of bias for illustrative purposes (Allen et al., 2005).

5.1.6 *Estimating the Load Factor*

Estimating the load factor to encompass load related statistics before beginning the final calibration process is an important step in the calibration process. When load statistics are available, Allen et al. (2005) provided the following equation to estimate the load factor:

$$\gamma_Q = \lambda_Q\left(1 + n_\sigma COV_Q\right) \quad 45$$

where λ_Q is the mean of the bias of the load, n_σ is a constant representing the number of standard deviations from the mean to achieve a desired probability of exceedance and COV_Q is the coefficient of variation (σ/μ) of the bias for the load. A value of two for n_σ was recommended by Allen et al. (2005) and corresponds to a probability of exceeding any factored load of about two percent. This value is also assumed to correspond to the Strength Limit state by Nowak (1999) and Nowak and Collins (2000). It is important to note that increasing the mean of the bias or coefficient of variation results in an increase in the load factor.

A number of measured and predicted load values for soil nails have been compiled by Lazarte (2011) and the summary of these statistics can be seen in Table 5.1. A load factor of about 1.5 is calculated with the use of these statistics; however, load factors of 1.0, 1.35, 1.5, 1.6 and 1.75 can be used to account of various loading conditions on the SNWs (Lazarte, 2011).

5.1.7 *Load Values Found in Literature*

The measured load values shown in Table 5.2, were collected from 11 instrumented SNWs within the United States and abroad (Byne et al., 1998; Oregon DOT, 1999). The predicted values were estimated from simplified methods developed by Byne et al. (1998) using the conditions present in the SNWs (GEC, 2003; Lazarte, 2011). The bias data was incorporated into the pullout resistance factor calibration in the NCHRP Report 701 and a lognormal distribution was fit to the head (highest bias values in the data set) of the data (Table 5.1; Lazarte, 2011).

Table 5.1: Statistics of bias for maximum nail loads (Lazarte, 2011).

Load Parameters						
Number of Points in Database	Distribution Type	Mean of Bias	Standard Deviation	Coefficient of Variation	Log Mean of Bias	Log Standard Deviation
N		λ_Q	σ_Q	COV_Q	μ_{LN}	σ_{LN}
13	Lognormal	0.912	0.290	0.32	-0.140	0.31

Table 5.2: Summary of normalized measured and predicted maximum nail load (Lazarte, 2011).

No.	Case	Normalized Measured Load, T_m	Normalized Predicted Load, T_p	Bias of Load
1	Cumberland Gap, 1988	0.54	1.05	0.51
2	Polyclinic	0.56	0.94	0.59
3	I-78, Allentown	0.68	1.07	0.63
4	Guernsey, U.K.	0.51	0.71	0.72
5	Swift-Delta Station 2	1.11	1.43	0.78
6	Oregon-3-A	0.81	0.98	0.82
7	Swift-Delta Station 1	0.81	0.97	0.84
8	Peasmarsh, U.K.	0.58	0.65	0.89
9	Oregon-2-B	1.05	1.10	0.95
10	IH-30, Rockwall, Section B	1.06	0.99	1.01
11	Oregon-1-A	0.96	0.80	1.11
12	San Bernardino (R)	1.08	0.83	1.20
13	San Bernardino (L)	1.13	0.83	1.36

5.1.8 *Monte Carlo Simulation*

Monte Carlo simulations can be used to generate numerous load and resistance values based on their statistical parameters such as very low resistance values or very high load values. These cases may not be obtained during testing but have the possibility of occurring in the field.

The Monte Carlo technique uses random numbers to extrapolate the CDF values at both ends of the distribution (Allen et al., 2005; Lazarte, 2011). Random numbers generated by the Monte Carlo simulation are incorporated into the calibration process by regarding those generated numbers as u_{ia} (Section 5.1.5) and allows for the Monte Carlo method to be a curve

fitting and extrapolation tool. For this procedure to be effective, a large amount (typically 10,000 or greater) of random numbers need to be generated (Lazarte, 2011).

In summary, the random numbers generated by the Monte Carlo simulation are guided by the load and resistance statistical distribution (Section 5.1.5) to estimate all (or most) values that could possibly be measured by testing. This allows the comparison of the resistances and loads by the limit state function and the resistance factors to be calibrated with a predetermined load factor.

5.1.9 *Calibration Procedures*

Procedures for calibrating resistance factors with Monte Carlo simulations can be seen in FHWA (2001); Lazarte (2011); and Yu et al. (2012). These studies generally follow the same calibration procedure as:

1. establish a limit state function that incorporates the resistance and load factors,
2. estimate the statistical parameters (μ and σ) from the resistance and load bias values by fitting CDFs,
3. select a value for β_T or the corresponding P_f,
4. calculate or select load factors based on load statistics or loads scenarios that the structure may be designed for,
5. perform a Monte Carlo simulation by the following procedure:
    - o estimate an initial value for the resistance factor,
    - o generate a large amount random numbers and incorporate them into Equations 41 or 42 to obtain load or resistance bias values, and
    - o input random load and resistance bias values into the limit state equation;
6. calculate the P_f by comparing the number of times the limit state function is below zero to the total number of simulations ($count(g \leq 0)$),
7. compare the target and calculated P_f as:

$$P_f(\%) = \frac{count(g \leq 0)}{N} * 100 \quad (46)$$

where N is the number of Monte Carlo simulations,

8. repeat steps 1 through 7 until the β_T and β or target P_f and calculated P_f are sufficiently similar.

5.1.10 *Review of Soil Nail Pullout Resistance Factors in Literature*

Several pullout resistance factors for soil nails and ground anchors can be found in literature. The pullout resistance for ground anchors has been calculated based on the factor of safety calibration and is 0.7 for cohesive soil (AASHTO, 2007) and the NCHRP Report 701 presents presumptive nominal pullout values of between 0.5 and 0.7.

Fully calibrated pullout resistance factors ($\emptyset_{PO}$) can be seen in the NCHRP Report 701. These values encompass a wide range of load factors and a variety of soil types (Table 5.3). While the clay/fine-grained soil calibration is mostly based on data collected from a few locations in California and calibrated with the Strength Limit state equation. Methods used to estimate the ultimate bond strength of the soil nail for the NCHRP Report 701 can be seen in Section 2.1.3, while prediction methods are based on recommended values, and local experience (Lazarte, 2011).

Table 5.3: Summary of calibration of resistance factors for soil nail pullout for various load factors (modified from Lazarte, 2011).

Material	Number of Points in Database	λ_Q				
		1.75	1.60	1.50	1.35	1.00
	N	$\emptyset_{PO}$				
Sand/Sandy Gravel	82	0.82	0.75	0.70	0.63	0.47
Clay/Fine-Grained	41	0.90	0.82	0.77	0.69	0.51
Rock	26	0.79	0.72	0.68	0.61	0.45
All	149	0.85	0.78	0.73	0.66	0.49

5.2 Analysis Procedure

The following procedure was conducted to calibrate pullout resistance factors for the Databases shown in Appendix A, while the probability of failure was determined using the following (Strength Limit Level II).

1. Load values were not available from this project, so values from the NCHRP Report 701 (Table 5.2) and the lognormal distribution statistics as shown in Table 5.1 were used.
2. Bias values were calculated for all test results (and databases) shown in Appendix A.
3. Mean and standard deviation values for the normal and lognormal distribution were calculated by the following procedure (Allen et al., 2005):
    a. [5]bias data was arranged and ranked (i) from lowest to highest order such that $bias_1 \leq bias_2 \leq \cdots \leq bias_n$,
    b. the probability of occurrence (p) was calculated by:

$$p = \frac{i}{n+1} \quad (47)$$

    where n is the total number of data values,
    c. the inverse normal function was calculated with Excel for each bias value by:

$$z = NORMSINV(p) \quad (48)$$

    d. results were than plotted as shown in Figure 5.5 through Figure 5.8,
    e. normal and lognormal distributions were fit to the tail (low bias values) by trial and error (μ_{PO} and σ_{PO} results are shown in Table 5.4).
4. A database with μ_{PO} and σ_{PO} values was selected for the pullout resistance[6].
5. Selected a pullout resistance factor and load factor for the trial.
6. Generated 15,000 random numbers for each of the two variables (pullout resistance and load).

---

[5] This procedure (a through e) was only conducted for databases with only uncensored data points.
[6] The remaining steps were conducted for databases with and without censored values.

7. Calculated the pullout resistance (R_n) and load (T_{max}) using Equation 41 or 42, substituting R_n or T_{max} for X. This was completed for all 15,000 random numbers and an example of the results is shown in Figure 5.9.
8. The 15,000 randomly generated R_n and T_{max} values were paired and imputed into Equation 40.
9. Found the number of cases where $g \leq 0$ out of the 15,000 calculated limit state values ($count(g \leq 0)$).
10. Calculated the probability of failure (Equation 46) with N =15,000.
11. Repeated steps 5 through 10 until a probability of failure near 1.0 percent ($\beta_T \approx 2.33$) was obtained (Yu et al., 2012).
12. Conducted 50 trials for each resistance factor with a probability of failure near 1.0 percent, an example is shown in Figure 5.10.

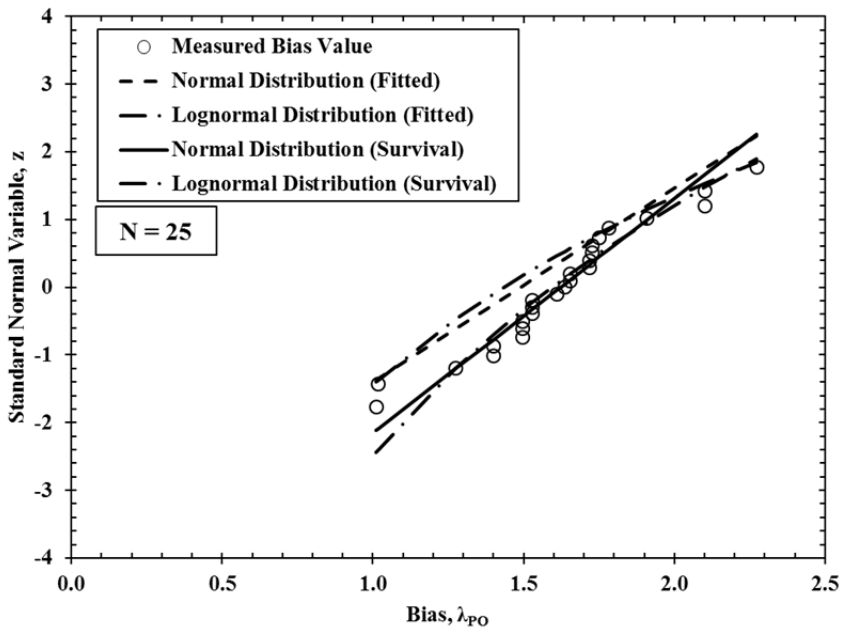

Figure 5.5: Standard normal variable as a function of bias for Database 1.

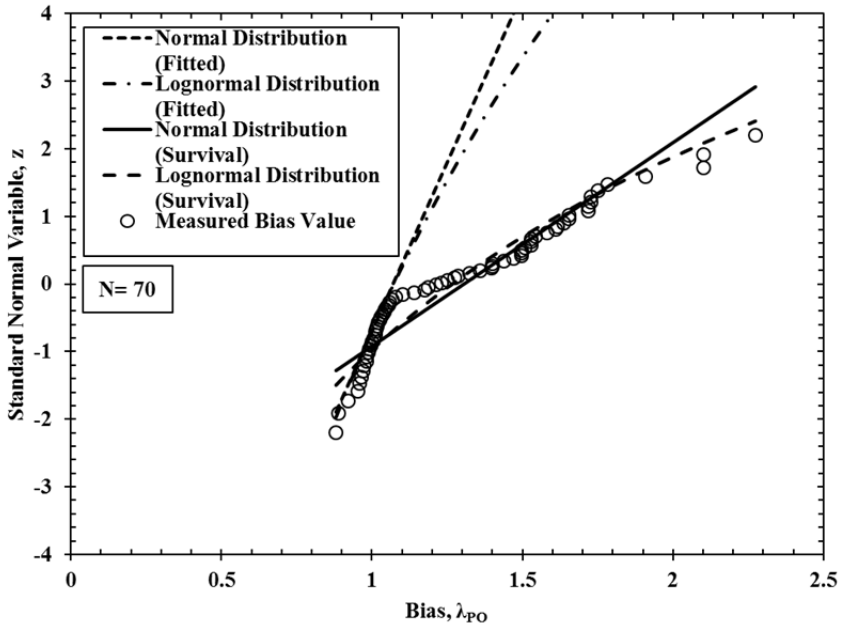

Figure 5.6: Standard normal variable as a function of bias for Databases 1 and 2.

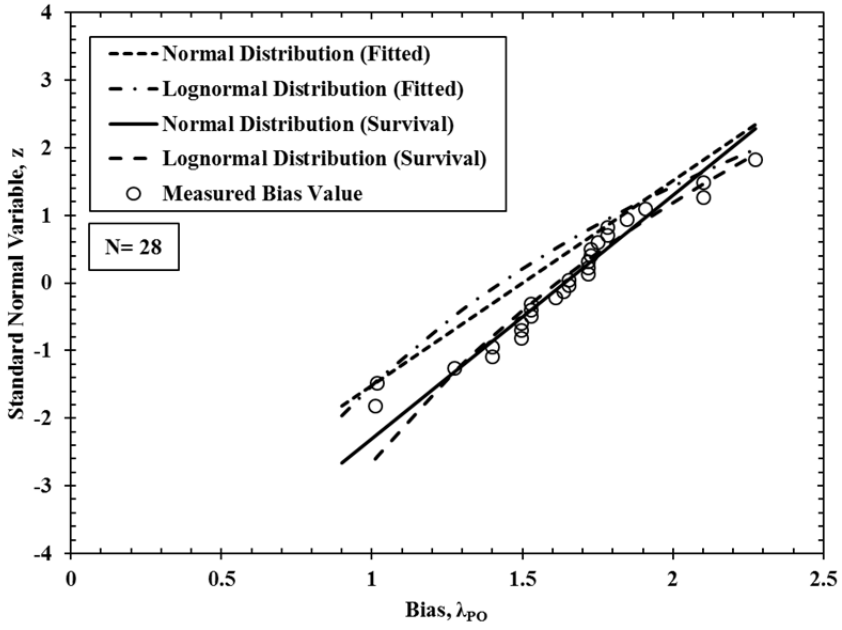

Figure 5.7: Standard normal variable as a function of bias for Databases 1 and 4.

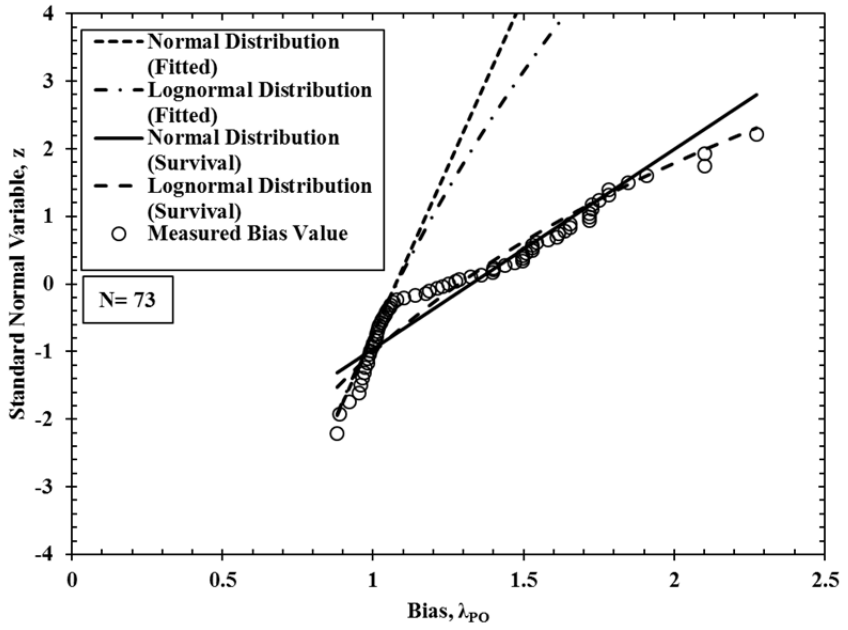

Figure 5.8: Standard normal variable as a function of bias for Databases 1, 2 and 4.

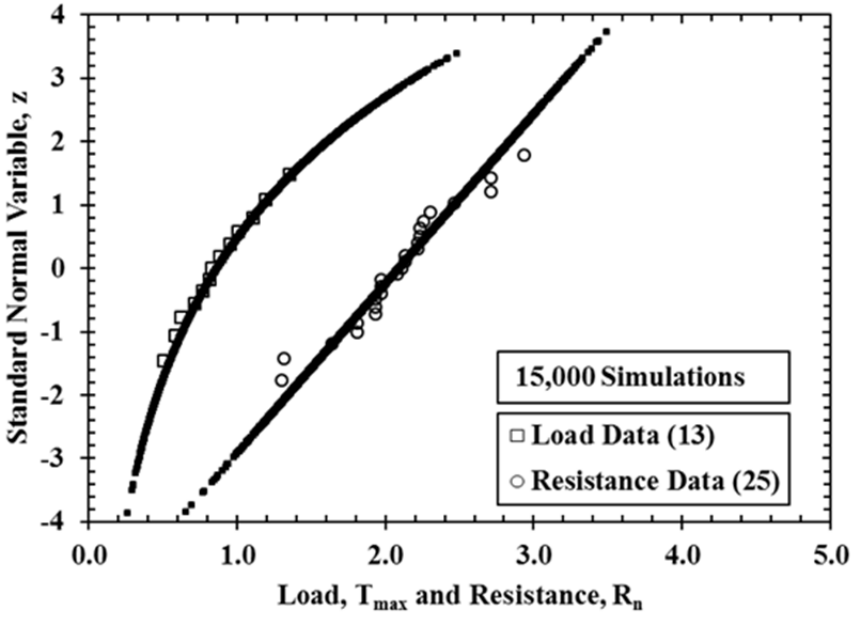

Figure 5.9: Example of Monte Carlo curve fitting of load and resistance.

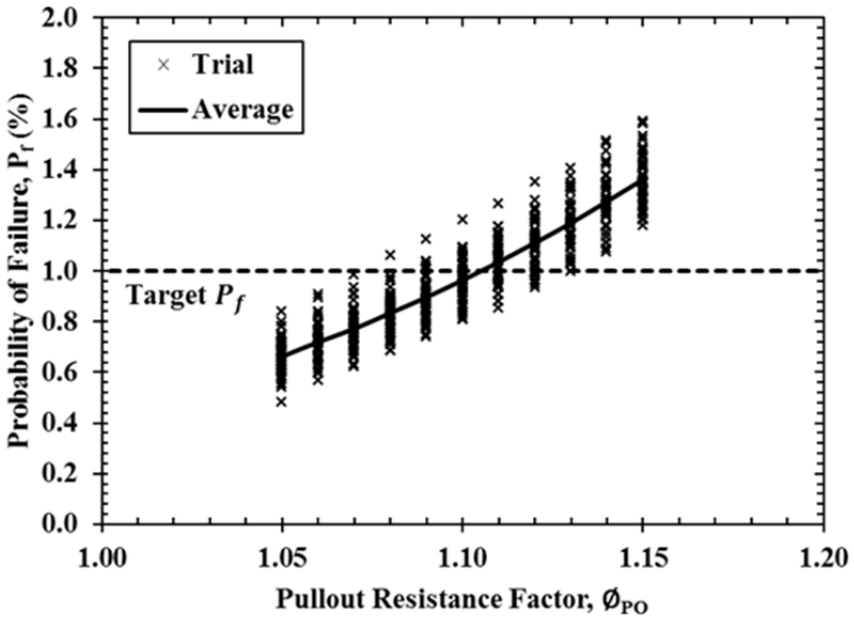

Figure 5.10: Example of probability of failures for various pullout resistance factors.

5.3 Results and Conclusions

A culmination of results shown in Chapters 2, 3 and 4 and LRFD calibration conducted with the procedure shown in Section 5.2, concluded in the pullout resistance factors shown in Table 5.4. When analyzing these results, it is important to remember the concepts and results noted in the previous chapters (especially Chapters 2 and 3). Conclusions from Figure 5.5 through Figure 5.8 are stated subsequently:

- Although the Survival Analysis' distributions fit the overall trend of the data, they tend to overestimate the lower tail test data.
- It can be seen in Figure 5.5 that the fitted curves fit the lower tail of the data, but tend to underestimate much of the rest of the data.
- The distributions estimated by Survival Analysis in Figure 5.6 greatly underestimate the tail data, while the fitted curves greatly underestimate much of the data but fit well to data in the tail.

- The fitted distribution curves fit to the tail and head of the data in Figure 5.7, while the distributions calculated by Survival Analysis fit well to all but the two data points found in the tail.
- Comparison between the measured and estimated distributions in Figure 5.8 show very similar trends to those shown Figure 5.6.
    - This infers that incorporating PLAXIS results into the distributions resulted in little change or benefit.

Although calibrated pullout resistance factors are shown in Table 5.4, graphical methods allow for easy comparison between fitted and Survival Analysis distributions, and databases and cumulative databases (Figure 5.11 through Figure 5.18). A baseline of NCHRP Report 701 results are shown in every figure, and conclusions and comparison of results are listed following.

- All calibrated pullout resistance factors in Database 1 are shown to be higher than the NCHRP Report 701 (Figure 5.11). The Survival Analysis distributions showed a much greater increase than those fitted to the data.
    - It can be seen in Section 2.3 (Figure 2.8) that Database 1 showed a trend toward higher bias values with only a few results near the 1:1 line. This can be compared to the many tests having bias values near or below 1.0 in the NCHRP Report 701 and resulted in Database 1 having a greater mean of the bias (greater values of $\emptyset_{PO}$).
    - Although the normal and lognormal distributions calculated by Survival Analysis, fit the general trend of the data, they overestimated the tail of the data (Section 3.3, Figure 3.5). These distributions did not account for these measured tail values and caused large changes in the calculated probability of failure. As it is recommended that the distribution should be fit to the tail of the data, these pullout resistance factors should be used with caution.

- A slight decrease in $\emptyset_{PO}$ was calibrated when adding Database 2 to Database 1. While a noticeable decrease was calculated for the Survival Analysis distributions. The normally distributed Survival Analysis values are lower than the NCHRP Report 701 while the rest of the distributions have almost identical $\emptyset_{PO}$ (Figure 5.12).
    - As stated before (Section 2.3), Database 2 had a trend toward lower bias values when compared to Database 1. As a result, when the databases are combined the mean of the bias decreased and more variability was added (higher standard deviation). When the bias decreases and the standard deviation increases, lower $\emptyset_{PO}$ values are the outcome.
    - Section 3.3, Figure 3.5 presents that the calculated Survival Analysis distributions underestimated the measured values at the tail, with the normal distribution underestimated the bias values the greatest. A conservatively calibrated value for the $\emptyset_{PO}$ was the result of the tail underestimation. It is interesting that the lognormal distribution resulted in the same $\emptyset_{PO}$ as both of the fitted distribution and since the normal distribution had the greatest conservatism, resulted in the lowest $\emptyset_{PO}$ values.
- A slight increase in $\emptyset_{PO}$ is shown in Figure 5.13 for when the PLAXIS results (Database 4) were incorporated with Database 1. All results were at least 0.14 above the NCHRP Report 701 calibrated values.
    - Section 2.3, Figure 2.10 showed the addition of three predicted failed test did not have much effect on the trend as shown in Figure 5.10 and no additional values near the 1:1 line were incorporated. The PLAXIS results fit within the general trend of the failed test (Database 1) and thus resulted in greater confidence in testing data. Greater confidence in the data resulted in a lower standard deviation and since the mean remained almost constant, greater $\emptyset_{PO}$ values were calibrated.

- Similar to only Database 1 results, incorporating PLAXIS predictions resulted in an overestimate of the tail by the calculated Survival Analysis distributions as seen in Figure 3.7 (Section 3.3). As a result, it is important to use caution when using these pullout resistance factors as they do not accurately represent the lowest measured bond resistance values. It is also important to note that since the normal and lognormal Survival Analysis distribution results are very similar, very similar $\emptyset_{PO}$ were calibrated.

- Little change in the calibrated $\emptyset_{PO}$ values were found when Database 4 was incorporated into databases 1 and 2, in some cases the values were the same while others were 0.01 greater (Figure 5.14).
  - As stated earlier (Section 2.3), Database 4 did not have a great effect on trends of Database 1 (although the standard deviation decreases), and thus did not have a great effect when Databases 1 and 2 were combined.
  - Similar trends to when Databases 1 and 2 were combined for the Survival Analysis results were shown when Database 4 was added. As a result, conclusions made previously for Cumulative Databases 1 and 2 can be concluded when Database 4 was incorporated (Figure 3.8, Section 3.3).
- Combining Database 3 with Database 1 resulted in higher $\emptyset_{PO}$ values from Survival Analysis, and substantially higher values than the NCHRP Report 701 (0.3 or greater) are obtained. Results of combining Databases 1 and 3 are shown in Figure 5.15.
  - As noted in Section 2.3, the greatest bias values are those of non-failed tests and resulted in a slightly greater bias trend than with only Database 1. This induced a greater mean of the pullout resistance bias and greater uncertainty in the testing results. The increase in bias and slightly higher standard deviation values for Survival Analysis results lead to the higher calibrated $\emptyset_{PO}$ values.

- Survival Analysis shown in Section 3.3, Figure 3.9 for the combination of Databases 1 and 3 showed a slight overestimate of the three lowest measured values but show conservatism for the rest of the tail data. It is interesting to note that although the normal and lognormal distributions showed a very similar trend, lognormal $\emptyset_{PO}$ values had a tendency to be at least 0.04 greater than the normally distributed pullout resistance factors. Since the lowest measured values were not represented in the Survival Analysis distributions, the calibrated $\emptyset_{PO}$ should be used with caution.

- The lowest $\emptyset_{PO}$ values of any database or cumulative database are calculated when Databases 1, 2 and 3 are combined and normally distributed. It is shown in Figure 5.16 that the lognormally distributed Survival Analysis results remained above the NCHRP Report 701 results.
  - It was stated previously, that the mean decreased and standard deviation increases when Databases 1 and 2 were combined, and that the uncertainty increased when Database 3 was added to Database 1. As a result, the standard deviation for the Survival Analysis normal distribution is the highest of all the cumulative databases (Table 5.4), and thus the lowest calibrated $\emptyset_{PO}$ values are the result.
  - The calculated distributions by the SAS® program for Survival Analysis and combining Databases 1, 2 and 3 resulted in a substantial conservatism for the tail of the data (Figure 3.10). This fact is evident in the low $\emptyset_{PO}$ calibrated (especially the normal distribution) as shown in Table 5.4 and these values are highly conservative.
- When Databases 1, 4 and 5 are compiled, the highest $\emptyset_{PO}$ values were calibrated. Thus adding PLAXIS and non-failed tests to Database 1, resulted in greater $\emptyset_{PO}$ values.

- The highest values for the bias were seen in non-failed tests as shown in Section 2.3 (Figure 2.14), and resulted in an increase in the mean of the bias. Although slightly higher mean of the bias values were seen when Databases 1 and 3 were combined, the addition of PLAXIS results and subsequently subtraction of these non-failed tests from Database 3 (Database 5) resulted in a decrease in standard deviation. Thus, possessing slightly lower mean values and lower standard deviation values than just Databases 1 and 3 resulted in higher calibrated $\emptyset_{PO}$ values.
- Again, the lowest measured bias values are overestimated by the Survival Analysis distributions while other tail data is underestimated (Figure 3.11, Section 3.3). An overestimated $\emptyset_{PO}$ was the result of the tail overestimation and these values should be used with caution.

- When all of the literature and this study values are combined (Databases 1, 2, 4 and 5), some of the lowest $\emptyset_{PO}$ were calibrated.
  - As stated in Section 2.3, results when all of the data are combined are very similar to the combination of Databases 1, 2 and 3. Thus similar results for the calibrated resistance factors were calculated.
  - The distributions underestimated the bias values for the tail of the data as shown in Section 3.3, Figure 3.12. The relatively low resistance factors calibrated are the result of this tail conservatism.

Table 5.4: Summary of calibrated pullout resistance factors.

Database(s)	Distribution	Analysis Method	Number of Tests Included		Mean (μ_{PO})	Standard Deviation (σ_{PO})	ϕ_{PO}				
			Failed	Non-Failed			$\gamma_Q = 1.00$	$\gamma_Q = 1.35$	$\gamma_Q = 1.50$	$\gamma_Q = 1.60$	$\gamma_Q = 1.75$
1	Normal	Fitted	25	0	1.490	0.350	0.61	0.82	0.91	0.97	1.06
	Lognormal	Fitted	25	0	0.360	0.250	0.66	0.89	0.98	1.05	1.15
	Normal	Survival	25	0	1.622	0.289	0.78	1.04	1.16	1.24	1.35
	Lognormal	Survival	25	0	0.467	0.187	0.79	1.07	1.20	1.28	1.40
2	Lognormal	Fitted	45	0	0.030	0.050	0.51	0.69	0.77	0.82	0.90
1 and 2	Normal	Fitted	70	0	1.070	0.100	0.58	0.78	0.87	0.92	1.01
	Lognormal	Fitted	70	0	0.070	0.100	0.58	0.78	0.87	0.93	1.01
	Normal	Survival	70	0	1.305	0.332	0.49	0.67	0.74	0.78	0.86
	Lognormal	Survival	70	0	0.236	0.243	0.58	0.78	0.87	0.93	1.02
1 and 4	Normal	Fitted	28	0	1.500	0.330	0.65	0.86	0.96	1.03	1.12
	Lognormal	Fitted	28	0	0.356	0.235	0.69	0.90	1.00	1.07	1.16
	Normal	Survival	28	0	1.639	0.278	0.79	1.07	1.19	1.28	1.39
	Lognormal	Survival	28	0	0.479	0.180	0.81	1.09	1.21	1.29	1.41
1, 2 and 4	Normal	Fitted	73	0	1.075	0.100	0.58	0.78	0.87	0.93	1.02
	Lognormal	Fitted	73	0	0.075	0.105	0.58	0.78	0.87	0.93	1.01
	Normal	Survival	73	0	1.325	0.339	0.50	0.67	0.74	0.79	0.86
	Lognormal	Survival	73	0	0.250	0.247	0.59	0.79	0.88	0.94	1.03
1 and 3	Normal	Survival	25	22	1.849	0.392	0.81	1.09	1.21	1.29	1.41
	Lognormal	Survival	25	22	0.605	0.239	0.85	1.15	1.27	1.36	1.49
1, 2 and 3	Normal	Survival	45	22	1.474	0.449	0.42	0.57	0.63	0.68	0.74
	Lognormal	Survival	45	22	0.354	0.316	0.58	0.79	0.88	0.94	1.02
1, 4 and 5	Normal	Survival	28	19	1.821	0.370	0.81	1.10	1.22	1.30	1.43
	Lognormal	Survival	28	19	0.588	0.225	0.85	1.15	1.28	1.36	1.49
1, 2, 4 and 5	Normal	Survival	73	19	1.466	0.439	0.44	0.59	0.65	0.70	0.76
	Lognormal	Survival	73	19	0.348	0.308	0.59	0.79	0.88	0.94	1.04

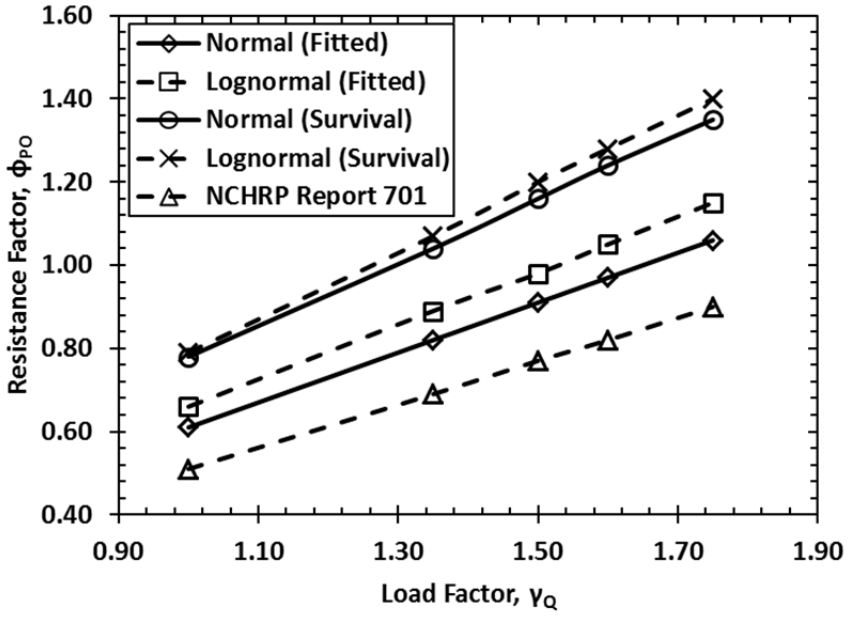

Figure 5.11: Load and resistance factors for fitted and Survival Analysis, normally and lognormally distributed from Database 1.

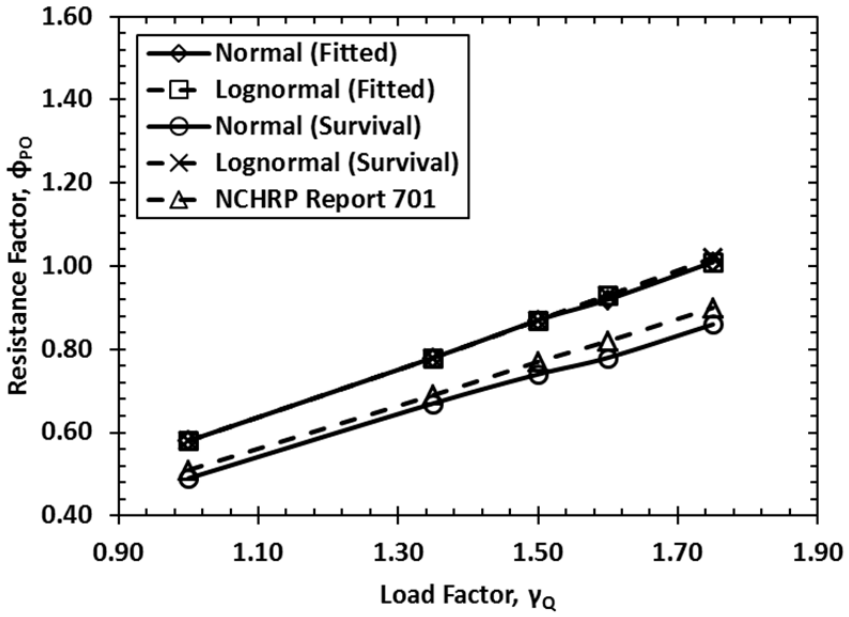

Figure 5.12: Load and resistance factors for fitted and Survival Analysis, normally and lognormally distributed from Databases 1 and 2.

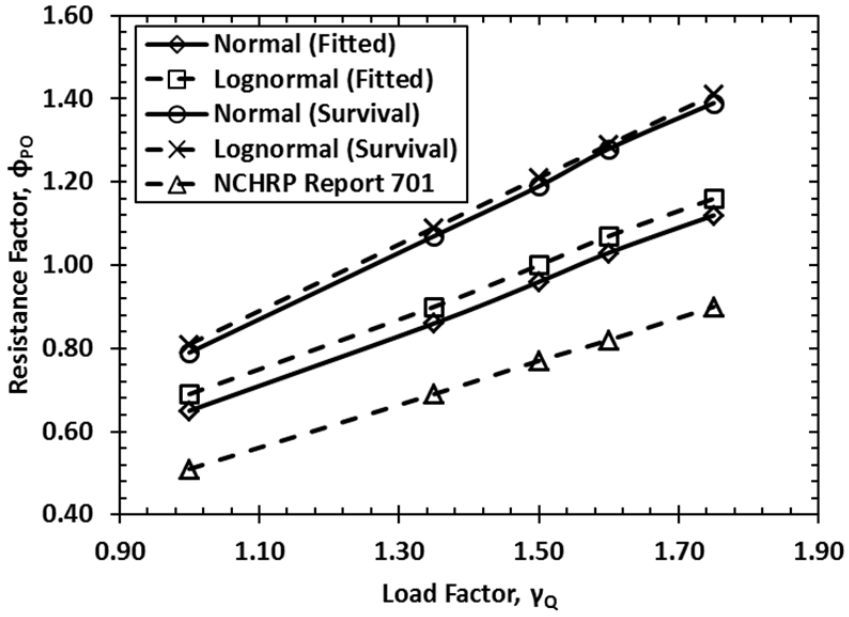

Figure 5.13: Load and resistance factors for fitted and Survival Analysis, normally and lognormally distributed from Databases 1 and 4.

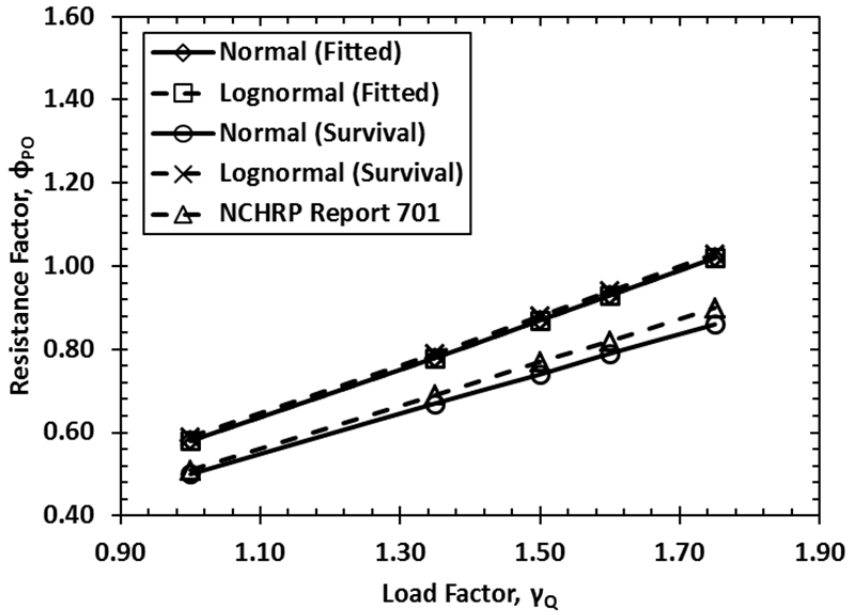

Figure 5.14: Load and resistance factors for fitted and Survival Analysis, normally and lognormally distributed from Databases 1, 2 and 4.

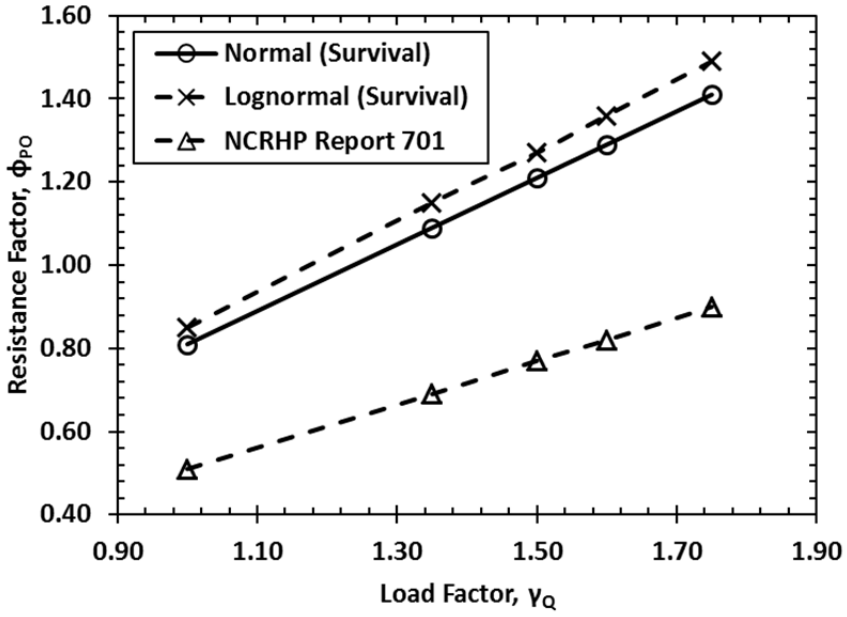

Figure 5.15: Load and resistance factors for Survival Analysis, normally and lognormally distributed from Databases 1 and 3.

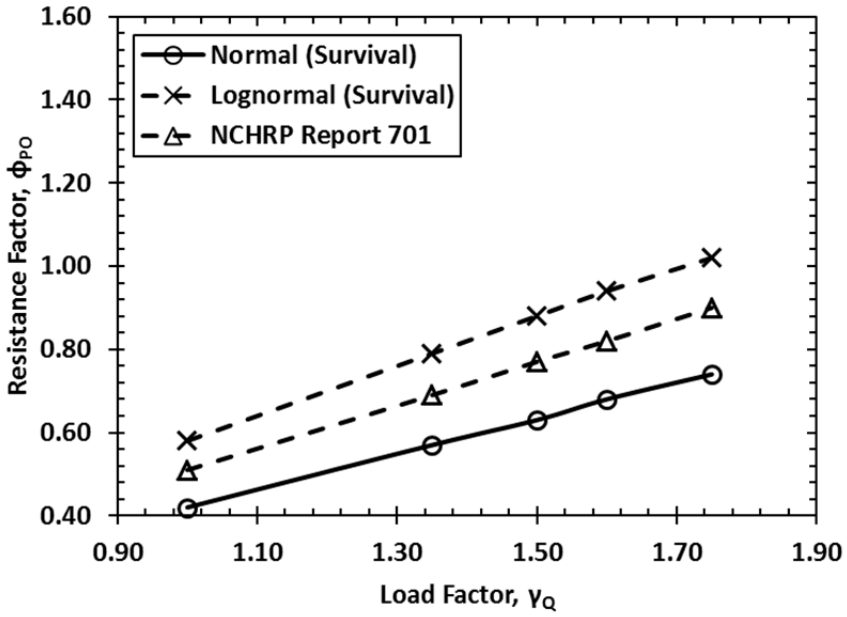

Figure 5.16: Load and resistance factors for Survival Analysis, normally and lognormally distributed from Databases 1, 2 and 3.

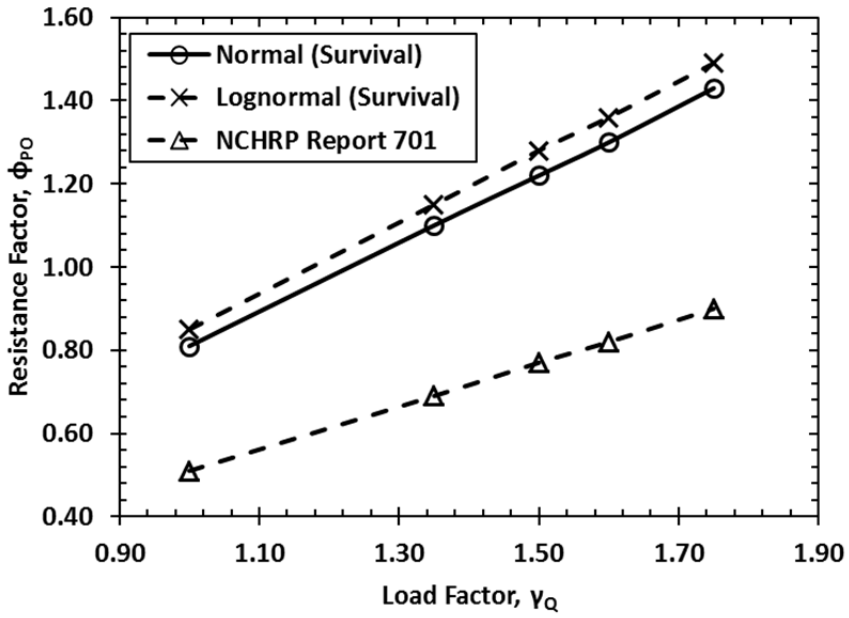

Figure 5.17: Load and resistance factors for Survival Analysis, normally and lognormally distributed from Databases 1, 4 and 5.

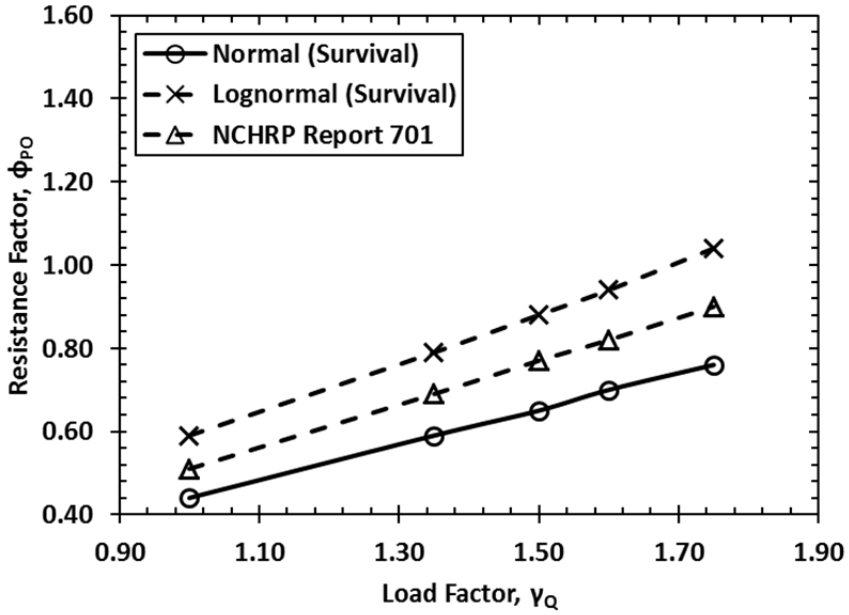

Figure 5.18: Load and resistance factors for Survival Analysis, normally and lognormally distributed from Databases 1, 2, 4 and 5.

Chapter 6

SNAILZ

6.1 Literature Review and Background

6.1.1 *Capabilities and Limitations*

SNAILZ models bi-linear and tri-linear failure planes that can exist at or beyond the toe of the SNW. The analysis is conducted with a fully balanced force equilibrium equation with only the soil interslice forces (Caltrans, 2007). For the SNW analysis to be conducted, the following information is required:

- search limit,
- wall geometry,
- reinforcement parameters, and
- soil parameters (up to 7 soil layers).

Additional information may be added to enhance the usefulness of SNAILZ for design purposes as follows:

- earthquake acceleration,
- surcharge(s),
- slope below and above the wall,
- external horizontal force,
- water surface, and
- specified failure plane (Caltrans, 2007).

Although SNAILZ is ASD based, it has the possibility to incorporate a limited amount of LRFD method analysis, but required that the resistance factors be calibrated with a load factor of 1.0. As stated in Section 5.1.1.2, the design is consistent with the Service Limit state when the global factor of safety (FS_G) and load factors are equal to 1.0. In addition, the option “pre-factored” in SNAILZ must be selected for the soil

parameters to affect the FS_G. This selection also allows for reduced values of pullout and facing resistance, nail tensile and requires the following equations to be employed and imputed into SNAILZ (Lazarte, 2011):

$$\varphi(input) = \tan^{-1}(\emptyset_s \tan\varphi) \quad 49$$

$$c'(input) = c'\emptyset_s \quad 50$$

$$q(input) = q_u BSF \quad 51$$

$$Facing\ resistance\ (input) = facing\ resistance * \emptyset_{FF} \quad 52$$

$$Tensile\ resistance\ (force, imput) = tensile\ resistance(force) * \emptyset_T \quad 53$$

$$Tensile\ resistance\ (stress, input) = tensile\ resisance\ (stress) * \emptyset_T \quad 54$$

where φ is the friction angle of the soil, q_u is ultimate pullout resistance of the soil nail, BSF is the bond stress factor (or pullout resistance factor, $\emptyset_{PO}$) and the other parameters are defined in Table 6.1.

Table 6.1: Resistance factors for overall stability (Lazarte, 2011).

Resistance Factor	Value
Soil Shear Resistance, $\emptyset_s$	0.65
Nail Pullout Resistance, $\emptyset_{PO}$	0.49
Nail Tendon Resistance, $\emptyset_T$	0.56
Nail Head Resistance, $\emptyset_{FF}$	0.67

A comparison between the ASD and LRFD methods with SNAILZ were presented in the NCRHP Report 701. This comparison resulted in little change in the SNW layout between the two design methods, and was due to the BSF and $\emptyset_{PO}$ values of the ASD and LRFD methods being very similar. As a result, changing design methodologies from ASD to LRFD with only resulted in a change of the design format (Lazarte, 2011).

6.2 Analysis Procedure

Soil nail walls that were constructed for the LBJ Express construction project can be seen in Figure 6.1 and Figure 6.2. Additional necessary SNW properties are shown in Table 6.2 and calculations are in Appendix C. The effective cohesion and effective friction angle are a result of many Consolidated Undrained Triaxial Tests conducted by Terracon throughout the project site (Table D.1), while the yield stress of reinforcement and punching shear are used in SNW design by Craig Olden, Inc. LRFD resistance factors for soil shear resistance and nail resistances used for this study are found from the NCHRP Report 701 (Table 6.1). Incorporating those parameters, comparison between ASD and LRFD methods with a load factor equal to 1.0 was conducted with the following procedure.

1. ASD method was completed with soil properties in Figure 6.1 and the length of the nail was adjusted until a global factor of safety (FS_G) equal to 1.5 was achieved. This provided a soil nail length for use in the ASD to LRFD comparison.
2. To verify that LRFD is equal to the ASD method when adjusted soil parameters (Table 6.2) were incorporated and FS_G of 0.97 was computed; only the soil parameters from Step 1 were changed to adjusted values (Appendix C) and comparison was made.
3. LRFD method (load factor of 1.0) was utilized in SNAILZ by adjusting the soil nail length until a FS_G value was equal 1.0, for $\emptyset_{PO}$ of between 0.4 to 0.85 in 0.05 increments (encompassing all calibrated resistance factors).

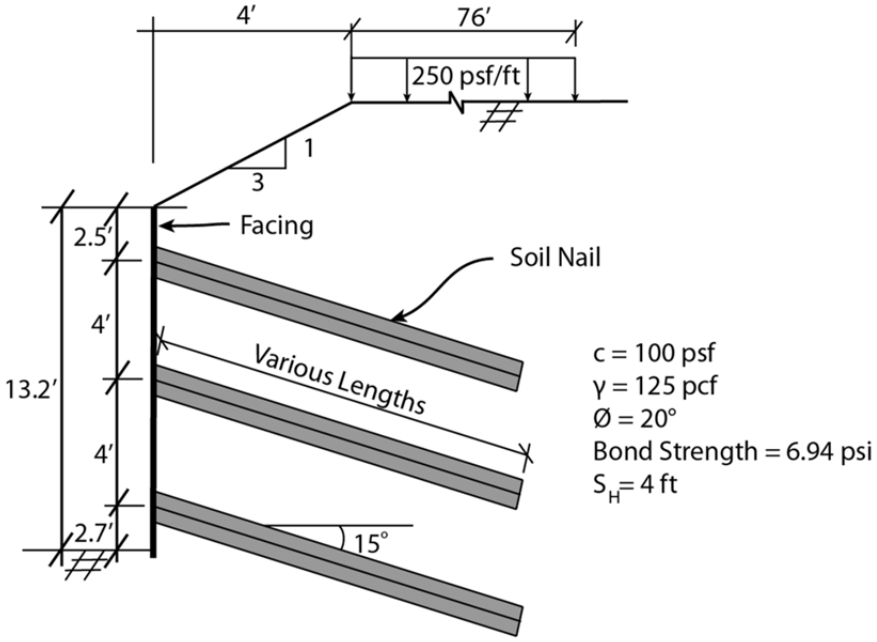

Figure 6.1: Soil nail wall layout 1 for comparison in SNAILZ.

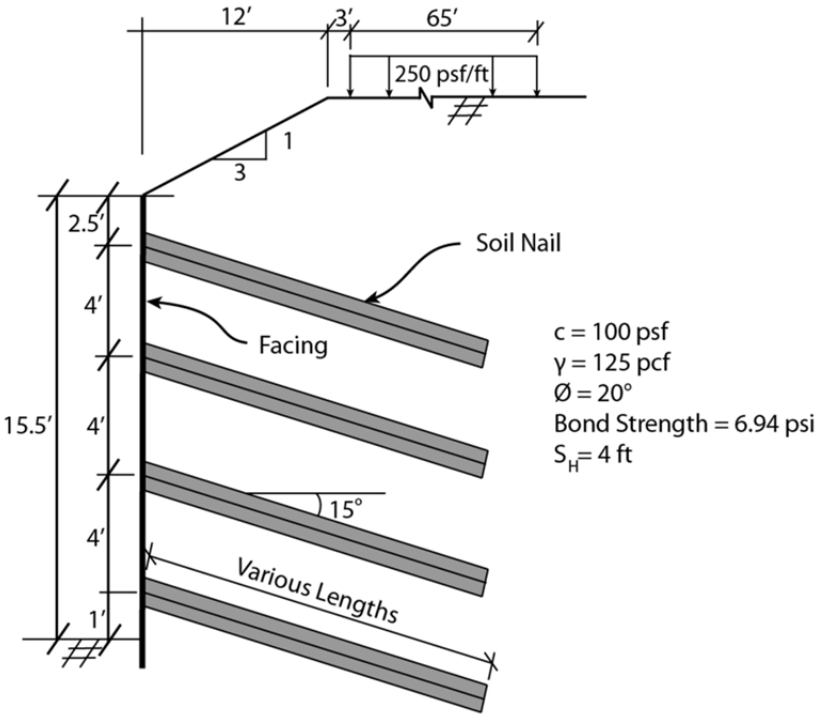

Figure 6.2: Soil nail wall layout 2 for comparison in SNAILZ.

Table 6.2: Soil nail wall and soil properties.

Parameter	Value
Unit Weight, Adjusted (pcf)	125.0
Effective Friction Angle, Adjusted (Degrees)	13.3
Effective Cohesion, Adjusted (psf)	65.0
Yield Stress of Reinforcement (ksi)	41.3
Punching Shear (kips)	35.8
Diameter of Grouted Hole (inch)	6.0
Bar Diameter (inch)	1.0
BSF	0.5

6.3 Results and Conclusions

Required soil nail length results from the procedure shown in Section 6.2 are shown in Table 5.4, Figure 6.3 and Figure 6.4. These calculated lengths incorporate calibrated resistance factors (Table 5.4, Section 5.3) for a load factor of 1.0, and results and conclusions of the analysis are listed subsequently.

- As the resistance factor increased, the required soil nail length decreased.
    - A higher pullout resistance factor results in a higher ultimate bond strength of the soil nail and thus less length is required to provide the same resistance and FS_G.
- Comparison between ASD ($FS_G = 1.5$) and LRFD ($\lambda_Q = 1.0,\ FS_G = 0.97$) methods with the BSF equal to $\emptyset_{PO}$ resulted in the same required nail length. This confirmed that the two methods can be related and compared by using the previously mentioned procedure.
- The required nail length between the ASD method and the largest $\emptyset_{PO}$ calibrated in this study was 6.5 feet, a different of 28.3 percent (Table 6.3) for both SNWs. This resulted in a substantial length difference and as a result, potential cost savings.

Table 6.3: Comparison of required nail length using ASD and LRFD methods.

Design Method	BSF	Φ_{PO}	Layout 1		Layout 2	
			Nail Length (ft)	Percent Difference (%)	Nail Length (ft)	Percent Difference (%)
ASD ($FS_G = 1.5$)	0.5	-	23.0	-	24.0	-
LRFD ($\lambda_Q = 1.0$)	-	0.40	27.5	+19.6	28.0	+17.4
LRFD ($\lambda_Q = 1.0$)	-	0.45	25.0	+8.7	26.0	+8.7
LRFD ($\lambda_Q = 1.0$)	-	0.50	23.0	0.0	24.0	0.0
LRFD ($\lambda_Q = 1.0$)	-	0.55	21.5	-6.5	22.5	-6.5
LRFD ($\lambda_Q = 1.0$)	-	0.60	20.5	-10.9	21.5	-10.9
LRFD ($\lambda_Q = 1.0$)	-	0.65	19.5	-15.2	20.5	-15.2
LRFD ($\lambda_Q = 1.0$)	-	0.70	18.5	-19.6	19.5	-19.6
LRFD ($\lambda_Q = 1.0$)	-	0.75	17.5	-23.9	19.0	-21.7
LRFD ($\lambda_Q = 1.0$)	-	0.80	17.0	-26.1	18.5	-23.9
LRFD ($\lambda_Q = 1.0$)	-	0.85	16.5	-28.3	17.5	-28.3

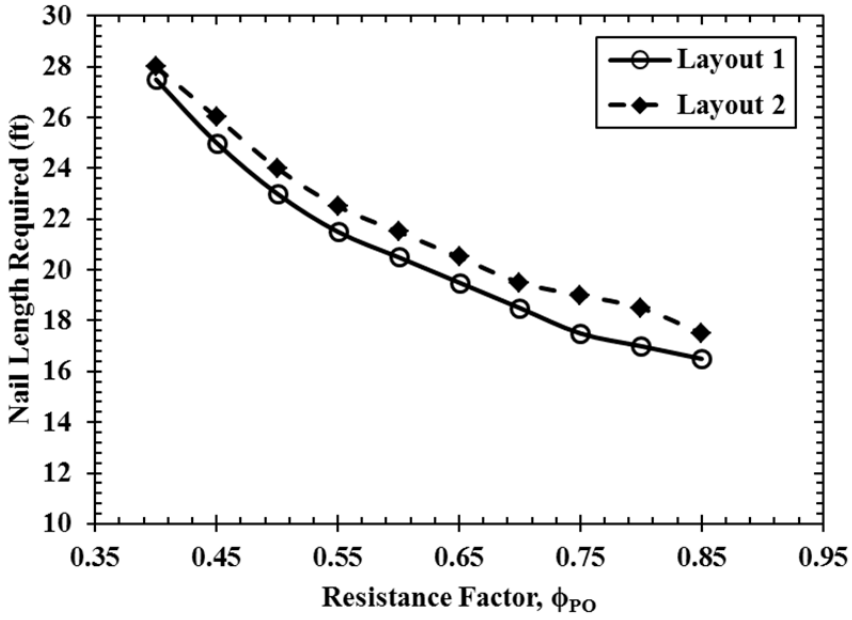

Figure 6.3: Required soil nail length with various resistance factors calculated by SNAILZ (λ_Q = 1.0).

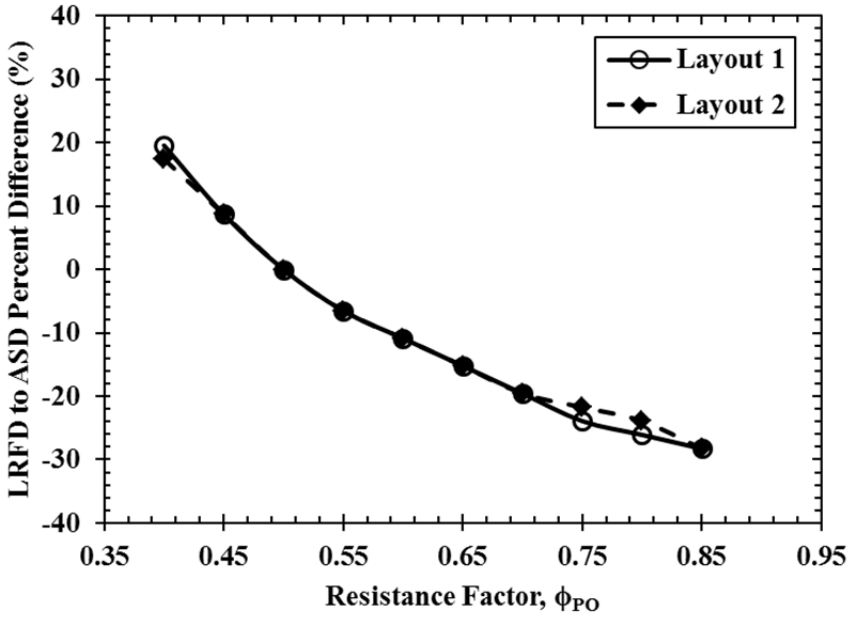

Figure 6.4: Percentage difference in nail length between LRFD and ASD methods for various resistance factors calculated by SNAILZ (λ_Q = 1.0).

Chapter 7

General Results and Conclusions

The main objective of achieving a greater understanding of the soil nail bond strength between cohesive soil and grout in North Dallas Texas was achieved through the use of the following:

- analysis of the verification test data,
- Survival Analysis,
- PLAXIS 2D,
- LRFD resistance factor calibration, and
- SNAILZ.

Important information, results, comments and conclusions of the entire study are stated subsequently.

- Three failure criteria were implemented to define the ultimate bond strength between soil and nail and allowed for 25 verification tests to be interpreted as meeting failure criteria.
- Soil nail test data found in literature and from this study (failed, non-failed, and PLAXIS predicted) were separated into databases and then combined to conduct Survival Analysis and LRFD resistance factor calibration.
    - Testing results found in the NCHRP Report 701 tended to have a bias around 1.0, while testing results from North Dallas Texas were shown to have a tendency toward greater bias values.
- Survival Analysis was conducted to either incorporate non-failed test data into the normal or lognormal distributions or to fit distributions to the databases.
    - Calculated Survival Analysis had a tendency to overestimate the tail of the data, resulting in resistance factors that should be used with caution.

- Non-failed tests were successfully incorporated in the databases and tended to increase the mean and standard deviation of the distributions.

- PLAXIS 2D using the Axisymmetric and either the Mohr-Coulomb or Hardening Soil models were successful in fitting to the failed test results and in predicting the failure of three verification tests.
  - The cohesion and friction angle for the PLAXIS models have a tendency toward higher values than what was shown in the Consolidated Undrained Triaxial Tests within the project area.
  - The initial elastic modulus from the Triaxial Tests results showed a substantial overestimation of the E values calibrated in PLAXIS.
  - An overestimate by the Triaxial Testing E_{50} results compared to values in PLAXIS was shown when the MC model was used to characterize the soil.
  - PLAXIS calibrated E_{50}^{ref} values for the HS model showed a tendency to follow the average E_{50} values interpreted from Triaxial Tests results.
- Pullout resistance factor LRFD calibration was successfully conducted for the various databases and load factors of 1.0, 1.35, 1.5, 1.6 and 1.75.
  - Fitted distributions to the data showed a tendency toward slightly underestimating tail data while considerably underestimating the rest of the data.
  - Survival Analysis distributions fit the data set as a whole, but tended to overestimate tail data. This led to resistance factors that did not incorporate the lowest measured data and thus should be used with caution.

- Comparison between the ASD method and LRFD (load factor of 1.0) was successfully conducted using SNAILZ.
    - Implementing LRFD calibrated resistance factors allowed for a decrease in the required soil nail length for the majority of calibrated resistance factors and could lead to substantial cost savings.
- It should be noted that the calibrated resistance factors are biased towards soils within the testing region and may not accurately represent cohesive soils in other areas.

Appendix A

Soil Nail Test Databases

Table A.1: Database 1 – verification tests from North Dallas meeting failure criteria.

No.	Type of Natural Materal	Soil Type	Location	Bond Length, L_B (ft)	Unbonded Length L_U (ft)	Drill-Hole Diameter, D_{DH} (in.)	Nail Bar Diameter, D_B (in.)	Design Load, DL (kips)	Test Design Load, DL (kips)	Estimated Pullout Resistance, Q (kips/ft)	Predicted Resistance (kips)	Measured Resistance (kips)
1	Fine-grained	Clay	Dallas, TX	17	3	6	1	13.3	13.5	1.6	26.7	27.0
2	Fine-grained	Clay	Dallas, TX	10	3	6	0.75	7.9	8.0	1.6	15.7	16.0
3	Fine-grained	Clay	Dallas, TX	10	3	6	0.75	7.9	10.0	1.6	15.7	20.0
4	Fine-grained	Clay	Dallas, TX	10	3	6	0.75	7.9	11.0	1.6	15.7	22.0
5	Fine-grained	Clay	Dallas, TX	10	3	6	1	7.9	11.0	1.6	15.7	22.0
6	Fine-grained	Clay	Dallas, TX	17	3	6	1	13.3	20.0	1.6	26.7	40.0
7	Fine-grained	Clay	Dallas, TX	17	3	6	1	13.3	20.0	1.6	26.7	40.0
8	Fine-grained	Clay	Dallas, TX	17	3	6	1	13.3	20.0	1.6	26.7	40.0
9	Fine-grained	Clay	Dallas, TX	10	3	6	0.75	7.9	12.0	1.6	15.7	24.0
10	Fine-grained	Clay	Dallas, TX	10	3	6	0.75	7.9	12.0	1.6	15.7	24.0
11	Fine-grained	Clay	Dallas, TX	10	3	6	0.75	7.9	12.0	1.6	15.7	24.0
12	Fine-grained	Clay	Dallas, TX	17	3	6	1	13.3	21.5	1.6	26.7	43.0
13	Fine-grained	Clay	Dallas, TX	7	3	6	1	5.5	9.0	1.6	11.0	18.0
14	Fine-grained	Clay	Dallas, TX	10	3	6	0.75	7.9	13.0	1.6	15.7	26.0
15	Fine-grained	Clay	Dallas, TX	10	3	6	0.75	7.9	13.0	1.6	15.7	26.0
16	Fine-grained	Clay	Dallas, TX	10	3	6	1	7.9	13.5	1.6	15.7	27.0
17	Fine-grained	Clay	Dallas, TX	10	3	6	1	7.9	13.5	1.6	15.7	27.0
18	Fine-grained	Clay	Dallas, TX	7	3	6	1	5.5	9.5	1.6	11.0	19.0
19	Fine-grained	Clay	Dallas, TX	7	3	6	1	5.5	9.5	1.6	11.0	19.0
20	Fine-grained	Clay	Dallas, TX	12	3	6	1	9.4	16.5	1.6	18.8	33.0
21	Fine-grained	Clay	Dallas, TX	10	3	6	0.75	7.9	14.0	1.6	15.7	28.0
22	Fine-grained	Clay	Dallas, TX	10	3	6	0.75	7.9	15.0	1.6	15.7	30.0
23	Fine-grained	Clay	Dallas, TX	10	3	6	1	7.9	16.5	1.6	15.7	33.0
24	Fine-grained	Clay	Dallas, TX	10	3	6	1	7.9	16.5	1.6	15.7	33.0
25	Fine-grained	Clay	Dallas, TX	7	3	6	1	5.5	12.5	1.6	11.0	25.0

Table A.2: Database 2 – test results from the NCHRP Report 701 (Lazarte, 2011).

No.	Type of Natural Materal	Soil Type	Location	Bond Length, L_B (ft)	Unbonded Length L_U (ft)	Drill-Hole Diameter, D_{DH} (in.)	Nail Bar Diameter, D_B (in.)	Design Load, DL (kips)	Test Design Load, DL (kips)	Estimated Pullout Resistance, Q (kips/ft)	Predicted Resistance (kips)	Measured Resistance (kips)
1	Fine-grained	Sandy Clay	San Luis Obispo, CA	11	18	6	1 (6)	15.8	17.6	1.6	35.2	31
2	Fine-grained	Sandy Clay	San Luis Obispo, CA	13	13	6	0.875	15.8	20.8	1.6	41.6	37
3	Fine-grained	Clay	Solana Beach, CA	15.3	6.5	8	1	22	16.83	1.1	33.66	31
4	Fine-grained	Clay	Solana Beach, CA	17	4	8	1	22	18.7	1.1	37.4	35.7
5	Fine-grained	Clay	Solana Beach, CA	16	7.5	8	1	22	17.6	1.1	35.2	33.8
6	Fine-grained	Clay	Solana Beach, CA	16.75	6.5	8	1	22	18.425	1.1	36.85	35.6
7	Fine-grained	Clay	Solana Beach, CA	16.8	6.5	8	1	22	18.48	1.1	36.96	35.9
8	Fine-grained	Clay	Solana Beach, CA	15.4	6.5	8	1	22	16.94	1.1	33.88	33
9	Fine-grained	Clay	Solana Beach, CA	16.4	12.5	8	1	22	18.04	1.1	36.08	35.4
10	Fine-grained	Clay	Solana Beach, CA	15.25	13.5	8	1	22	16.775	1.1	33.55	33
11	Fine-grained	Clay	Solana Beach, CA	13	14	8	1	22	14.3	1.1	28.6	28.3
12	Fine-grained	Clay	Guadalupe River, CA	10	15	8	0.875	13.6	13.6	1.4	27.2	27
13	Fine-grained	Clay	Solana Beach, CA	13	8	8	1	22	14.3	1.1	28.6	28.5
14	Fine-grained	Clay	Solana Beach, CA	14.5	12	8	1	22	15.95	1.1	31.9	31.9
15	Fine-grained	Clay	Solana Beach, CA	14.2	8.8	8	1	22	15.62	1.1	31.24	31.4
16	Fine-grained	Clay	Solana Beach, CA	14.2	9.3	8	1	15.6	15.62	1.1	31.24	31.6
17	Fine-grained	Clay	Solana Beach, CA	15	8.2	8	1	22	16.5	1.1	33	33.5
18	Fine-grained	Clay	Solana Beach, CA	15.4	17.8	8	1	22	16.94	1.1	33.88	34.6
19	Fine-grained	Clay	Solana Beach, CA	16.75	6.5	8	1	22	18.425	1.1	36.85	37.8
20	Fine-grained	Clay	Solana Beach, CA	12	10.5	8	1	22	13.2	1.1	26.4	27.2
21	Fine-grained	Clay	Solana Beach, CA	15.5	7.7	8	1	22	17.05	1.1	34.1	35.3
22	Fine-grained	Clay	Solana Beach, CA	15.5	8	8	1	22	17.05	1.1	34.1	35.5
23	Fine-grained	Clay	Solana Beach, CA	17.8	5	8	1	22	19.58	1.1	39.16	40.9

Table A.2 – *Continued*

24	Fine-grained	Clay	Solana Beach, CA	17.3	5.7	8	1	22	19.03	1.1	38.06	40
25	Fine-grained	Clay	Solana Beach, CA	16.8	6.25	8	1	22	18.48	1.1	36.96	39
26	Fine-grained	Clay	Solana Beach, CA	17.25	5.7	8	1	22	18.975	1.1	37.95	40.2
27	Fine-grained	Clay	Solana Beach, CA	16.8	6	8	1	22	18.48	1.1	36.96	39.4
28	Fine-grained	Clay	Guadalupe River, CA	7.5	15	8	0.875	13.6	10.2	1.4	20.4	22
29	Fine-grained	Clay	Guadalupe River, CA	10	20	6	0.875	13.6	13.6	1.4	27.2	30
30	Fine-grained	Clay	Guadalupe River, CA	10	15	8	0.875	13.6	13.6	1.4	27.2	31
31	Fine-grained	Clay	Guadalupe River, CA	10	15	8	0.875	13.6	13.6	1.4	27.2	32
32	Fine-grained	Silty Clay	Chattanooga, TN	8	NA	6	1	16	16	2.0	32	38
33	Fine-grained	Clay	Guadalupe River, CA	10	20	6	0.875	13.6	13.6	1.4	27.2	33
34	Fine-grained	Clay	Guadalupe River, CA	10	15	8	0.875	13.6	13.6	1.4	27.2	33.5
35	Fine-grained	Clay	Guadalupe River, CA	10	15	8	0.875	13.6	13.6	1.4	27.2	34
36	Fine-grained	Clay	Guadalupe River, CA	10	20	6	0.875	13.6	13.6	1.4	27.2	35
37	Fine-grained	Clay	Guadalupe River, CA	10	15	8	0.875	13.6	13.6	1.4	27.2	36
38	Fine-grained	Clay	Guadalupe River, CA	10	15	8	NA	13.6	13.6	1.4	27.2	37
39	Fine-grained	Clay	Guadalupe River, CA	10	15	8	0.875	13.6	13.6	1.4	27.2	38
40	Fine-grained	Sandy Lean Clay	San Luis Obispo, CA	10	10	6	0.875	15.8	16	1.6	32	46
41	Fine-grained	Clay	Guadalupe River, CA	10	15	8	0.875	13.6	13.6	1.4	27.2	40
42	Fine-grained	Clay	Guadalupe River, CA	10	20	8	0.875	13.6	13.6	1.4	27.2	41
43	Fine-grained	Clay	Guadalupe River, CA	10	15	8	0.875	13.6	13.6	1.4	27.2	42
44	Fine-grained	Clay	Guadalupe River, CA	10	15	8	0.875	13.6	13.6	1.4	27.2	43
45	Fine-grained	Clay	Guadalupe River, CA	10	15	8	0.875	13.6	13.6	1.4	27.2	44

Table A.3: Database 3 – verification tests from North Dallas not meeting failure criteria.

No.	Type of Natural Materal	Soil Type	Location	Bond Length, L_B (ft)	Unbonded Length, L_U (ft)	Drill-Hole Diameter, D_{DH} (in.)	Nail Bar Diameter, D_B (in.)	Design Load, DL (kips)	Test Design Load, DL (kips)	Estimated Pullout Resistance, Q (kips/ft)	Predicted Resistance (kips)	Measured Resistance (kips)
1	Fine-grained	Clay	Dallas, TX	17	3	6	1	13	13	1.6	26.7	27
2	Fine-grained	Clay	Dallas, TX	17	3	6	1	13	13	1.6	26.7	27
3	Fine-grained	Clay	Dallas, TX	10	3	6	0.75	8	8	1.6	15.7	26
4	Fine-grained	Clay	Dallas, TX	10	3	6	0.75	8	8	1.6	15.7	26
5	Fine-grained	Clay	Dallas, TX	10	3	6	0.75	8	8	1.6	15.7	26
6	Fine-grained	Clay	Dallas, TX	10	3	6	0.75	8	8	1.6	15.7	26
7	Fine-grained	Clay	Dallas, TX	10	3	6	0.75	5	5	1.6	15.7	26
8	Fine-grained	Clay	Dallas, TX	10	3	6	0.75	8	8	1.6	15.7	26
9	Fine-grained	Clay	Dallas, TX	10	3	6	0.75	8	8	1.6	15.7	26
10	Fine-grained	Clay	Dallas, TX	10	3	6	0.75	8	8	1.6	15.7	26
11	Fine-grained	Clay	Dallas, TX	10	3	6	0.75	8	8	1.6	15.7	26
12	Fine-grained	Clay	Dallas, TX	10	3	6	0.75	8	8	1.6	15.7	26
13	Fine-grained	Clay	Dallas, TX	10	3	6	0.75	8	8	1.6	15.7	26
14	Fine-grained	Clay	Dallas, TX	10	3	6	1	8	8	1.6	15.7	26
15	Fine-grained	Clay	Dallas, TX	10	3	6	0.75	8	8	1.6	15.7	26
16	Fine-grained	Clay	Dallas, TX	10	3	6	0.75	11	11	1.6	15.7	26
17	Fine-grained	Clay	Dallas, TX	17	3	6	1	9	9	1.6	26.7	45
18	Fine-grained	Clay	Dallas, TX	10	3	6	0.75	8	8	1.6	15.7	27
19	Fine-grained	Clay	Dallas, TX	17	3	6	1	13	13	1.6	26.7	47
20	Fine-grained	Clay	Dallas, TX	7	3	6	0.75	5	5	1.6	11.0	26
21	Fine-grained	Clay	Dallas, TX	12	3	6	1	9	9	1.6	18.8	45
22	Fine-grained	Clay	Dallas, TX	12	3	6	1	9	9	1.6	18.8	45

Table A.4: Database 4 – verification tests that were predicted by PLAXIS to fail.

No.	Type of Natural Materal	Soil Type	Location	Bond Length, L_B (ft)	Unbonded Length, L_U (ft)	Drill-Hole Diameter, D_{DH} (in.)	Nail Bar Diameter, D_B (in.)	Design Load, DL (kips)	Test Design Load, DL (kips)	Estimated Pullout Resistance, Q (kips/ft)	Predicted Resistance (kips)	Measured Resistance (kips)
1	Fine-grained	Clay	Dallas, TX	10	3	6	0.75	8	8	1.6	15.7	27
2	Fine-grained	Clay	Dallas, TX	10	3	6	0.75	8	8	1.6	15.7	28
3	Fine-grained	Clay	Dallas, TX	10	3	6	0.75	8	8	1.6	15.7	29

Table A.5: Database 5 – verification tests from North Dallas not predicted or seen to fail.

No.	Type of Natural Materal	Soil Type	Location	Bond Length, L_B (ft)	Unbonded Length, L_U (ft)	Drill-Hole Diameter, D_{DH} (in.)	Nail Bar Diameter, D_B (in.)	Design Load, DL (kips)	Test Design Load, DL (kips)	Estimated Pullout Resistance, Q (kips/ft)	Predicted Resistance (kips)	Measured Resistance (kips)
1	Fine-grained	Clay	Dallas, TX	17	3	6	1	13	13	1.6	26.7	27
2	Fine-grained	Clay	Dallas, TX	17	3	6	1	13	13	1.6	26.7	27
3	Fine-grained	Clay	Dallas, TX	10	3	6	0.75	8	8	1.6	15.7	26
4	Fine-grained	Clay	Dallas, TX	10	3	6	0.75	8	8	1.6	15.7	26
5	Fine-grained	Clay	Dallas, TX	10	3	6	0.75	5	5	1.6	15.7	26
6	Fine-grained	Clay	Dallas, TX	10	3	6	0.75	8	8	1.6	15.7	26
7	Fine-grained	Clay	Dallas, TX	10	3	6	0.75	8	8	1.6	15.7	26
8	Fine-grained	Clay	Dallas, TX	10	3	6	0.75	8	8	1.6	15.7	26
9	Fine-grained	Clay	Dallas, TX	10	3	6	0.75	8	8	1.6	15.7	26
10	Fine-grained	Clay	Dallas, TX	10	3	6	0.75	8	8	1.6	15.7	26
11	Fine-grained	Clay	Dallas, TX	10	3	6	1	8	8	1.6	15.7	26
12	Fine-grained	Clay	Dallas, TX	10	3	6	0.75	8	8	1.6	15.7	26
13	Fine-grained	Clay	Dallas, TX	10	3	6	0.75	11	11	1.6	15.7	26
14	Fine-grained	Clay	Dallas, TX	17	3	6	1	9	9	1.6	26.7	45
15	Fine-grained	Clay	Dallas, TX	10	3	6	0.75	8	8	1.6	15.7	27
16	Fine-grained	Clay	Dallas, TX	17	3	6	1	13	13	1.6	26.7	47
17	Fine-grained	Clay	Dallas, TX	7	3	6	0.75	5	5	1.6	11.0	26
18	Fine-grained	Clay	Dallas, TX	12	3	6	1	9	9	1.6	18.8	45
19	Fine-grained	Clay	Dallas, TX	12	3	6	1	9	9	1.6	18.8	45

Appendix B

Verification Test Results, PLAXIS 2D Fittings and Predictions

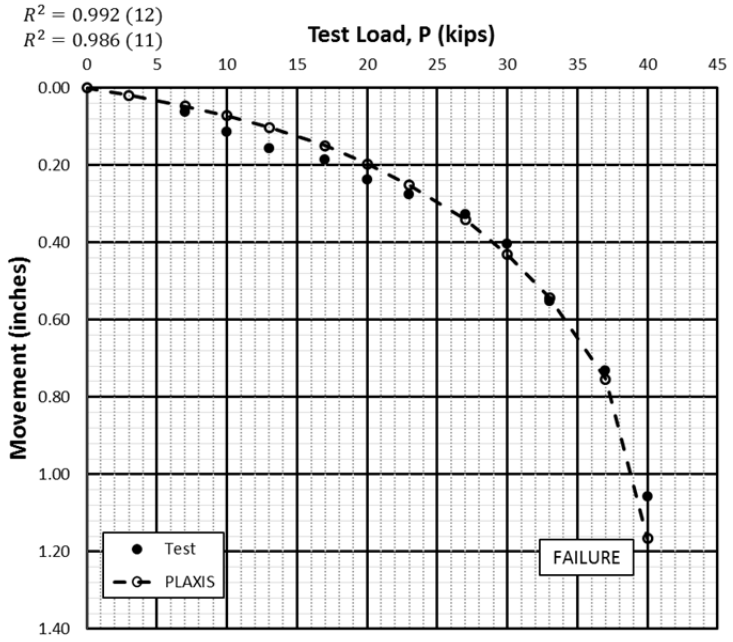

Figure B.1: Verification test data and PLAXIS (HS) fitting of Database 1(1).

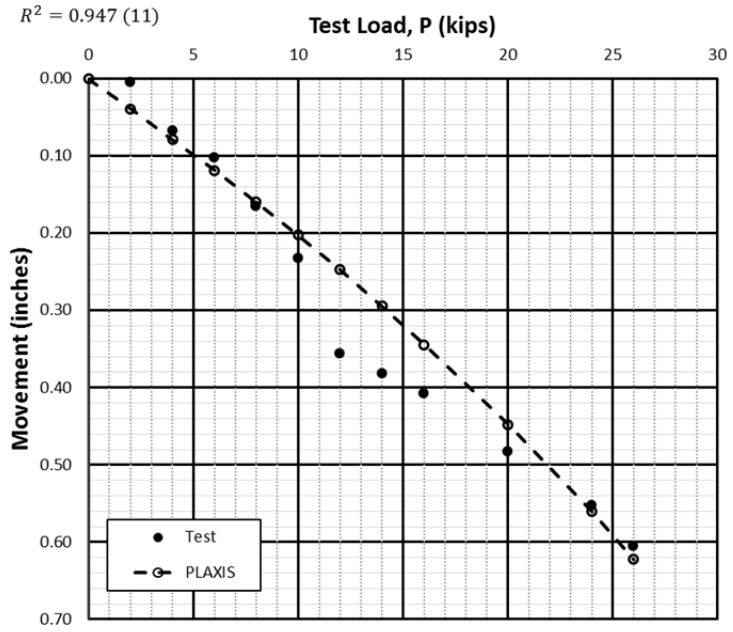

Figure B.2: Verification test data and PLAXIS (MC) fitting of Database 1(2).

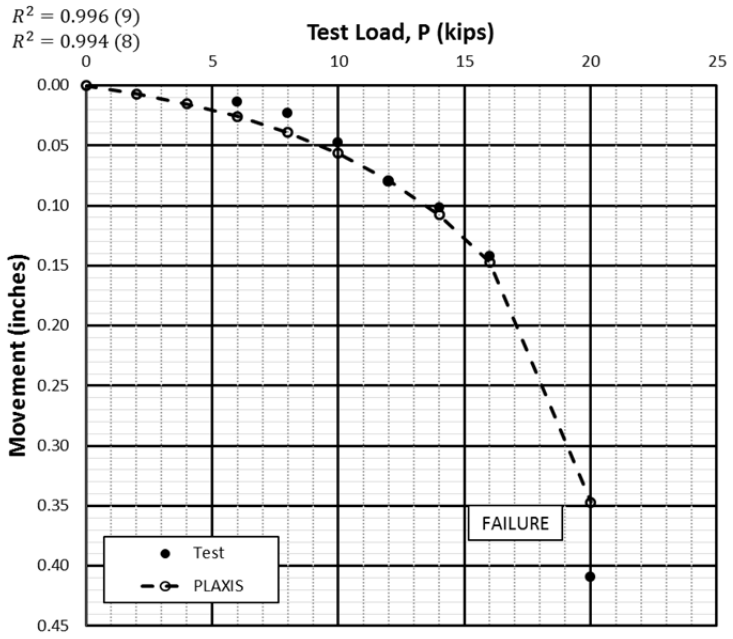

Figure B.3: Verification test data and PLAXIS (HS) fitting of Database 1(3).

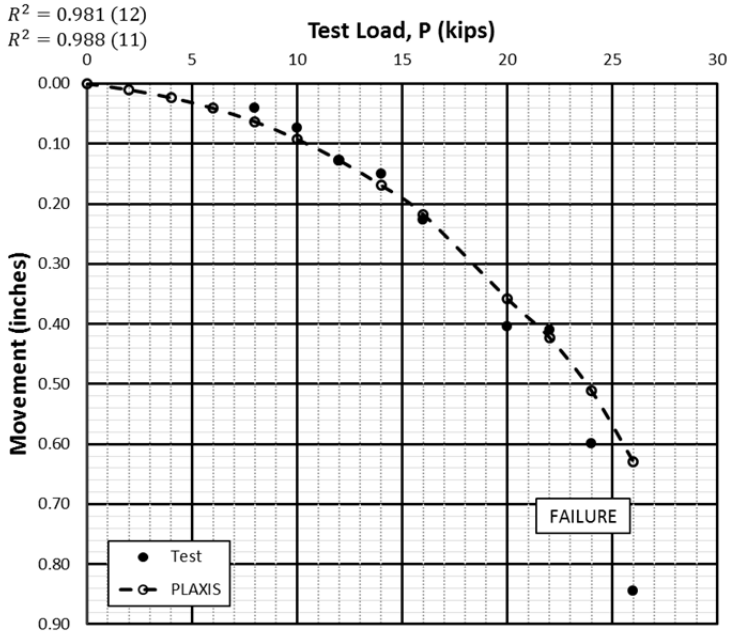

Figure B.4: Verification test data and PLAXIS (HS) fitting of Database 1(4).

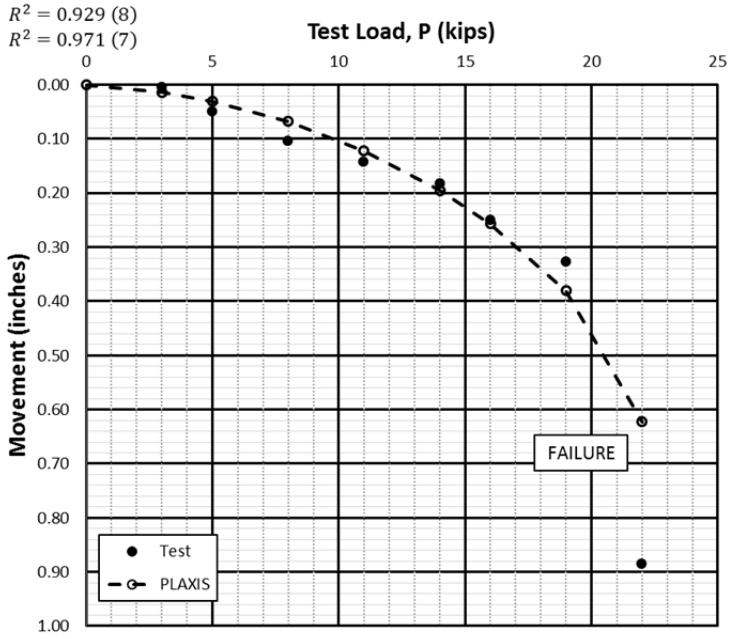

Figure B.5: Verification test data and PLAXIS (HS) fitting of Database 1(5).

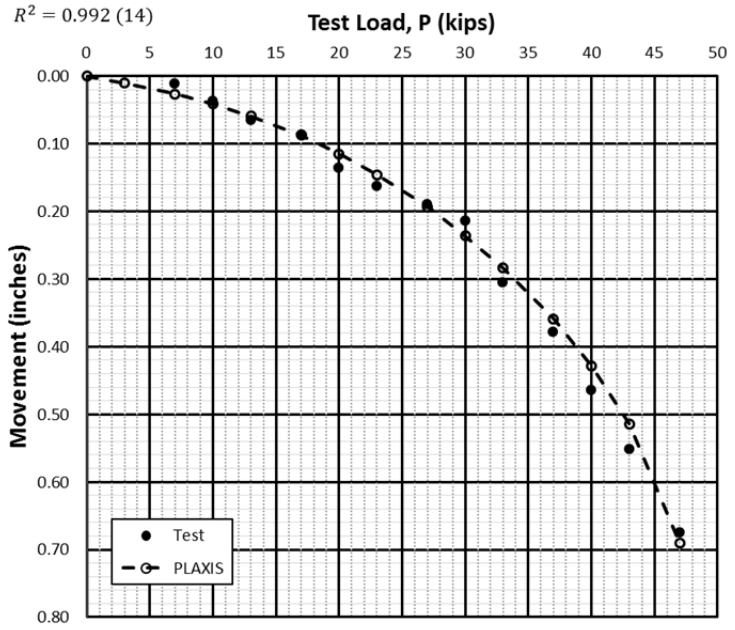

Figure B.6: Verification test data and PLAXIS (HS) fitting of Database 1(6).

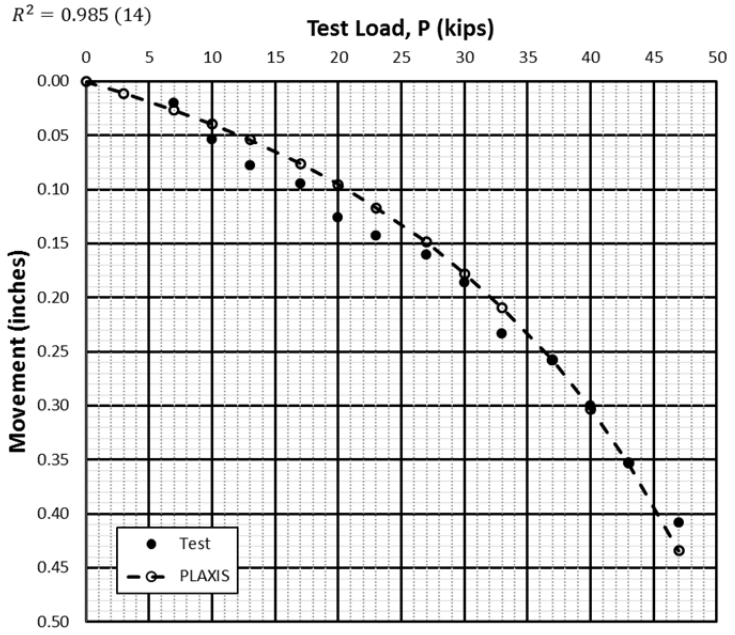

Figure B.7: Verification test data and PLAXIS (HS) fitting of Database 1(7).

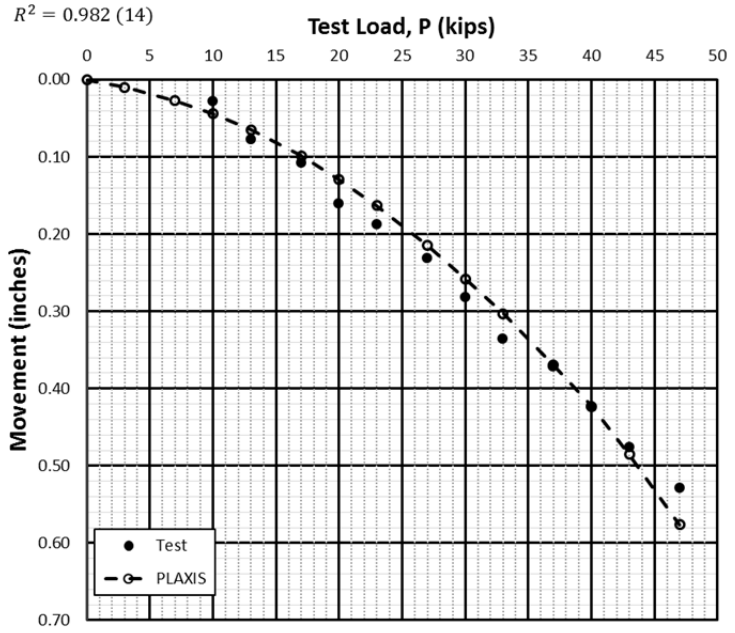

Figure B.8: Verification test data and PLAXIS (HS) fitting of Database 1(8).

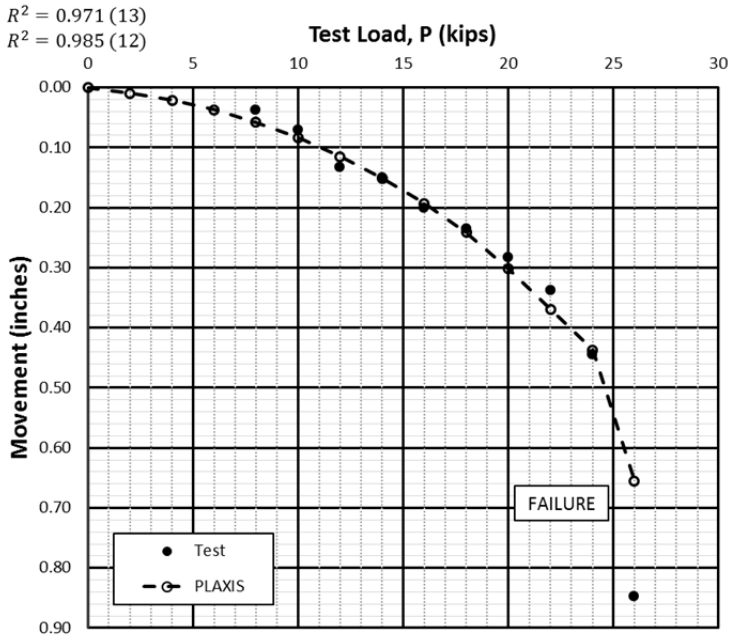

Figure B.9: Verification test data and PLAXIS (HS) fitting of Database 1(9).

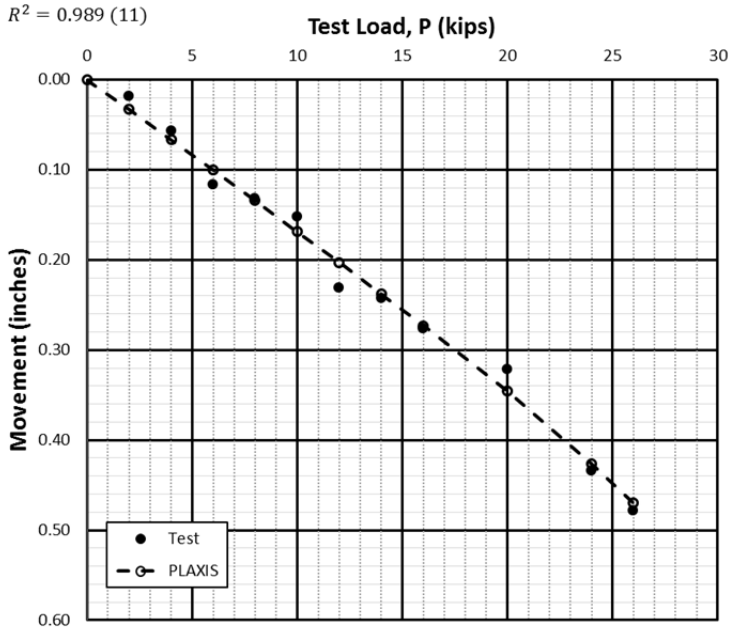

Figure B.10: Verification test data and PLAXIS (MC) fitting of Database 1(10).

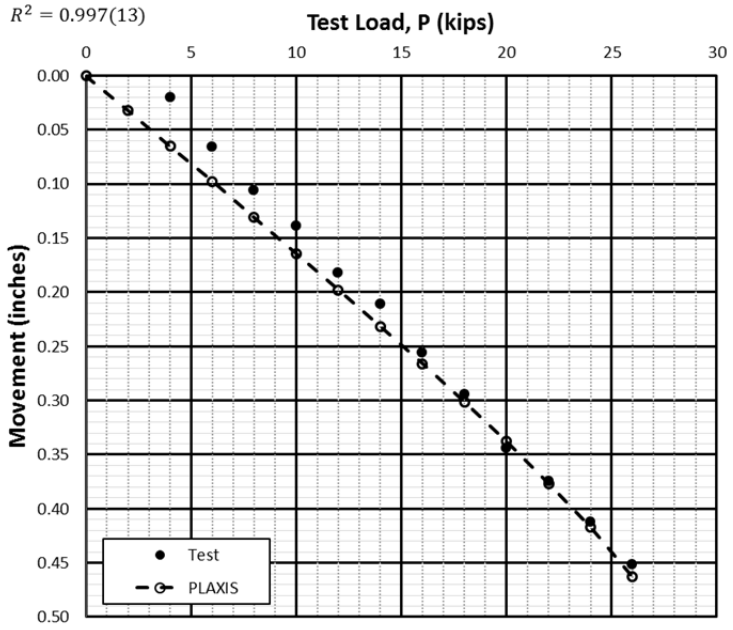

Figure B.11: Verification test data and PLAXIS (MC) fitting of Database 1(11).

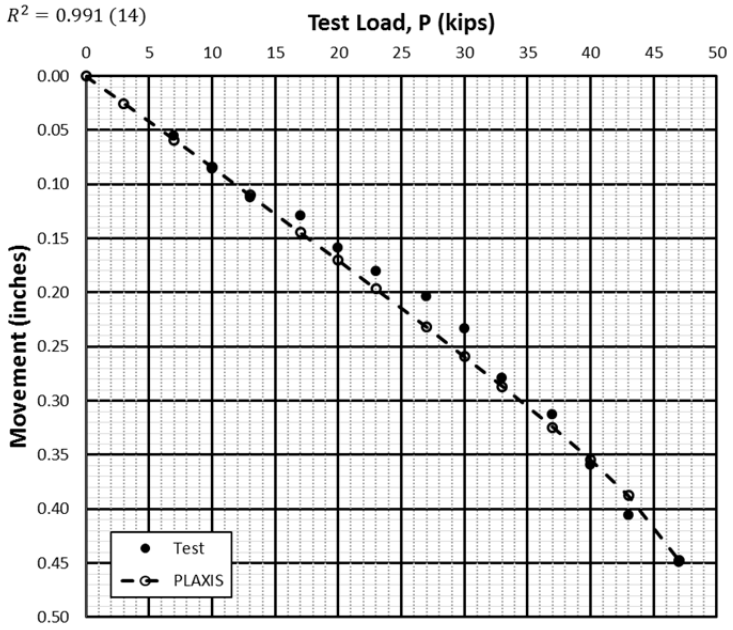

Figure B.12: Verification test data and PLAXIS (MC) fitting of Database 1(12).

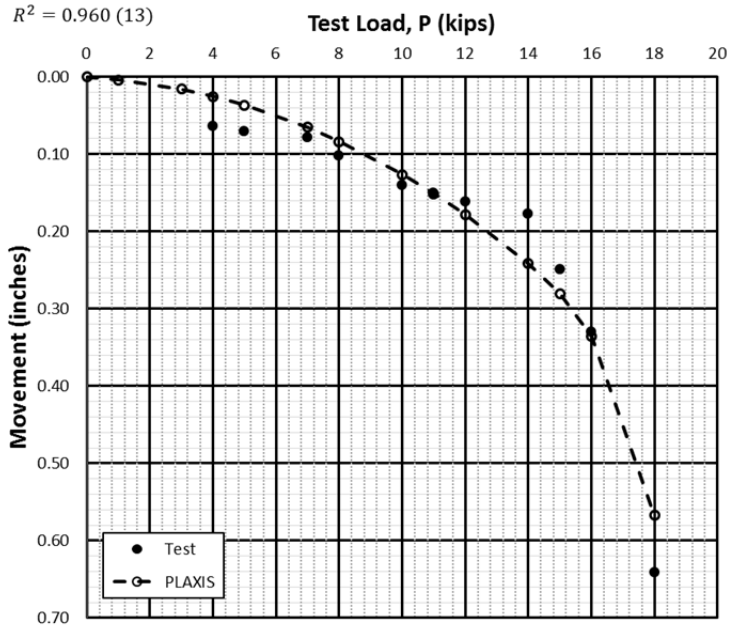

Figure B.13: Verification test data and PLAXIS (HS) fitting of Database 1(13).

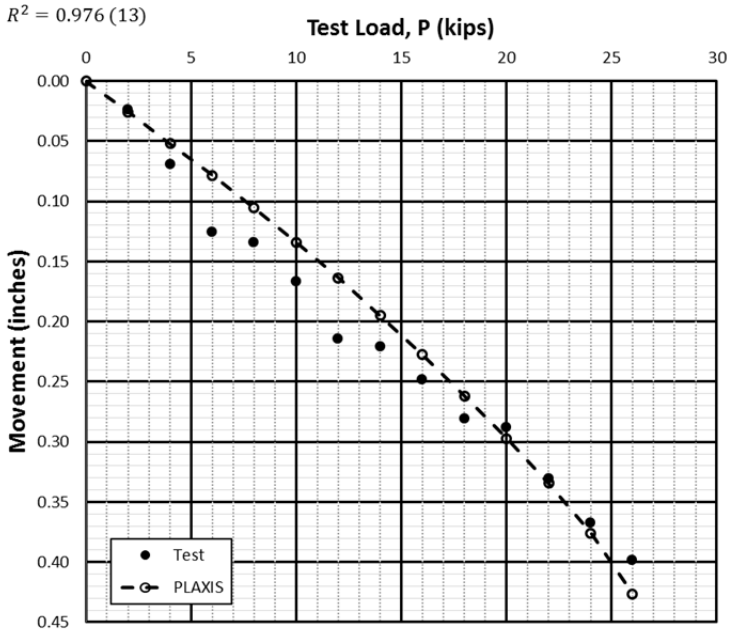

Figure B.14: Verification test data and PLAXIS (MC) fitting of Database 1(14).

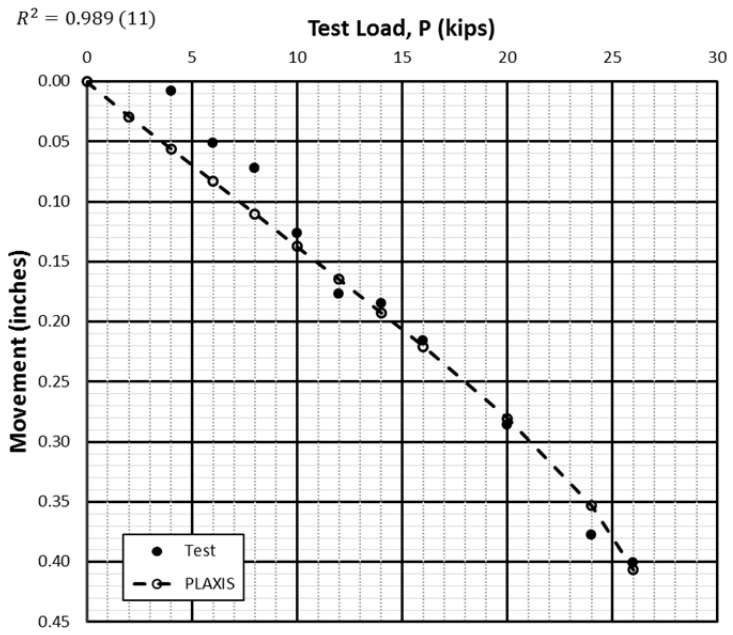

Figure B.15: Verification test data and PLAXIS (MC) fitting of Database 1(15).

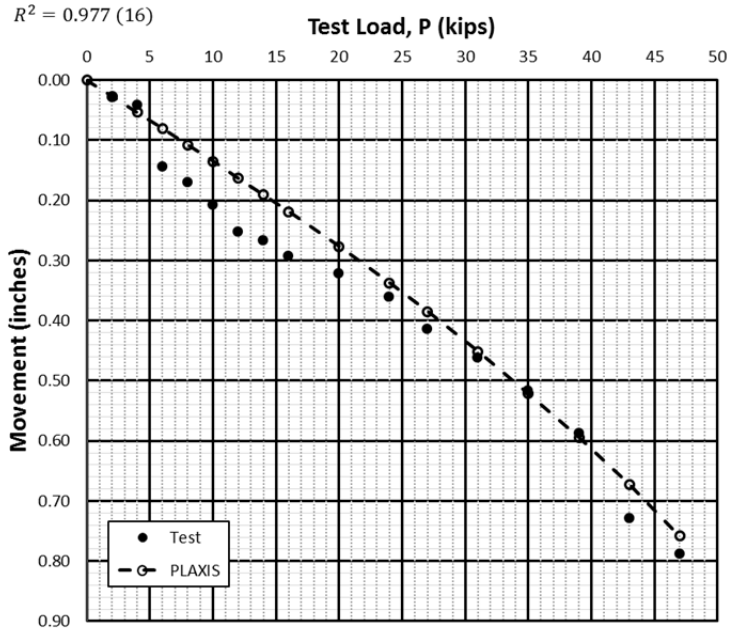

Figure B.16: Verification test data and PLAXIS (MC) fitting of Database 1(16).

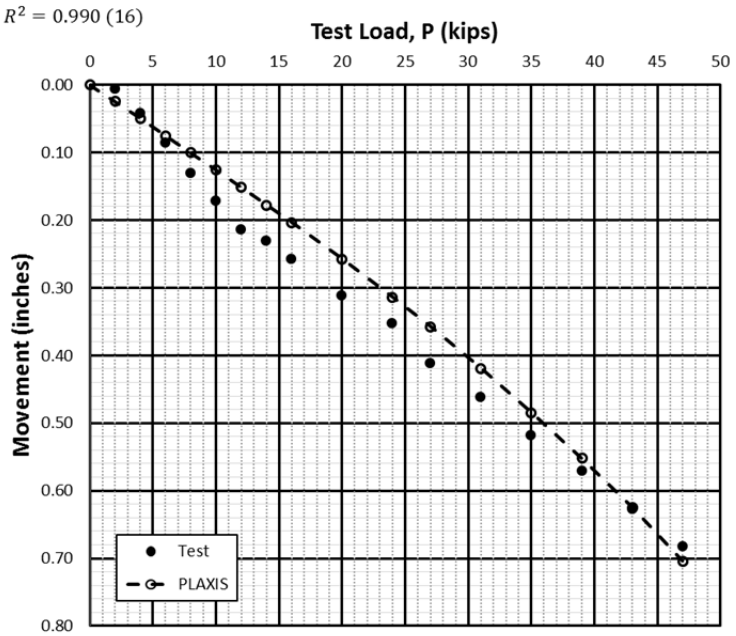

Figure B.17: Verification test data and PLAXIS (MC) fitting of Database 1(17).

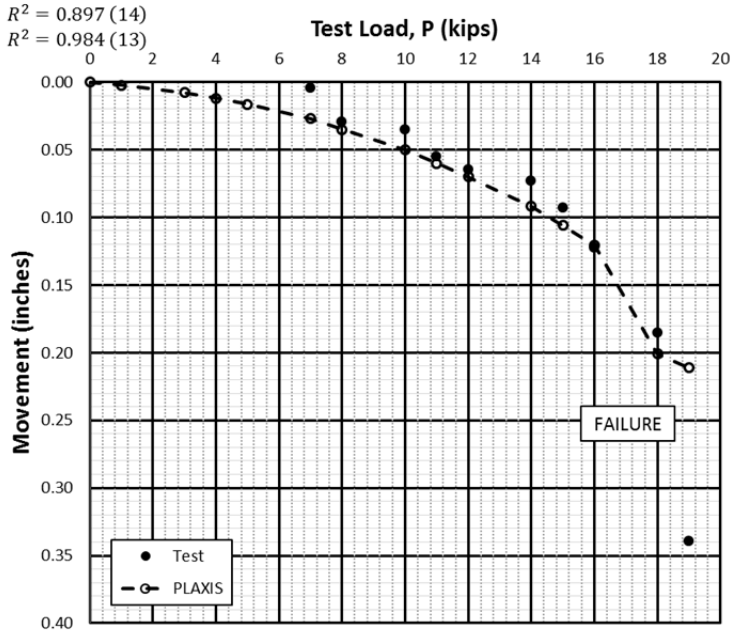

Figure B.18: Verification test data and PLAXIS (HS) fitting of Database 1(18).

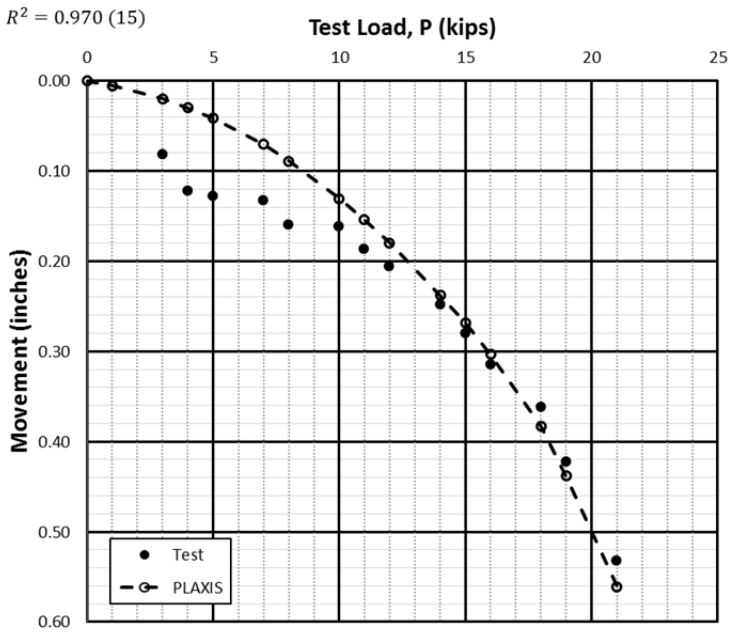

Figure B.19: Verification test data and PLAXIS (HS) fitting of Database 1(19).

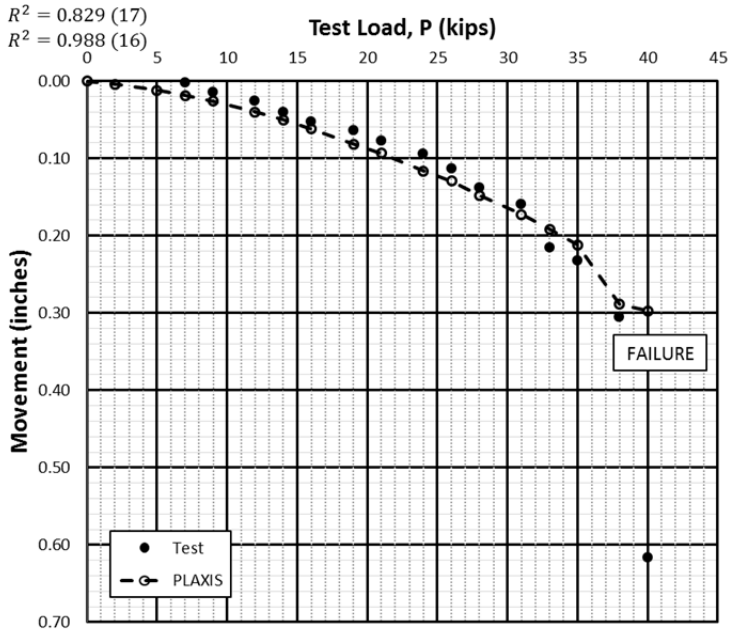

Figure B.20: Verification test data and PLAXIS (HS) fitting of Database 1(20).

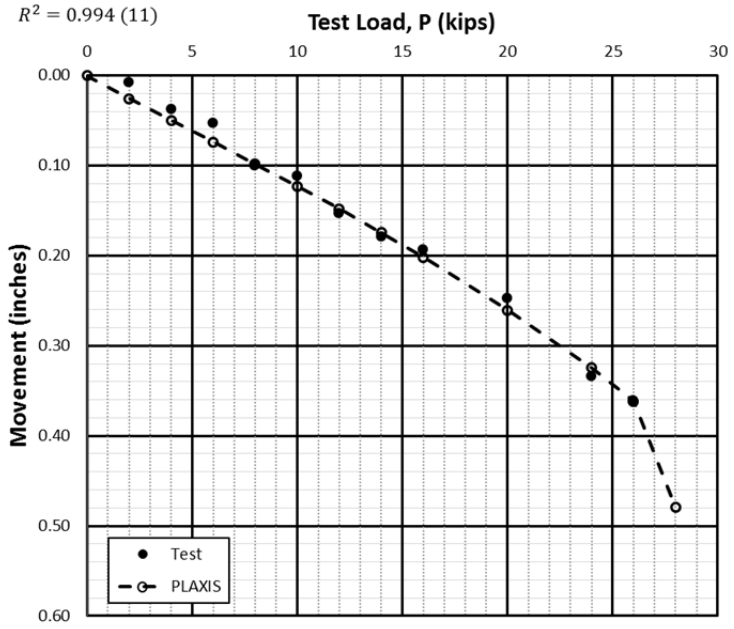

Figure B.21: Verification test data and PLAXIS (MC) fitting of Database 1(21).

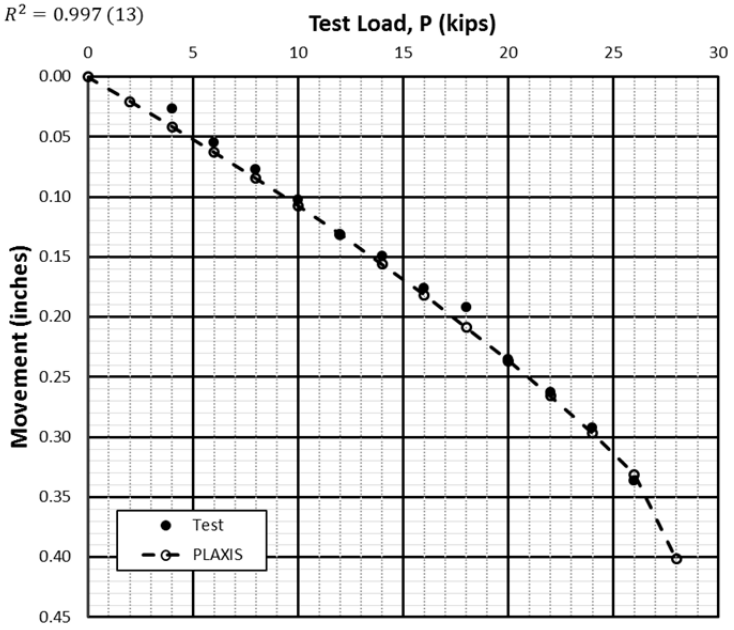

Figure B.22: Verification test data and PLAXIS (MC) fitting of Database 1(22).

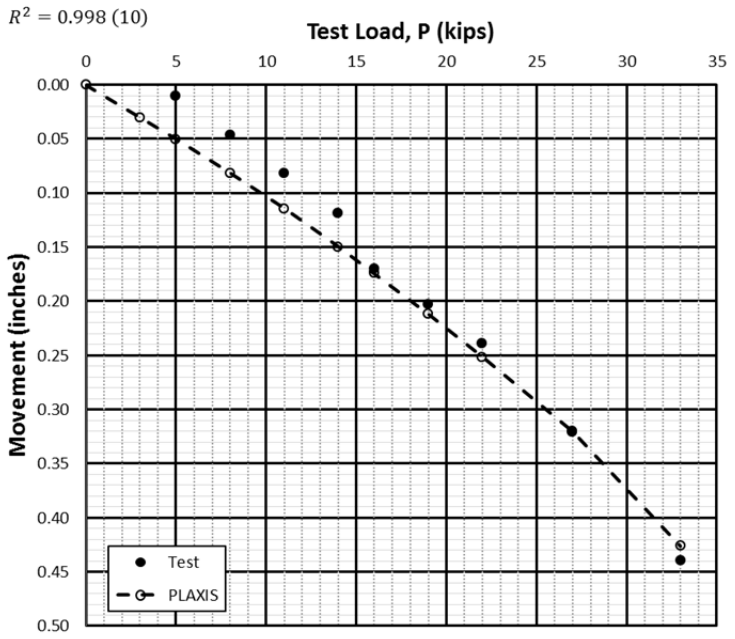

Figure B.23: Verification test data and PLAXIS (MC) fitting of Database 1(23).

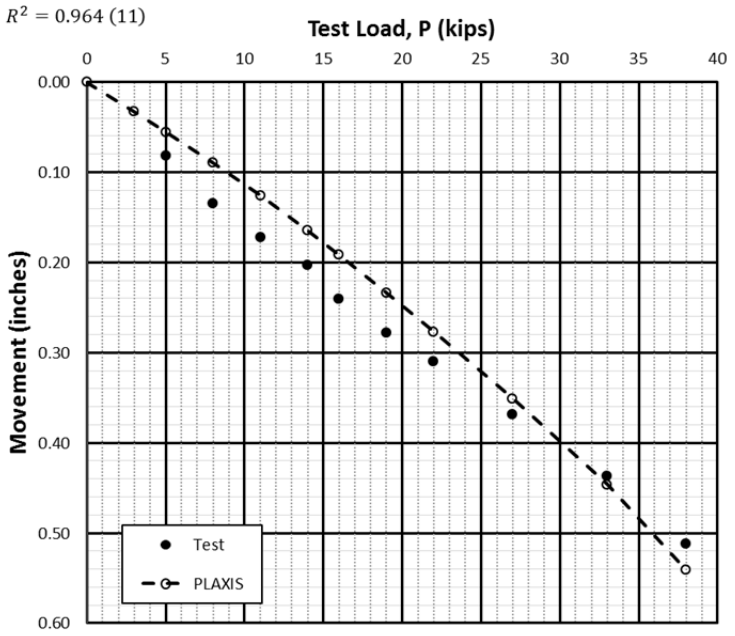

Figure B.24: Verification test data and PLAXIS (MC) fitting of Database 1(24).

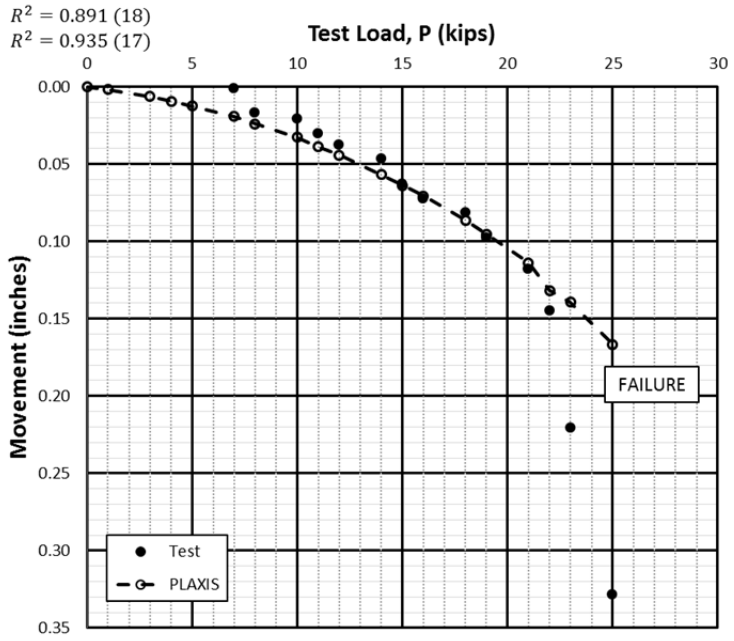

Figure B.25: Verification test data and PLAXIS (HS) fitting of Database 1(25).

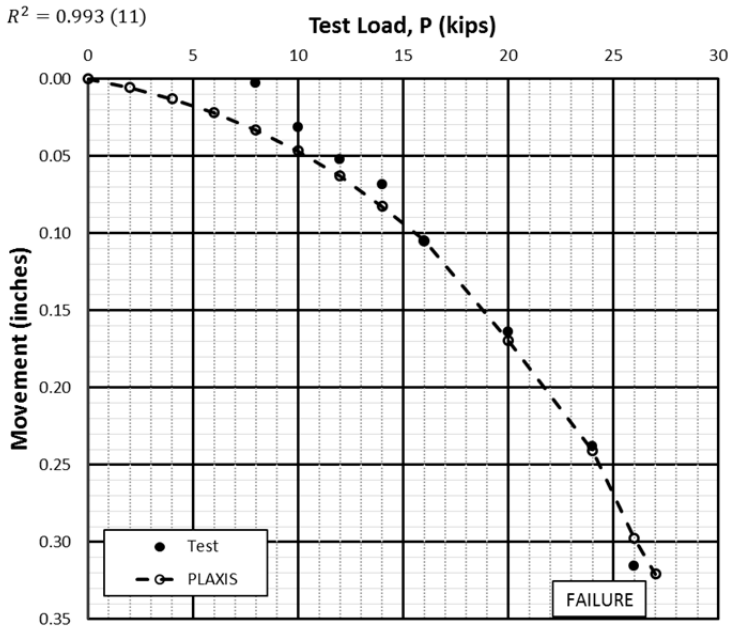

Figure B.26: Verification test data and PLAXIS (HS) fitting and prediction of Database 4(1).

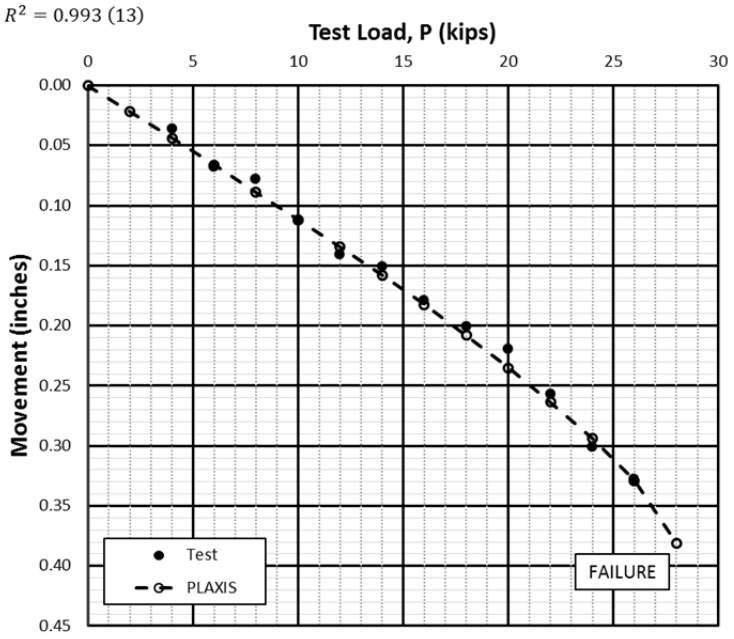

Figure B.27: Verification test data and PLAXIS (MC) fitting and prediction of Database 4(2).

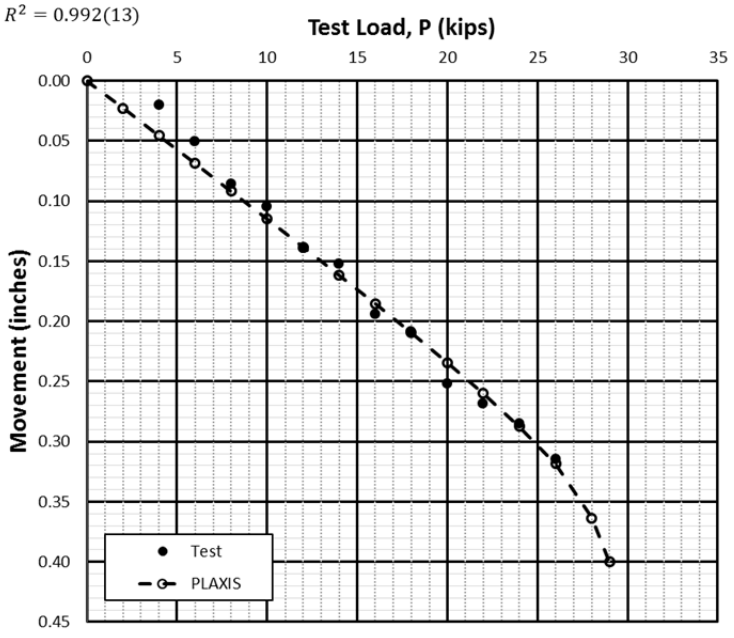

Figure B.28: Verification test data and PLAXIS (MC) fitting and prediction of Database 4(3).

Table B.1: Results of PLAXIS 2D verification test fitting for the MC model.

Database (No.)	1(2)	1(10)	1(11)	1(12)	1(14)	1(15)	1(16)	1(17)	1(21)	1(22)	1(23)	1(24)
γ (lb/ft^3)	110	110	110	110	110	110	110	110	110	110	110	110
e	0.50	0.50	0.50	0.50	0.50	0.50	0.50	0.50	0.50	0.50	0.50	0.50
E (lb/ft^2)	80,000	95,000	85,000	125,000	125,000	105,000	130,000	130,000	120,000	160,000	145,000	130,000
ν'	0.3	0.3	0.3	0.3	0.3	0.3	0.3	0.3	0.3	0.3	0.3	0.3
c (lb/ft^2)	1,100	1,000	900	1,000	1,000	550	1,650	1,650	850	1,070	1,050	1,200
Φ (°)	28	27	27	26	28	24	32	32	28	28	27	28
Ψ (°)	0	0	0	0	0	0	0	0	0	0	0	0
R_{inter}	1.0	1.0	1.0	1.0	1.0	1.0	1.0	1.0	1.0	1.0	1.0	1.0
Overburden (lb/ft^2)	500	1100	990	1320	500	1980	500	1100	660	500	500	500
Failure load (kip)	16	24	24	43	26	26	31	27	28	28	33	33
Length (ft)	10	10	10	17	10	10	10	10	10	10	10	10

Table B.2: Results of PLAXIS 2D verification test fitting for the HS model.

Database (No.)	1(1)	1(3)	1(4)	1(5)	1(6)	1(7)	1(8)	1(9)	1(13)	1(18)	1(19)	1(20)	1(25)
E_{50}^{ref} (lb/ft^2)	75,000	375,000	250,000	260,000	210,000	160,000	250,000	270,000	350,000	1,000,000	250,000	925,000	1,300,000
E_{oed}^{ref} (lb/ft^2)	75,000	375,000	250,000	260,000	210,000	160,000	250,000	270,000	350,000	1,000,000	250,000	925,000	1,300,000
E_{ur}^{ref} (lb/ft^2)	225,000	1,125,000	750,000	780,000	630,000	480,000	750,000	810,000	1,200,000	3,000,000	750,000	2,775,000	3,900,000
m	0.80	0.80	0.80	0.80	0.80	0.80	0.80	0.80	0.80	0.80	0.80	0.80	0.80
e_{int}	0.5	0.5	0.5	0.5	0.5	0.5	0.5	0.5	0.5	0.5	0.5	0.5	0.5
c (lb/ft^2)	650	600	825	600	950	1000	1100	900	680	675	680	925	850
Φ (°)	25	23	27	23	26	28	28	27	24	24	24	27	28
Ψ (°)	0	0	0	0	0	0	0	0	0	0	0	0	0
Overburden (lb/ft^2)	1320	825	500	500	770	1320	440	500	500	500	500	330	500
e	0.50	0.50	0.50	0.50	0.50	0.50	0.50	0.50	0.50	0.50	0.50	0.50	0.50
γ (lb/ft^3)	110	110	110	110	110	110	110	110	110	110	110	110	110
R_{inter}	1.00	1.00	1.00	1.00	1.00	1.00	1.00	1.00	1.00	1.00	1.00	1.00	1.00
Failure Load (kip)	30	20	20	22	40	30	40	24	18	19	19	40	25
Length (ft)	17	10	10	10	17	17	17	10	7	10	7	12	10

Appendix C

Calculations

PLAXIS Calculations

Table C.1: Soil nail parameters.

Parameter	Value
3 day strength of concrete, f'_c (psi)	2,500
Elastic modulus of bar, E_{bar} (ksi)	29,700
Bar diameter, D_n (inch)	1.0
Soil nail diameter, D_{SN} (inch)	6.0

$$E_g = 57{,}000\sqrt{f'_c} = 57{,}000\sqrt{2500} = 2{,}850{,}000\ psi$$

$$A_n = \pi\left(\frac{D_n}{2}\right)^2 = \pi\left(\frac{1}{2}\right)^2 = 0.442\ in^2$$

$$A = \pi\left(\frac{D_{SN}}{2}\right)^2 = \pi\left(\frac{6}{2}\right)^2 = 28.27\ in^2$$

$$A_g = A - A_n = 28.27 - 0.44 = 27.83\ in^2$$

$$E_{eq} = E_n\left(\frac{A_n}{A}\right) + E_g\left(\frac{A_g}{A}\right) = 29700\left(\frac{0.442}{28.27}\right) + 2850\left(\frac{27.83}{28.27}\right) = 3269\ ksi = 470000\ ksf$$

$$EA = \frac{E_{eq}}{S_H}\left(\frac{\pi D_{DH}^2}{4}\right) = \frac{3269}{1}\left(\frac{\pi(6)^2}{4}\right) = 92428\,\frac{kip}{ft}$$

$$EI = \frac{E_{eq}}{S_H}\left(\frac{\pi D_{DH}^4}{64}\right) = \frac{3269 * 144}{1}\left(\frac{\pi\left(\frac{6}{12}\right)^4}{64}\right) = 1444\ kip - ft^2/ft$$

SNAILZ Calculations

$$\varphi\ (input) = \tan^{-1}(\emptyset_s \tan\varphi) = \tan^{-1}(0.65 * \tan 20) = 13.3°$$

$$c\ (input) = \emptyset_s * c = 0.65 * 100 = 65\ psf$$

$$q = (\emptyset_{PO}\ or\ BSF)q_u = (\emptyset_{PO}\ or\ BSF)6.94\ psi$$

$$Facing\ resistance\ (Punching\ shear) = nominal * \emptyset_{FF} = 53.4 * 0.67 = 35.8\ kips$$

$$Tensile\ resistance\ (Yield\ stress\ of\ reinforcement) = nominal * \emptyset_T = 74 * 0.56 = 41.3\ ksi$$

Appendix D

Consolidated Undrained Triaxial Test Results

Table D.1: Consolidated Undrained Triaxial Test results along the project length (Terracon).

Boring No.	E-9			E-16		E-18			E-19			E-27		
Sample Depth (ft)	12 to 14			22.5 to 23		13 to 15			11 to 14			12 to 14		
Description of Specimens	Brown Clay			Brown Clay		Brown Clay			Light Brown Clay			Light Brown Sandy Clay		
LL (%)	47			81		72			69			60		
PL (%)	15			33		25			24			21		
PI	32			48		47			45			39		
Percent Passing No. 200 Sieve (%)	82			95		Not Reported			92			88		
Effective Stress Friction Angle (°)	27.8			25.4		22			21.6			17.8		
Effective Stress Cohesion (psf)	570			200		497			53			423		
Specimen	A	B	C	A	B	A	B	C	A	B	C	A	B	C
Consolidation Stress (psi)	10	20	40	15	45	5	15	30	12	24	47.8	15	25	45
Ultimate Deviator Stress (psi)	38.8	42.4	58.7	23.2	47.3	17.9	16.7	25.9	8.2	11.9	24.6	15.1	19.9	29.1
Dry Density (psf)	107.6	107.3	108.8	106.6	101.6	98	101.9	92.4	93.1	92.7	99.7	96.3	97.7	101.8
Modulus of Elasticity, E_0 (psf)	312,000	979,200	1,872,000	720,000	720,000	270,000	468,000	1,152,000	2,592,000	2,592,000	1,728,000	316,800	316,800	504,000
Modulus of Elasticity, E_{50} (psf)	264,000	288,000	468,000	446,400	262,800	134,640	331,200	201,600	259,200	230,400	288,000	288,000	198,000	360,000

Table D.1 – *Continued*

E-29			E-31			E-53			E-100			E-112			W-7		
29 to 31			11 to 15			8 to 10			14 to 16			8 to 10			26 to 30		
Brown Clay			Brown Clay			Brown Clay			Brown Clay			Brown Clay			Brown Clay		
59			47			41			63			58			60		
29			16			18			24			27			23		
30			31			23			39			31			37		
Not Reported			78			Not Reported			Not Reported			Not Reported			84		
23.8			22.6			26.8			27.5			26.6			26.4		
1133			671			460			617			370			434		
A	B	C	A	B	C	A	B	C	A	B	C	A	B	C	A	B	C
13	26	52	10	20	40	7.3	15	35	19.7	21.7	27.7	10	21.8	45	10.2	20	39.9
32.6	39.2	74.1	3209	30	39.9	17.5	26.2	35.3	37.1	40.5	55.3	21.2	23.5	43.2	26.4	32.7	37.4
102.2	104.9	106.8	102.2	100.3	100	104.5	100.3	100.6	99.9	101.4	98.1	99.3	100.4	102.6	113	106.8	1115.3
-	1,080,000	1,440,000	820,800	864,000	1,440,000	432,000	864,000	1,152,000	720,000	748,800	1,209,600	468,000	604,800	1,728,000	403,200	540,000	763,200
-	763,200	1,195,200	93,600	547,200	270,000	64,800	147,600	1,152,000	132,000	50,400	648,000	234,000	316,800	540,000	32,571	264,000	480,000

Table D.1 – *Continued*

W-9			W-11			W-14			W-30			W-120			W-128		
24 to 28			24 to 28			28 to 30			6.5 to 10			6 to 10			8 to 10		
Tan Clay			Light Brown Clay			Brown Clay			Light Brown Sandy Clay			Light Brown Clay			Brown Clay		
61			75			81			70			58			57		
22			24			26			23			21			24		
39			51			55			47			37			33		
Not Reported			95			Not Reported			85			86			89		
22.8			24.5			22.6			22			26.4			25.4		
328			225			390			0			434			653		
A	B	C	A	B	C	A	B	C	A	B	C	A	B	C	A	B	C
9.9	20	40	10	20	40	10	20	40	7.2	14.9	30	7.5	15	30	10	25	45
16.8	29	35.5	18.1	21.7	35.8	19	20.1	30.2	7.8	10.5	21.1	24.7	35	37	28.6	38.3	45.4
18.2	19.1	18.9	107.8	108.2	101.8	94.1	95.4	101.9	95.4	93.1	93.8	100.4	100.3	102.8	105.3	105.1	107.1
360,000	374,400	403,200	403,200	576,000	921,600	475,200	720,000	576,000	345,600	345,600	489,600	360,000	480,000	720,000	468,000	648,000	921,600
194,400	266,400	316,800	194,400	576,000	388,800	266,400	133,200	81,600	104,400	331,200	338,400	55,200	88,800	240,000	95,400	219,600	547,200

References

AASHTO. (2007). *LRFD Bridge Design Specification*. Washington, D.C.: 4th Edition, American Association of State Highway and Transportation Officials.

Allen, T. M., Nowak, A., and Barthurst, R. (2005). *Calibration to Determine Load and Resistance Factors for Geotechnical and Structural Design*.TRB Circular E-C079, Transportation Research Board, Washington, D.C.

Ann, T. S., Cheang, W., Hai, O. P., and Tan, D. (2004a). *Finite Element Analysis of A Soil Nailed Slope-Some Recent Experience.* 3rd Asian Regional Conference on Geosynthetics, GeoAsia, 183-192.

Ann, T. S., Hai, O. P., and Lum, C. W. (2004b). *Simulation of Soil Nail's Dynamic Pullout Response*. Plaxis Bulletin, (15): 10-12.

Baecher, G. B., and Christian, J. T. (2003). *Reliability and Statistics in Geotechnical Engineering*. Hoboken, NJ: Wiley.

Bolton, M. D. (1986). *The Strength and Dilantancy of Sands*. Geotechnique, 35(1); 65-78.

Brinch-Hansen, J. (1963). *Discussion of Hyperbolic Stress-Strain Response: Cohesive Soils*. Journal of Soil Mechanics and Foundation Engineering, American Society of Civil Engineers, Vol. 89, No. 4, pp. 241-242.

Byne, R. J., Cotton, D., Porterfield, J., Wolschlag, C., and Ueblacker, G. (1998). *Manual for Design and Construction Monitoring of Soil Nail Walls.* Report: FHWA-SA-96-69R, Federal Highway Administration, Washington, D.C.

Caltrans. (2007). *A User's Manual for the SNAILZ Program*, Version 2.02-Updated PC Version. Retrieved from Division of New Technology, Material and Research, Office of Geotechnical Engineering, California Department of Transportation, Sacramento, California: http://www.dot.ca.gov/hq/esc/geotech

Clouterre. (1993). *Recommendations Clouterre 1991.* (Trans.: Soil Nailing Recommendations 1991), English Translation, Presses de l'EcoleNationale des PontsetChaussees, Paris, France.

Cox, D. R., and Hinkley, D. V. (1984). *Analysis of Survival Data*. New York, NY: Chapman and Hall.

Craig Olden, Inc. (2013). *Verification and Proof Testing Results.*

Davisson, M. T. (1972). *High Capacity Piles*. Proceedings of Lecture Series on Innovations in Foundation Construction, American Society of Civil Engineers, Illinois Section, Chicago, pp. 81-112.

De Beer, E. E. (1967 and 1968). *Proefondervindlijkebijdrage tot de studie van het grensdraagvermogen van zandonderfunderingen op staal*. Tijdshift der OpenbarVerken van Belgie No. 6 (1967) and No 4, 5 and 6 (1968).

Duncan, J. M., and Chang, C. Y. (1970). *Nonlinear Analysis of Stress and Strain in Soil. ASCE Journal of the Soil Mechanics and Foundation Division*, (96); 1629-1653.

FHWA. (2001). *Load and Resistance Factor Design (LRFD) for Highway Bridge Substructures. Washington*, D.C.: Publication FHWA HI-98-032, Federal Highway Administration.

Google Inc. (2013). *Google Map of Dallas and Surrounding Area*.

Hawkins, D.L (2013). *SAS® Code for Parametric Survival Analysis.*

Hirary, A., and Kulhawy, F. H. (2002). *On the Interpretation of Drilled Foundation Load Test Results*. In Deep Foundation 2002 (GSP 116), ASCE, Reston, VA., pp. 1018-1028.

Irwin, J. O. (1947). *The Standard Error of an Estimate of Expectational Life*. Journal of Hygiene, No. 47, 471-476.

Kaplan, E. L., and Meier, P. (1958). *Nonparametric Estimation from Incomplete Observations*. Journal of the American Statistical Association, 53(282), 457-481.

Koutsoftas, D. C. (2000). *High Capacity Steel H-Piles in Franciscan Rock*. In Proceedings of Geo-Denver, Denver, Colorado, ASCE, Reston, VA, 157-177.

Lazarte, C. A. (2011). *Proposed Specifications for LRFD Soil-Nailing Design and Construction.* Washington, D.C.: NCHRP Report 701, Transportation Research Board.

Lazarte, C. A., Elias, V., Espinoza, R. D., and Sabatini, P. J. (2003). *Soil Nail Walls.* Washington, D.C.: Geotechnical Engineering Circular No. 7, Publication FHWA-IF-03-017, Federal Highway Administration.

Lee, E. T., and Wang, J. W. (2003). *Statistical Methods for Survival Data Analysis.* Hoboken, New Jersey: Third Ed. John Wiley & Sons.

Lengkeek, A., and Peters, M. (n.d.). S*imulation of Soil Nail in Large Scale Direct Shear Test*. Plaxis Practice, 12-15.

Nowak, A. S. (1999). *Calibration of LRFD Bridge Design Code*. Washington, D.C.: NCHRP Report 368, Transportation Research Board, National Research Council.

Nowak, A. S., and Collins, K. R. (2000). *Reliability of Structures*. New York: McGraw-Hill.

Oregon DOT (1999). *Monitoring of Soil Nailed Walls at the Highway 217 and Highway 26 Interchange.* Final Report, State Planning and Research, Project 270, Oregon Department of Transportation.

PLAXIS.(2011). *PLAXIS User Manual*.Delft University of Technology & PLAXIS by the Netherlands.

PTI (2005). *Recommendations for Prestressed Rock and Soil Anchors*; 4th ed. Phoenix, Arizona: Post-Tensioning Institute.

Randolph, M. F., and Wroth, P. (1978). *Analysis of Deformation of Vertically Loaded Piles*.Journal of Geotechnical Engineering div., Vol. 104.

Singh, V. P., and Sivakumar Babu, G. L. (2010). *2D Numerical Simulations of Soil Nail Walls*. Geotech. Geo. Eng., 28:299-309.

Sivakumar Babu, G. L. and Singh, V. P. (2009). *Simulation of Soil Nail Structures using PLAXIS 2D*. Plaxis Bulletin, 16-21.

Terracon Consulting Engineers and Scientist. (2013). *Consolidated Undrained Triaxial Test Results.*

Trinity Infrastructure LLC.(2013). *General Information Related to Design of Construction of Soil Nail Walls in North Dallas Texas.*

Van Langen, H. (1991). *Numerical Analysis of Soil-structure Interaction*. Dissertation: Delft University of Technology.

Wang, Z., and Richwien, W. (2002). *A Study of Soil-Reinforcement Interface Friction*. Journal of Geotechnical and Geoenvironmental Engineering, 128(1), 92-94.

Yu, X., Murad, Y., Abu-Farsakh, M. Y., Yoon, S., Tsai, C., and Zhang, Z. (2012).*Implementation of LRFD of Drilled Shafts in Louisiana*. Journal of Infrastructure Systems, American Society of Civil Engineering, 18(2), 103-112.

Zhang, M., Song, E., and Chen, Z. (1999). *Ground Movement Analysis of Soil Nailing Construction by three-dimensional (3-D) Finite Element Modeling (FEM)*. Computers and Geotechnics, (25); 191-204.

Biographical Information

Brett DeVries received his Bachelor of Science degree in Civil Engineering from North Dakota State University in the spring of 2011. He then spent the following summer working in the Geotechnical Lab at the Universidad de Burgos in Spain and was admitted to the University of Texas at Arlington in Spring 2012. At which he completed his Masters of Science in Civil Engineering in the summer of 2013. Brett's current plans are to continue his education and complete a Doctor of Philosophy in Civil Engineering from the University of Texas at Arlington.